BLAST DAMAGE MITIGATION IN SUBMERGED SYSTEMS. PHASE I: INTERNAL EXPLOSION

BLAST DAMAGE MITIGATION IN SUBMERGED SYSTEMS. PHASE I: INTERNAL EXPLOSIONS

By

YASSER ALI MAHMOUD ALI KHALIFA

B.Sc., M.A.Sc.

A Thesis Submitted to the School of Graduate Studies in Partial Fulfillment of the Requirements for the Degree of Doctorate of Philosophy

McMaster University

September 2015

Doctor of Philosophy (2015)	McMaster University
(Civil Engineering)	Hamilton, Ontario

TITLE:	Blast Damage Mitigation in Submerged Systems. Phase I: Internal Explosions
AUTHOR:	Yasser Ali Mahmoud Ali Khalifa
	B.Sc., M.A.Sc. (Military Technical Collage)
SUPERVISORS:	Dr. Wael W. El-Dakhakhni
	Dr. Michael Tait (Co-Supervisor)
NUMBER OF PAGES:	xix, 188

ABSTRACT

This thesis is focused on quantifying the dynamic performance of lightweight metal sandwich systems under confined explosions, where this effort represents the first of a multi-phase comprehensive research program that is focused on developing blast damage mitigation techniques in submerged structures. A confined explosion occurrence inside such facilities may lead to paralyzing all operations depending on the functions of the affected sections. Subsequently, using sacrificial cladding placed as a physical barrier over critical components that might be vulnerable to a potential explosion is considered to be an effective blast damage mitigation technique. Furthermore, sandwich panels can be an ideal system to be used as sacrificial cladding, as it can be manufactured to possess high stiffness-to-weight ratio and superior energy absorption capabilities. Consequently, an experimental program was performed to investigate the performance of lightweight cold-formed steel sandwich panels under both quasi-static loads and confined explosions, where a total of fifty-seven sandwich panels were tested, considering various core configurations, different core sheet thickness, and different blast load intensity levels.

The American ASCE/SEI 59-11 and The Canadian CSA/ S850-12 blast design standards predict the dynamic response of a structure component based on the static resistance function by applying dynamic increase factors. Subsequently, the static resistance functions for the proposed panel configurations were investigated experimentally and compared with the introduced analytical model, in order to quantify accurately the inelastic panel response. The quasi-static test program was performed in two stages, where the first included eighteen single layer core sandwich panels, which represented *longitudinal* and *transverse corrugated* core configurations. The results of the first stage configurations demonstrated an efficient strength and stiffness, but showed a lack in energy absorption capabilities and ductility capacity. Therefore, in the second stage, different core configurations were developed, including twenty-one panels representing *Bi-directional* and *X-core* double layered core configurations and its counterpart *Uni-directional* single layer core configuration. The results of the second stage demonstrated an enhancement in the ductility and energy absorption capabilities compared to the configurations tested in the first stage. The residual deformations and failure modes demonstrated were assessed and discussed in details, where web crippling, local buckling and global buckling induced by shear or flexure were determined. In general the static resistance functions for each tested panel were used to quantify the panels' yield loads, ultimate capacities, and corresponding displacement levels. Moreover, the influences of both the core configuration and the core sheet thickness on the panels' stiffness, ductility levels and energy absorption were quantified.

Based on the conclusions of the static testing and considering the ductility, capability of energy absorption, and the behavior beyond the elastic zone, two different core configurations were chosen to be tested under confined explosions. Eighteen panels were tested in a cylindrical shape blast chamber representing a typical submerged structure under different scaled distances ranged from 2.82 to 1.09 m/kg$^{1/3}$, in order to demonstrate different damage state levels in accordance with the blast design standards (ASCE/SEI 59-11, CSA/ S850-12). In the blast testing results, the incident and reflected pressure time histories of the blast wave were measured, while the modified Friedlander equation was used to fit the first positive phase of the reflected pressure histories. In addition, the displacement response histories of the back face of the tested panels were recorded. The measured values of peak incident pressure, peak reflected pressure, incident impulse and the reflected impulse were compared to the predicted values using ConWep (Hyde 1990) considering the spherical explosion, and have shown a good agreement. Furthermore, the failure modes and the post blast damage were determined and compared to the static observations.

In order to complement the experimental program, a nonlinear inelastic single degree of freedom model was developed in order to predict the dynamic response of the sandwich panels. The model used the recorded blast load and the static resistance while applying the dynamic increase factors recommended by the standards (ASCE/SEI 59-11, CSA/ S850-12). The model results were in a good agreement with the experimental data. Furthermore, the different ductility and support rotation values obtained experimentally and predicted analytically were related to the different damage levels specified by blast standards. Finally, the influence of sandwich panel core configuration on the dynamic blast response of the tested sandwich panels was discussed.

KEYWORDS: Blast Loads; Cold formed steel; Confined explosion; Energy absorption; Flexural stiffness; Lightweight structure; Sacrificial cladding; Sandwich panel; Submerged structures; Uniform loading.

ACKNOWLEDGEMENTS

All Praise and thanks to Almighty Allah for giving me a chance and support to finish this study. I would like to express my sincere gratitude to my parents, who raised me to be the man I am today, may Allah bless them, and have mercy on them, and give them long healthy life, Amen. Thanks are due to my generous wife for her continuous support and encouragement, and being patient through the hard times. I would also like to sincerely apologise to my kids for being busy at work all time, and I hope that they will understand one day that it was for our all good.

I want to express my deepest gratitude and appreciation to my supervisors Dr. Wael El-Dakhakhni and Dr. Micheal Tait for their superior support and encouragement throughout my research. They have guided me through the way and gave me the opportunity to learn and understand how research should be conducted. It was a great honor to work with wonderful professors and within a research group like theirs.

Furthermore, I would like to thank Dr. Manuel Campidelli for the fruitful discussions and help through my research. My gratitude to my committee members Dr. Philip Koshy and Dr. Peijun Guo, who offered their valuable advices and suggestions during the development of this work.

Thanks are due to Kent Wheeler and Paul Heerema, of McMaster University's Applied Dynamics Laboratory, who helped me a lot and provided me with their technical support during the experimental phase. Moreover, I would like to express my respects and thanks to Mr. Bert von Rosen and Mr. Rick Guilbeault, as well as the Canadian Explosive Research Laboratory staff for conducting the blast tests and providing continuous support and guidance throughout my blast testing phase.

The Egyptian Armed Forces is gratefully acknowledged for the sponsorship, and their moral and financial support.

Finally, I would also like to thank my friends and colleagues at McMaster University, for their support and valuable discussion during my research, for you: Ahmed Ashour, Mustafa Syiam, Ahmed Siam, Mohamed Azzeldien, Shady Salem, Tarek El-Hashimy, Yasser El-Anany, and Omar El-Azizy, I am truly grateful.

CO-AUTHORSHIP

This thesis has been prepared and written in accordance to the rules for a sandwich thesis format required by the faculty of graduate studies at McMaster University. This thesis consists of the following papers:

Chapter 2

Khalifa, Y. A., Tait, M. J., and El-Dakhakhni, W. W. (2015), "***Sandwich Systems Performance under Blast Loads: Review***". Prepared to be submitted for publication.

The comprehensive literature review was performed by Yasser Khalifa. Chapter 2 was written by Yasser Khalifa. Dr. Michael Tait and Dr. Wael El-Dakhakhni provided technical guidance and reviewed the journal paper throughout its development phases.

Chapter 3

Khalifa, Y. A., Tait, M. J., and El-Dakhakhni, W. W. (2015), "***Out-of-Plane Behavior of Lightweight Metallic Sandwich Panels***". ASCE Journal of Performance of Constructed Facilities, submitted for publication in June 2015.

Experimental program design and analysis of experimental data were performed by Yasser Khalifa. Chapter 3 was written by Yasser Khalifa. Dr. Michael Tait and Dr. Wael El-Dakhakhni provided technical guidance and reviewed the journal paper throughout its development phases.

Chapter 4

Khalifa, Y. A., El-Dakhakhni, W. W., and Tait, M. J., (2015), "***Metallic Sandwich Panels Assessment under Quasi-Static Loading***". Elsevier, Journal of Engineering Structures, submitted for publication in July 2015.

Experimental program design and analysis of experimental data were performed by Yasser Khalifa. Chapter 4 was written by Yasser Khalifa. Dr. Michael Tait and Dr. Wael El-Dakhakhni provided technical guidance and reviewed the journal paper throughout its development phases.

Chapter 5

Khalifa, Y. A., El-Dakhakhni, W. W., and Tait, M. J., (2015), "***Performance of Lightweight Sacrificial Cladding under Confined Blast Loads***". ASCE Journal of Structural Engineering, submitted for publication in July 2015.

Experimental program design and analysis of experimental data were performed by Yasser Khalifa. Chapter 5 was written by Yasser Khalifa. Dr. Michael Tait and Dr. Wael El-Dakhakhni provided technical guidance and reviewed the journal paper throughout its development phases.

TABLE OF CONTENT

Chapter 1: Introduction

Chapter 2: Sandwich Systems Performance under Blast Loads: Review

Chapter 3: Behavior of Lightweight Metallic Sandwich Panels under Out-of-Plane Loading

Chapter 5: Performance of Lightweight Sacrificial Cladding under Confined Blast Loads

Chapter 6: Summary, Conclusions, and Recommendations for future research

LIST OF TABLES

LIST OF FIGURES

CHAPTER 1: INTRODUCTION

1.1 Background and problem statement

The current study represents the first of a multi-phase comprehensive research program that is focused on quantifying the response of submerged structures under both internal and underwater explosions. In addition, the program aims at developing practical blast damage mitigation techniques for the both aforementioned types of loading. Subsequently, the present work is focused on quantifying the dynamic performance of lightweight cold-formed steel sandwich panel systems under confined explosions, in order to facilitate their adoption as a sacrificial cladding installed on the internal walls of a submerged system to minimize internal explosion effects.

Compared to free-air explosion, a confined explosion could be more disastrous as it typically requires significantly less amount of explosives to cause the same damage level when the explosion is confined due to multiple refection effects. Such an explosion can also paralyze most facility operations depending on the location and the size of explosion. The nature of a confined explosion wave is also very complex to define, due to the target structure shape and dimensions that affects the reflections in the blast wave. The problem is magnified in the case of submerged structures, which are typically not designed to withstand confined blast loads. Designing structures to resist and sustain blast loads has been the solicitude of governments and military engineers for decades. More recently two North American Standards, namely the ASCE/SEI 59-11 and the CAN/CSA S850-12, were published to address the need for civilian blast resistant construction in addition to the re-introduction of the seminal US Army Technical Manual TM 5-1300 into a Unified Facility Criteria document UFC 3-340-02 (2008). In addition to design related codes, other guidelines have focused on describing actions needed for planning, preparing and mitigating the risk of blast hazard (e.g. FEMA-452, 2005 and GSA 2003).

The dissertation attempts to evaluate the effects of using sacrificial cladding, as an efficient method to mitigate the risk of blast hazard in a vessel simulating a submerged structure. The sacrificial cladding system is thus expected to provide adequate energy absorption capabilities through plastic deformations, and subsequently protecting the main structure. The proposed sacrificial cladding constitute a sandwich panel system that, in addition to possessing high energy absorption capability, have high strength and stiffness to weight ratio, which makes it ideal for blast hazard mitigation applications. The dissertation also attempts to tackle some sandwich panel disadvantages such as high cost and complex manufacturing techniques.

Finally, it should also be noted that there is no general analytical method available in literature to accurately predict the resistance function of sandwich panels, which is a key aspect in developing guidelines for sacrificial cladding sandwich panel response predictions under blast. As such, there is a critical need to develop an experimental blast result database, and corresponding idealized resistance functions, in order to facilitate benchmarking data for blast response prediction codes.

1.2 Scope

Mitigating internal (confined) blast load effects is a key aspect within any holistic facility protection scheme. On the other hand, relevant experimental data in open literature pertaining to characteristics of blast-induced pressure wave is scarce. In addition, predicting the non-elastic behavior of sandwich panels with different core configurations is complex because of the multitude of possible failure modes and the effect of dynamic loading on the response.

Moreover, there is a need to overcome the high cost of manufacturing sandwich panels using simple and cost-effective techniques.

The dissertation investigates the capabilities of lightweight cold-formed steel sandwich panels, with different cross sectional configurations, to serve as sacrificial cladding. To minimize cost, available off-the-shelf corrugated sheets with various profiles were used to construct different core configurations such as *longitudinal corrugated, transverse corrugated, Bi-directional corrugated* and *X*-core configurations. Furthermore, simple joining (manufacturing) technique was evaluated by testing the panels under both static and blast loads. The work included the development of a test setup to evaluate the static resistance under out-of-plane uniform loading, using an air bag, followed by data analysis in order to evaluate the behavior of the tested configurations, and to select those configurations that were more suited as sacrificial cladding. The selection was accompanied by a preliminary dynamic analysis in order to determine the scaled distances for the blast tests, which lead to different damage levels according to the both the American and Canadian standards (ASCE 2011, CSA 2012). Following the confined blast tests, an analytical model, using the established resistance function, was developed and verified by comparing its results with the experimental results.

Finally, it is expected that the results and findings of this dissertation would influence the development of lightweight cost-effective metal sandwich panels to be used as sacrificial cladding under confined explosions inside submerged structures.

1.3 Objectives

The objectives of this research are as follows:

1. Present the characteristics of confined blast pressure wave, and highlight the complex nature of the confined explosions. In addition, introduce the advantages and

disadvantages of sandwich panels, and the use of sacrificial cladding in blast risk mitigation.

2. Propose new metal sandwich panels that can be used in blast applications, by using available off-the-shelf materials and simple joining technique to produce a low-cost rapid blast mitigation product
3. Quantify the quasi-static resistance function experimentally for the proposed sandwich configurations, and analyze the results to choose the configuration(s) that most fit as sacrificial cladding in blast application.
4. Study the influence of core configuration and core sheet thickness on the characteristics of the performance of the sandwich panels under out-of-plane loading, and determine the failure mode(s) for the tested configurations.
5. Assess the performance of the sandwich panels under different scaled distances using live explosives in confined blast chamber, and relate the observed damages to the damage states specified by both the American and Canadian standards (ASCE 2011, CSA 2012).
6. Develop a nonlinear inelastic analytical model to predict the dynamic behavior of the sandwich panels, using the experimental static resistance, to be used later for further investigation.

1.4 Organization of the dissertation

The current research investigates the performance of lightweight cold-formed steel sandwich panels subjected to confined explosions, which can be used as sacrificial cladding in submerged structures. Three experimental stages accompanied by analytical modeling were performed to provide better understanding of the dynamic response of the proposed sandwich configurations under both quasi-static and confined blast loads. The dissertation content are as follows:

- Chapter 1 presents the problem statement, motivation, and the objectives of the research.
- Chapter 2 gives an overview in the literature on the state-of-the art for the dynamic response of sandwich panels under blast loads, considering analytical, numerical and experimental methods. The sandwich panels were classified according to its fabrication materials into three types: metallic, hybrid-metallic and composite sandwich panels.
- Chapter 3 contain the description of the quasi-static experimental program, test matrix of first stage (single layer core panels), test setup and instrumentation, results and data analysis, and the influence of core configuration and core sheet thickness on (elastic flexure stiffness, ductility, and energy absorption).
- Chapter 4 describes the second stage (double layer core panels and its opponent with single layer) of the quasi-static experimental program, test matrix, results and data analysis, and the influence of core configuration and core sheet thickness on (elastic flexure stiffness, ductility, and energy absorption).
- Chapter 5 presents the description of the confined blast experimental program, test setup and instrumentation, results and data analysis including the pressure wave characteristics, peak displacements, inelastic analysis results, ductility exhibited by different configurations under different scaled and related to damage levels specified by standards.
- Chapter 6 contains the dissertation summary, main conclusions, and recommendation for future work.

1.5 Blast phenomena

An explosion is defined as a rapid increase in volume and release of energy in an extreme manner, usually accompanied with the generation of high temperatures and release of gases. Detonation of high explosives creates supersonic shock wave (pressure wave), burst, and fragments (Baker et al. 1983). On the other hand, subsonic explosions are created by low explosives through a slower burning process known as deflagration.

The blast loads can be evaluated based on charge weight and stand-off distance (Cole 1948). The energy released by an explosion is typically assessed according to the TNT (Trinitrotoluene) charge weight equivalent. Several factors and approaches might be used to compute the equivalent TNT weight for another explosive, in order to predict blast pressure or impulse, these factors are tabulated in different references such as (Dusenberry 2010).

1.5.1 Open-air Explosion

The typical pressure-time curve that would describe explosions occurring in open air was introduced independently by several researchers during and after the World War II. Fig. 1.1 shows a typical pressure time curve for a blast wave (Baker et al. 1983). The pressure time curve consists of two phases; the positive pressure (pushing) phase, where incident pressure rise at the wave front from ambient pressure (P_o) to ($P_o+P_s^+$) at time of arrival (t_a), then follows an exponential decay until pressure drops down to ambient pressure at time of (t_a+T^+). The second phase is called negative (suction) phase, where pressure decrease until a peak negative pressure ($P_o+P_s^-$). Typically, time of the pressure wave is relatively very small, for that the structure component respond is mainly affected by the impulse more than the value of the peak pressure. The specific impulse of the positive phase is given by:

$$Is = \int_{-ta}^{ta+T+} P(t)dt \tag{1}$$

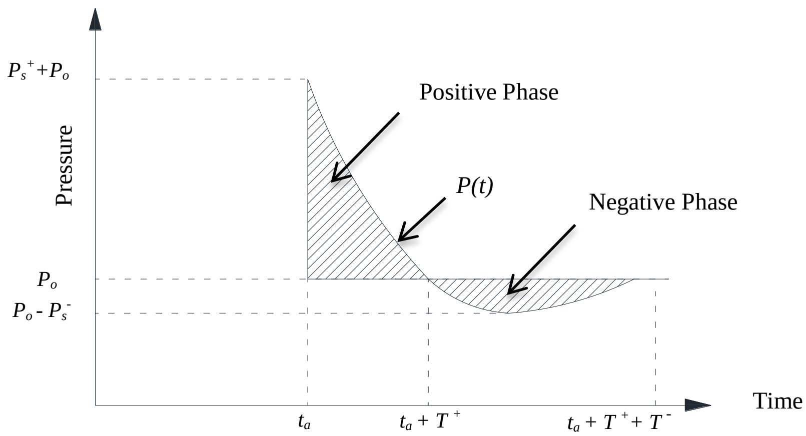

Fig. 1.1 Pressure time curve of blast wave (Baker et al. 1983).

The distance between the center of the charge and the structure is referred to as the stand-of-distance, which has a major effect on the imparted energy to the structure. Consequently, the explosion scenario can be classified also from stand-of-distance point of view as follows: Far-field explosion, localized explosion, and full contact explosion. Each type is specified with different pressure distribution on the considered structure and its accompanied failure.

Usually the positive phase only is considered whereas the negative phase is not taken into consideration. However in particular cases such as corrugated roofs and glass panels, the influence of negative phase pressure on the response of a structure could be similar or may be more than that of positive phase (Krauthammer 2008).

1.5.2 Underwater Explosion

Underwater explosions differ from open-air ones due to the incompressible and denser fluid, which increases its ability for energy transfer and increases the Mach number to about 4.3

times. The effects of an underwater explosion depend on a many factors as the distance from the explosion, explosion energy, explosion depth, and water depth (Cole 1948). The underwater explosions can be classified according to the depth of explosion to shallow and deep underwater explosion. Shallow explosion is specified with a crater formation at water surface, while it may or may not be formed for deep explosions.

Detonation underwater produces a gas bubble under high pressure releasing a primary shock wave with about half the total energy of the charge. The bubble starts to contract after losing its internal energy by the mean of surrounding pressure until it is compressed and its inner pressure increases. At that point, it starts to expand again forming second shock wave as shown in Fig. 1.2. This process is repeated until the total energy is vanished. For shallow underwater explosion, the gas bubble is released in air producing water surface crater (Kowsarinia et al. 2012). The dynamics of gas bubble release has not well defined by a mathematical model, approximate methods are used to predict underwater shock (Kowsarinia et al. 2012).

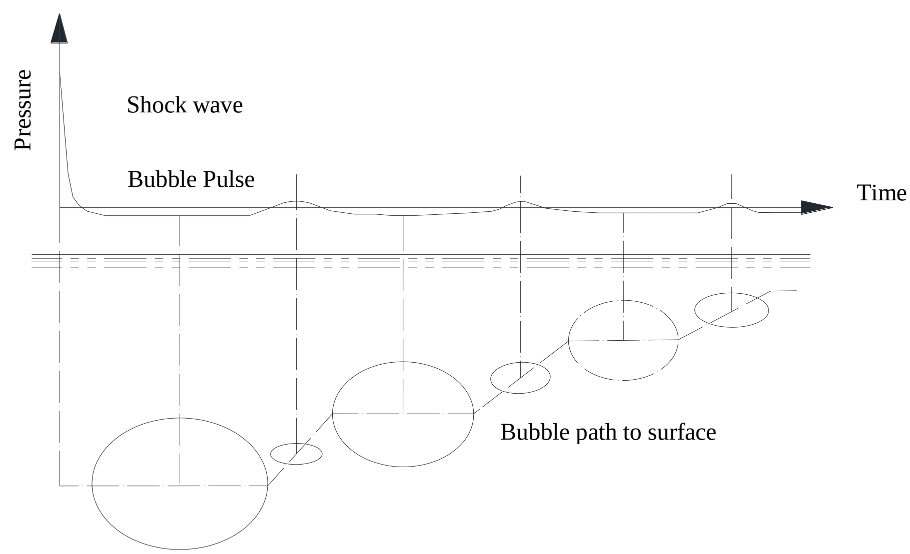

Fig. 1.2 Fluctuation of the gas bubble and its effect on pressure pulse (Kowsarinia et al. 2012).

1.5.3 Confined Explosion

Confined explosion is characterized by the complex reflection waves induced by the surrounding environment. However, the initial positive phase is argued to be similar to the open-air explosion with the same charge weight and stand-of-distance (Baker et al. 1983 and Krauthammer 2008).

Fig. 1.3 shows a typical time-pressure curve for a confined explosion, where a pseudo-static pressure is created after the reflections due to the unvented space. This pseudo-static pressure decays with time to ambient pressure due to ventilation and/or cooling of the hot gasses.

Confined explosions could be accidental or manmade, and may occur in different types of structures such as submerged structures, tunnels, buses, trains, and inside buildings. The expected damages due to confined blast can be much higher than its equivalent in open-air explosion (Smith 1994).

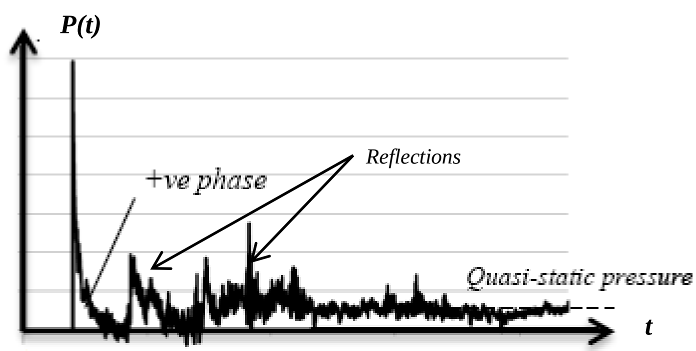

Fig. 1.3 Typical pressure-time history in confined explosion (Khalifa et al. 2015).

1.5.4 Modeling blast load

Open-Air and underwater large scale blast experiments using live explosives are key to investigate the performance of different structures under blast loads. However, performing those types of experiments is limited due to the associated high cost and security restrictions. subsequently, alternative test techniques have been proposed to investigate the dynamic response of sandwich panels under blast loads including shock tubes, water-hammers, and foam impact (Zhu et al. 2008, Yuen et al. 2010). Small explosive charge effects were simulated using gas gun (Hanssen et al. 2002), whereas aluminum foam impact was used by (Radford et al. 2006).

1.6 Blast loading computation

Computation of the blast loads is of specific interest to structural engineers dealing with blast resistant design. Extensive charts for predicting blast pressures and blast durations are found in UFC 3-340-02 (2008), which were based on wide experimental data and related equations.

1.6.1 Blast scaling law

Normalized description for the effects of blast can be given $(E/P_o)^{1/3}$, where E is the energy released (kJ) and P_o is the ambient pressure. For practice, the explosive charge weight (W) is expressed as equivalent mass of TNT, which results the Hokinson scaling law (Baker et al. 1983) that is given as a function of the dimensional distance parameter (scaled distance) $Z = R/W^{1/3}$, where R is the actual stand-off-distance from the explosive center. This approach shows that for different explosions that have equal scaled distance Z, will have the same blast wave characteristics.

1.6.2 Blast wave characteristic equations

Blast wave characteristics are defined in term of different parameters such as incident pressure, reflected pressure, pressure period and impulse. The values of these parameters for a particular charge weight and stand-of-distance are presented in diagrams and tables (UFC 3-340-

02 2008). Modified Friedlander equation is well known to describe pressure-time curve (Biggs 1964, Smith 1994) as

$$P(t) = P_o + P_{max}\left(1 - \frac{t}{t_d}\right)^{\frac{-bt}{t_d}} \tag{2}$$

where P_o and P_{max} are the ambient pressure and maximum pressure respectively, t is the time after the pressure arrival, t_d is the time of wave arrival. Kinney and Graham (1985) presented an equation for the maximum overpressure in terms of scaled distance for as

$$\frac{P_{max}}{P_o} = \frac{808\left[1+\left(\frac{Z}{4.5}\right)^2\right]}{\sqrt{1+\left(\frac{Z}{0.048}\right)^2}\sqrt{1+\left(\frac{Z}{0.32}\right)^2}\sqrt{1+\left(\frac{Z}{1.35}\right)^2}} \tag{3}$$

The impulse is a key characteristic of blast wave, as it correlates the effect of pressure and time, and computed as the area under the pressure-time curve. The equation proposed by Kinney and Graham (1985) for the impulse in terms of scaled distance and the weight of the explosives as

$$I = \frac{0.067\sqrt{1+\left(\frac{Z}{0.23}\right)^4}}{Z^2\sqrt[3]{1+\left(\frac{Z}{1.55}\right)^3}} * 100 * \sqrt[3]{W} \tag{4}$$

where impulse *(I)* is calculated in (Pa.s), Z in (m/kg$^{1/3}$), and W in (kg).

1.7 Response analysis of structures under blast loads

The dynamic response analysis of a structure subjected to blast loads can be carried out using different methods such as analytical, numerical and experimental. Each method has its characteristics and limitations in terms of accuracy to represent the actual problem. Brief discussion on each method will be presented next.

1.7.1 Analytical methods to predict dynamic structural response

The selection of appropriate analysis technique depends on the characteristics of loading and the anticipated mechanism of failure of the structural component. Flexural behavior is usually determined using single degree of freedom *SDOF* methods (Cole 1948, Smith 1994). For more complex behavior of components, multi-degree-of-freedom could be used (e.g. to predict shear failure). The latter analytical methods might require the use of explicit time-step numerical integration algorithms, ranging from constant velocity to linear acceleration techniques associated with relations that represent elastic and inelastic behavior of the structure. The concept of pressure-impulse (*P-I*) diagrams combine the different performance characteristics of a type of structural or nonstructural element under a required range of explosive loading.

1.7.1.1 Single-degree-of-freedom (SDOF)

A spring-mass SDOF system is widely used to predict the dynamic response of a structure subjected to broad different types of dynamic loading (Clough 1995, Chopra 2007), SDOF simulation of the real structure using its equivalent mass, damping and resistance function, provides the fundamental response mode which governs the overall component failure mode (Smith 1994).

The response of a *SDOF* under blast loading is extensively described in Biggs (1964), based on Rayleigh-Ritz approach for which representative shape functions for the flexural mode are assumed. Blast loading usually has a very short loading period relative to natural period of the structure, which results in impulsive response regime, and eliminating the damping effect which led to relationship between impulse (*I*) and ultimate resistance (R_m) (Biggs 1964) as

$$R_m = I\omega/(2\mu - 1)^{0.5} \qquad (5)$$

where (ω) is the natural frequency of structure and (μ) is the allowable ductility.

The equation of motion for such model is simplified in Biggs (1964) as

$$K_{lm}M\ddot{y} + Ky = P(t) \qquad (6)$$

where K_{lm} is load-mass factor, *M* is the structure mass, *k* is stiffness , and *P(t)* is loading function. The equation of motion involves the load-mass factor (K_{lm}), which has convenient values depending on the boundary conditions, strain range and case of loading. Values for (K_{lm}) are tabulated for beam, one-way slabs and two way slabs in (Biggs 1964).

1.7.1.2 Multi-degree-of-freedom (MDOF)

Multi-degree-of –freedom models (*MDOF*) are used for more accurate representing of spatial response of more complex structures, where it facilitate better distribution of dynamic loads and dynamic reactions by secondary element analyses, without having to generate an equivalent dynamic load. In addition, different failure modes can be represented. Sufficient short time-step should be considered to ensure accurate response and numerical stability.

1.7.1.3 Pressure-Impulse curves

Biggs (1964) introduced pressure-impulse diagram based on the *SDOF* concept. Pressure-impulse (P-I) curves combine the different performance characteristics of a type of structural or nonstructural components under a range of explosive loading which is similar to the response spectrum diagram of a *SDOF* system under seismic loading (Krauthammer 2008). As the name indicate, the diagrams are expressed in terms of the pressure and impulse combination that will result in a specific response (e.g. damage) level for a specific component(s) (Dusenberry 2010).

Fig. 1.4 shows a typical *P-I* diagram, in which three regimes (region) can be identified \ (Smith 1994). The response is specified to be within the impulsive regime (region I) if the ratio between loading time to natural period of the structure is relatively small, while it will be within the static regime (region III) if this ratio is relatively large, and finally, in between, the structure response is expected to be dynamic (region II) (Baker et al. 1983). All combinations of pressure and impulse that lie below or to the left of a *P-I* curve corresponds to a no-damage behavior, while all combinations of peak pressure and impulse that lie above or to the right to the *P-I* curve corresponds to expected damage.

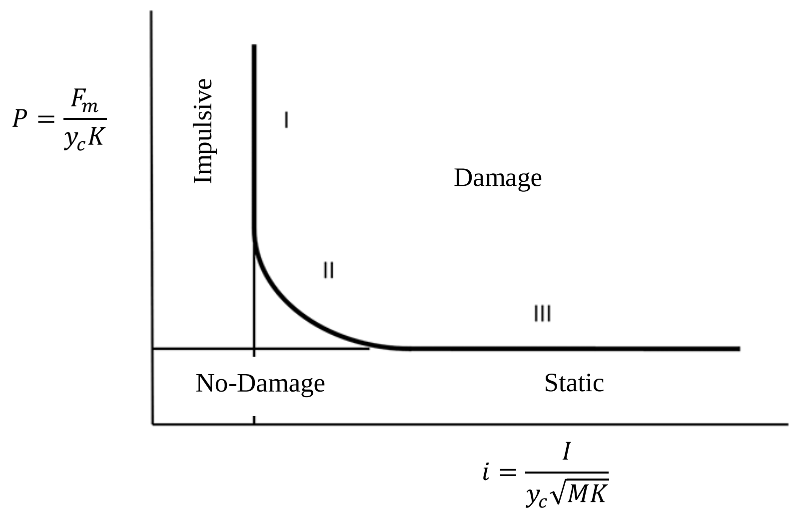

Fig. 1.4 Pressure-impulse diagram for elastic *SDOF* (Smith 1994).

1.7.2 Finite element analysis for structural response under blast loading

Finite element analysis (*FEA*) is a powerful method to carry out complex dynamic analysis as an effective alternate to experimental testing. FEA can account for nonlinearities associated with material, geometry, and loading. The response of an impulsively loaded structure could be computed using commercial software programs such as ANSYS-AUTODYN, LS-DYNA, and ABAQUS. Complicated structure systems and environmental effects could be interacted using FEA, where spatial deformations and internal stresses can be determined, which allows investigating the progress of structure failure and standing on the critical parameters. Typically, structures subjected to blast loads are forced beyond the elastic behavior, where forming plastic hinges and failure starts to take place.

1.7.3 Experimental assessment of structural response under blast loads

The experimental testing using live explosive is the most realistic and confident method to evaluate the dynamic behavior of a structure under blast loads. The experimental results are usually used to verify the precision of the analytical or numerical method to predict the dynamic response of a structure under blast loads. Nevertheless, the variability and uncertainties associated with blast phenomena and corresponding structure response may require repeating the test multiple times, in order to compute the average values, standard deviations, and the coefficient of variations corresponding to the parameters of interest. Researchers may not always be able to perform blast experimental testing due to its high expenses, logistics, and security regulations.

1.8 Reference

American Socity of Civil Engineers (ASCE) (2012). "Blast Protection of Buildings." ASCE/SEI 59-11, Reston, Virginia.

Baker, W.E., Cox, P.A., Westine, P.S., Kulesz, J.J., and Strehlow, R.A. (1983). “Explosion Hazard and Evaluation.” Oxford, New York, USA: Elservier Scientific Publishing Company.

Biggs, J. M. (1964). "Introduction to Structural Dynamics." New York, USA: McGraw-Hill Inc.

Canadian Standards Assiocation (CSA) (2012). "Design and Assessment of Buildings Subjected to Blast Loads." CSA S850-12. Mississauga, Ontario, Canada.

Chopra, A.K. (2007). “Dynamics of Structures.” Pearson Edition Inc., New-Jersey, USA, Third Edition.

Clough R. W., and Penzien, J., (1995) "Dynamics of Structures.", Computers & Structures Inc., University Ave.Berkeley, CA 94704USA.

COLE, R.H. (1948). "Underwater Explosions" Princeton University Press, Princeton, New Jersey.

Dusenberry, D.O. (2010). “Handbook for Blast Resistant Design of Buildings.” New-Jersey, USA: Wiley & Sons Inc., First Edition.

General Services Administration (GSA), (2003). "GSA Progressive Collapse Analysis and Design Guidelines for New Federal Office Buildings and Major Expansion Projects.", prepared by Applied Research Associates for GSA, Washington, D.C., 2003.

Hanssen, A.G., Enstock, L., and Langseth, M. (2002). "Close-range Blast Loading of Aluminium Foam Panels." International Journal of Impact Engineering 27: 593-618.

Khalifa, Y. A., El-Dakhakhni, W. W., and Tait, M. J., (2015), “Performance of Lightweight Sacrificial Cladding under Confined Blast Loads”. ASCE Journal of Structural Engineering, submitted for publication in July 2015.

Kinney, G.F. and Graham, K.J., “Explosive Shocks in Air”, Springer, 2nd Ed., Berlin, 1985.

Kowsarinia, E., Alizadeh, Y., Salavati, H. S. P. (2012). "Experimental Evaluation of Blast Wave Parameters in Underwater Explosion of Hexogen Charges." International Journal of Engineering, Transactions B: applications Vol. 25(1).

Krauthammer, T. (2008). “Modern Protective Structures.” New-York, USA: CRC Press, Taylor & Francis Group.

Radford, D.D., McShane G.J., Deshpande, V.S., and Fleck, N.A. (2006). "The Response of Clamped Sandwich Plates with Metallic Foam Cores to Simulated Blast Loading." International Journal of Solids and Structures 43(7-8): 2243-2259.

US Army Corps of Engineers, Naval Facilities Engineering Command, and Air Forces Civil Engineer Support Agency (2008), "Structures to Resist the Effect of Accidental Explosions." Unified Facilities Criteria, UFC 3-340-02.

Yuen, S.C.K., Nurick, G.N., Theobald, M.D., and Langdon, G.S. (2010). "Sandwich Panels Subjected to Blast Loading." Dynamic Failure of Materials and Structures: 297-325.

Zhu, F., Zhao, L., Lu, G., and Wang, Z. (2008). "Deformation and Failure of Blast-Loaded Metallic Sandwich Panels: Experimental Investigations." International Journal of Impact Engineering 35(8): 937-951.

Chapter 2: Sandwich Systems Performance under Blast Loads: Review

2.1 Abstract

Over the last two decades, the blast resistance of sandwich structures has received intensified interest as a result of its high stiffness to weight ratio and its ability to absorb energy relative to solid plates having the same mass. Sandwich panels have been efficiently employed as sacrificial cladding or sandwich structures under air/underwater blast loads. In this paper a comprehensive overview on the state-of-the art for the dynamic response of sandwich panels under blast loads is presented. This includes findings obtained using different methodologies (i.e. analytical, numerical and experimental) to investigation the behavior of sandwich panels. In this paper sandwich panels are categorized according to the material(s) used for fabrication: metallic, hybrid-metallic and composite sandwich panels. This paper also identifies areas in which limited research has been conducted and suggests potential future research areas.

Keywords: Blast loads, Confined blast, Finite element modeling, Fluid structure interaction, Numerical analysis, Open-air-blast, Sandwich panels, Sandwich Systems, Underwater blast.

2.2 Introduction

Recently, due to increased terrorist attacks on both civilian and military buildings, investigating the blast resistance of various structure and non-structure components has received interest from both engineering societies and government agencies. Design standards have been developed to resist the blast loads such as ASCE (2012) and CSA (2012). Sandwich panels are distinguished by their superior high stiffness/weight ratio and ability to absorb energy through their central core rather, which has encouraged their use in blast and impact applications.

2.3 Sandwich System Definition

A sandwich panel is a structure consisting of two face sheets joined in between by a lower density core material or structure. The separation of the face sheets by a lightweight core results in significant improvement in the stiffness of the section with only a small increase in the weight. Fig. 2.1 shows the influence of face sheet separation, for the case of a honeycomb type core, on elastic stiffness, flexural strength and weight of a sandwich panel (SANDCORE 2005).

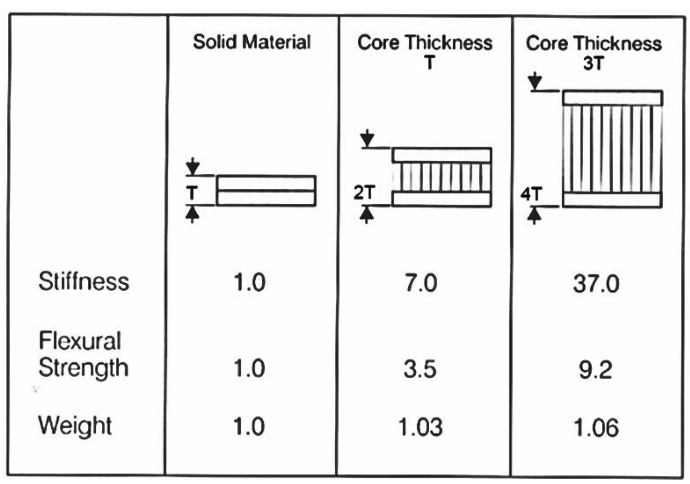

Fig.2.1 Influence of the facing separation with honeycomb core on elastic stiffness, flexural strength and weight of sandwich panel (SANDCORE 2005).

For blast applications, sandwich panels are often classified into two types. The first type is sacrificial cladding, which is fixed in front of main structure in order to absorb energy through the front face and the core. The second type is structural elements, which are used as main structural components. Its performance is primarily defined by the deformation of the back face.

Sandwich structures can also be classified according to the core as cellular, micro-architectural and macro-architectural (Yuen et al. 2010). In the present work, the sandwich panels are classified according to the material(s) used for fabrication: metallic, hybrid-metallic and composite sandwich structures. Based on this classification, an overview on the state-of-the art for the dynamic performance of the sandwich panels under blast loads is presented.

2.4 Metallic Sandwich Panels

Metallic sandwich panels are composed of metal face sheets and a core, which is usually steel or aluminum. In the early 1980’s the U.S. Navy fabricated sandwich panels using laser welding, initiated the first strength related investigations, which led to the first application as antenna platform for the U.S. Navy ships (Kujala 2005). Wiernicki et al. (1991) presented both elastic and plastic design equations for lightweight metallic corrugated core sandwich panels subjected to air blast loading. Between the 1990’s and 2000’s many European researchers and research projects were carried out to investigate the behavior and applications of steel sandwich panels, particularly in transportation applications (SANDWICH 2000, SANDCORE 2005). This led to the production of different core configurations (Gopichand 2012), as shown in Fig. 2.2.

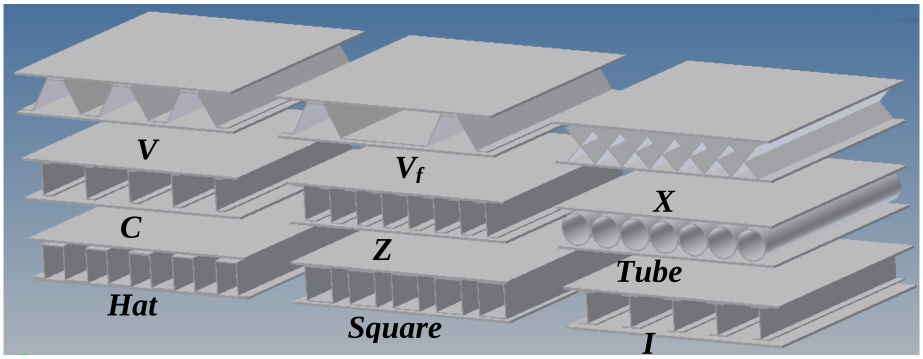

Types of core configurations

V, V_f, X

C, Z, Tube

Hat, Square, I

Fig.2.2 Different types of steel core configurations (redrawn from Gopichand 2012).

During the last several decades, sandwich panel performance under blast loading has been the focus of numerous studies. For example, Xue and Hutchinson (2003) used finite element modeling *FEM* to compare between the behavior of tetragonal truss core sandwich panels and solid plates with same material and mass. A uniformly distributed blast impulse and elastic-perfectly plastic material were assumed in the study. In addition, strain-rate and fracture of the material was neglected, although its importance had been showed in other studies. However, the sandwich panels were found to absorb twice the energy absorbed from solid plates.

Fleck and Deshpande (2004) proposed a simplified procedure, consisting of three stages, to analyze the dynamic response of one dimensional clamped sandwich beams. First, the fluid structure interaction *FSI* during blast inducing uniform velocity of front face. Second, the core compression where the front face and the core had the same velocity. Finally, the plastic bending and stretching of the back face sheet. Various topologies of core were also considered in the analysis and their response was compared to that of solid plates having equal mass. Performance charts were introduced to achieve optimal geometry resulting in the maximum blast resistance for a given mass of sandwich beam. It was found that a diamond-cell core provides the best blast resistance performance for both water and air blast.

Radford et al. (2006) used a metal foam projectile and *FEM* to compare between circular sandwich plates and solid plates having same masses. The sandwich plates comprised of AISI stainless steel face sheets and an aluminum alloy metal foam core. Pyramidal, square honeycomb, corrugated cores configurations and solid plates were considered. High-speed photography was used to record the transverse deflection. Experimental findings showed that the shock resistance of sandwich panels increased as the core thickness. Furthermore, sandwich panels constructed with the pyramidal core exhibited the highest mid-span deflections. Finally, the study highlighted the sensitivity of strain rate to the resistance of both solid and sandwich plates. The experimental results were found to be good with FEM results. The sandwich beams were found to exhibit lower displacements than solid beams with equivalent weight under nearby explosions. In addition, the square honeycomb core prevented crushing when subjected to lower impulses.

Tilbrook et al. (2007) investigated the dynamic crushing of stainless steel corrugated and Y-frame core sandwich panels under different impact values. The dynamic response of the cores was described using two mechanisms: (i) inertial stabilization of the webs against buckling and (ii) plastic wave effects. The peak stresses on the front and back faces were found to be approximately equal for impact velocities less than 30 ms^{-1} for the Y-frame core configurations and 60 ms^{-1} for the corrugated core configurations. For higher impact, the front face sheet stresses increased, while they remained relatively constant on the back face sheet.

Theobald and Nurick (2007) carried out numerical simulations in order to investigate the dynamic response of sacrificial cladding sandwich panel subjected to uniform blast loads. The panels consisted of mild steel face sheets and an annealed mild steel or 6063-T6 aluminum alloy tube core. Either five or nine tubes were used to fabricate the core, which is a parameter that affects the dynamic response. The buckling modes of the core tubes were observed to be irregular for small blast impulse, while they were symmetrical for the high blast impulse. The crush distance of the core was found to increase with an increase in the impulse, while decrease with the increase of number of tubes. In addition, steel tubes showed lower crushing distance than aluminum tubes under an equal mass of charge. *FEM* was used to determine the energy absorption by the core and face sheets, the results were found in good agreement with that of the experimental tests. The energy absorption was found to be improved by fewer tubes, thinner face sheets and uniformity of loading.

Børvik et al. (2008) proposed and tested a cost effective and lightweight protection concept for 20ft standard ISO container to be used as shelter in international operations. Extruded AA6005-T6 aluminum panels were proposed and filled with granular material to increase its blast resistance. Later, Børvik et al. (2009) investigated numerical modeling, using a Lagrangian model, to predict the dynamic response of a structure under blast loads. The proposed model was found to be in good agreement with results from ConWep (Hyde 1990) in describing the reflected pressure-time history. A comparison of experimental and numerical results was carried out and the difference in the deformation was found to be approximately 25%, which was due to the build-up of inner pressure in the non-vented container.

Zhu et al. (2008) presented a series of results obtained from ballistic testing and pendulum tests as well as finite element modeling (*FEM)*. The primary goal of this study was to investigate the response of metallic sandwich panels subjected to blast loads. The panels comprised of aluminum alloy face sheets and a honeycomb core. Different effective parameters were considered, including the thickness of honeycomb core foil, cell size, face sheet thickness and charge size. The experimental results were found to be in good agreement with those obtained from *FEM* for the sandwich panels investigated. Moreover, panels with relatively thicker face sheets and denser cores experience localized deformations in the front face sheet when subjected to larger charge sizes, while those with thinner face sheets, sparse core tended to deform globally when subjected to smaller charge sizes. An analytical study was subsequently performed by Zhu et al. (2009), which divided the deformation of sandwich panels into the following three phases: front sheets deformation, core crushing and overall bending and stretching of the panel structure. Later, an optimization study, aimed at minimizing the peak permanent deformation in square sandwich panels with a particular mass under different levels of impulse, was performed. The influences of: (i) ratio of the two side lengths, (ii) relative density of core, and (iii) core thickness were investigated. It was found that there exists an optimum core density and core depth that minimize the sandwich deflection.

Nurick et al. (2009) and Karagiozova et al. (2009) presented both experimental and numerical results from a research program focusing on the behavior of sandwich panels composed of aluminum alloy honeycomb core under the effect of localized and uniform blast loading. The response of the sandwich panel was compared with that of both mild steel plates and air-core sandwich panels. The failure modes were described in terms of crushing, tearing and deformation of sandwich panel components. The results showed that for uniform blast loading having an impulse greater than 20 Ns the resistance of the honeycomb sandwich panels exceeded that of the steel plates, while for an impulse less than 20 Ns the honeycomb sandwich panels experienced higher back face deformations than that of the air-core sandwich panels. The sandwich panels were found to have higher resistance and better performance under uniform blast loading compared to that obtained under localized blast loading. The load transferred to the back face sheet using a particular core material was found to depend on intensity of the load, thickness of the core and flexibility of the sandwich panel. It was concluded that a compromise between energy absorption of the core and load transfer to back face sheet must be made when designing sandwich panels.

Theobald et al. (2010) conducted a series of air-blast tests on sandwich panels consisting of steel face sheets with un-bonded aluminum foam (Alporas, Cymat) or hexagonal honeycomb cores. Two face sheet thickness values were considered in the study for each core material investigated. Findings from the results showed that face sheet thickness has an influence on the behavior of the panels, where the Alporas and honeycomb cores were found to have higher relative blast resistance when a thicker face sheet was used. Furthermore, thicker core honeycomb panels were found to have the highest resistance relative to other core materials, while Cymat core panels did not show any significant increase in behavior over that of solid plates.

McShane et al. (2010) used a water tube apparatus to assess the fluid structure interaction (*FSI)* effect on the response of free standing sandwich plates subjected to under water blast loads. Square honeycomb and corrugated cores stainless steel sandwich panels were examined. The total momentum and core compaction were determined as a function of core strength, front face mass and blast time constant, where *FSI* was analyzed using *FEM*. The results showed the importance of core topology and its influence on both the compressive strength and the crushing of the core, while it had minor effect on total momentum imparted to the sandwich panel.

Dharmasena et al. (2010) investigated five core configurations of rigidly supported stainless steel circular sandwich panels subjected to underwater impulsive loading using the experimental setup shown in Fig. 2.3. The specimens had diameter of 203 mm and core thickness of 90 mm. The core configurations were square-honeycomb, triangular honeycomb, multi-layer pyramidal truss, triangular corrugation and diamond corrugation. All specimens had a relative core density of approximately 5%. For the quasi-static compressive response, the honeycomb core configurations showed the highest initial peak strength followed by a significant softening behavior. The truss and corrugated core configurations were found to have a lower strength but exhibited a hardening behavior beyond yielding. For the case of dynamic impulse, the final transmitted momentum increased slowly with core strength. Crushable cores reduced the transmitted impulse by approximately 25% than that transmitted through rigid cores in a fully back supported sandwich structures.

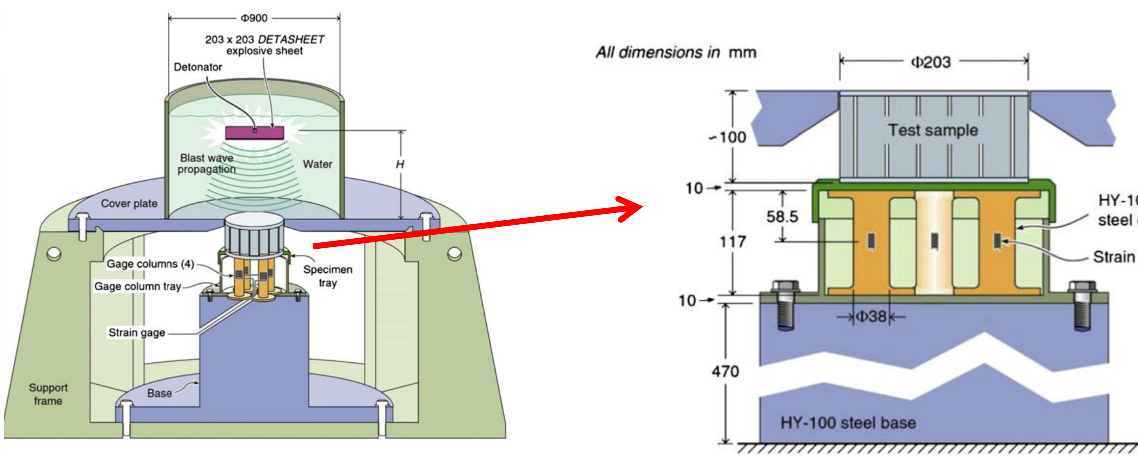

Fig.2.3 Sketch of the Dyno-crusher apparatus. The inset shows a detailed view of the specimen and four strain gauged columns used to measure the blast loads transmitted through by the sandwich panel (Dharmasena et al. 2010).

Shen et al. (2010) used ballistic pendulum testing to examine the response curved sandwich panels under blast loading. The sandwich panels were composed of two aluminum face sheets and an aluminum foam core. Two values of radii of curvature were considered to describe the influence of curvature on the response of sandwich panels. Several parameters were considered, such as core thickness, front face sheet thickness, radius of curvature and the magnitude of impulse. The curvature was found to have three major effects on the response. First, it reduced the pressure acting on the front face of sandwich panel by changing the reflective angle of the reflected blast wave. Second, wrinkling of the back face sheet (defined as a failure mode) was observed, which did not occur in the flat sandwich panels. Finally, a mixed deformation was defined between the bending and stretching deformation regimes along the circumferential direction, which did not exist in flat sandwich panels. Zhu et al. (2009) argued that the optimal thickness distribution for sandwich panels in order to resist blast loads is to have same equal face sheet thickness values for both the front and back faces. Nevertheless, Shen et al. (2010) presented, through a theoretical discussion that this is not the case for curved sandwich panels, as swapping the back and front faces had a minor influence on final deflection.

Rimoli et al. (2011) investigated the dynamic response of edge-clamped 6061-T6 aluminum corrugated core sandwich panels. Experimental tests and *FEM* were used to analyze the response of the panels under the impact of explosively driven wet sand. Detonation of spherical explosive charges encased by a concentric shell of wet sand placed at different standoff distances was used to apply the impact loading. The sandwich panels exhibited lower permanent deformation with a reduction of 15-20 % relative to that of solid plates of the same material and having the same mass. The response of the sandwich panels was found to vary with redistribution of mass among the core webs and face sheets. Finally, a configuration was identified that achieved a reduction in permanent deformation of 30 % relative to an equivalent solid plate.

Wang et al. (2011) carried out a numerical study on the dynamic response of asymmetric face sheet aluminum alloy sandwich panels. The effect of five different thickness ratios (ξ) of the front to back face sheets was considered on the peak deflection and energy absorption of the sandwich panels. It was shown that energy absorbed by the sandwich panel increased by decreasing (ξ), while changing (ξ) had a minor effect on the peak deflection. The analysis illustrated the effect of (ξ) on deformation mechanism of the sandwich panels, where the buckling of the back face sheet was higher for larger (ξ), while localized deformation (denting) of the front face sheet was observed for lower (ξ) values. The results were consistent with the results presented by Main and Gazonas (2008), who investigated the effect of mass distribution between facing sheets and the honeycomb core of sandwich panels. A one-dimensional system to quantify the energy absorption capacity under uniaxial crushing was used. The model was based on the well-established rigid perfectly plastic idealization for the cellular core. The same idealization was previously used to successfully model metal honeycombs and foam cores by Hanssen (2002).

Zhang et al. (2011) carried out analytical and numerical analyses to assess the role of foam filling on the blast resistance of sandwich panels. Stainless steel sandwich panels with trapezoidal cores were considered. The performance of the unfilled and metal foam filled sandwich panels was compared. It was found that the blast resistance of the filled sandwich panels was higher than that of the unfilled panels, where the foam was found to increase the inertial stabilization of the core webs while suppressing local buckling.

Cui et al. (2012) tested the dynamic response of metallic tetrahedral lattice core sandwich panels using a four cable ballistic pendulum, followed by analytical analysis (Cui et al. 2012) based on a three stage framework, previously presented by Fleck and Deshpande (2004). Identical face sheets with tetrahedral lattice core sandwich panels were tested and compared with hexagonal honeycomb core panels having the same core density. The tetrahedral lattice sandwich structures were manufactured using perforated metal sheet forming and welding technology. The peak permanent transverse deflection of the back face sheet was used to identify the impulsive resistance of the sandwich panels. Local deformations were observed in addition to global transverse deflections. Also, non-uniform compression was observed in the second stage of the tetrahedral lattice core damage, due to the inconsistent deformation of the front and back face sheets. Findings from this research work implied the superior performance of tetrahedral lattice sandwich panels over honeycomb core sandwich panels. This was consistent with the findings presented by Dharmasena et al. (2011), who investigated the response of metallic pyramidal lattice subjected to high intensity of impulsive loading in air through a series of experimental tests and *FEM*.

The response of metal sandwich panels subjected to multiple impulse shocks was investigated by Ebrahimi and Vaziri (2013). Sandwich panels with honeycomb and folded plate core were subjected to a maximum of three consecutive shocks. The face sheet deformations and core crushing strain at mid-span were used to define the performance of the sandwich panels. It was found that minimum face sheet deflection occurred in the square honeycomb core sandwich panels with a relative core density of 4-5 %. Failure diagrams were constructed to reveal the fracture and failure mechanisms for sandwich panels.

Liu et al. (2013) conducted a comparative study on the blast attenuation ability of sandwich panels with aluminum foam and mild steel plates. Different densities of closed-cell aluminum foam cores were manufactured using a molten body transitional foaming process. A reduction in the peak transmitted load of up to 61.5–64.7 % in sandwich panels, compared to that of mild steel plates was observed. Additional energy was dissipated by the formation and growth of cracks. The lower density of the core also induces a higher ratio of peak load incident to the peak load transmitted by the sandwich panel.

2.5 Hybrid-Metallic Sandwich Panels

Hybrid-metallic sandwich panels use a combination of metal and non-metal material, either for the face sheets or the core. Often cellular materials are used for the core in this type of sandwich structure, such as polymer foams or wood. Hybrid-metallic sandwich panels have several positive characteristics, such as highly fire resistant, high heat and sound isolation capabilities, ability of absorb significant energy.

Karagiozova et al. (2009) compared the response of sandwich panels with steel face sheets and a polystyrene core to their counterpart with an aluminum honeycomb core under blast loading. Blast loads were applied by the detonation of plastic explosive discs at near stand-off-distance. Further numerical analysis was carried out, which considered additional parameters, such as density, strength and thickness of the core on the response of the sandwich panels. Core thickness was found to affect the level of stress transmission to back face sheet. Moreover, the aluminum honeycomb core panels were found to absorb more energy relative to the polystyrene core panels.

Langdon et al. (2010) experimentally investigated the response of honeycomb cores sandwich panels with aluminum and glass-fiber epoxy composite face sheets under blast loads. The effect of core thicknesses on the response of the sandwich panels was considered by using two different core thickness values of 13mm and 25mm. Increasing the core thickness reduced the level of permanent deformation and panels with composite faces exhibited lower residual deflections than those with aluminum face sheets. Various failure modes were identified, such as core crushing, core shearing, de-bonding of the face sheet from the core, cracking of the composite face sheets, and tearing. Fig. 2.4 shows the first thickness response at 180mm stand-off distance and impulse of 4.7 Ns, where dishing and partial shear deformations observed. Localized impulse was found to reduce the global resistance of the panel, as damage was concentrated in the center area of the panel.

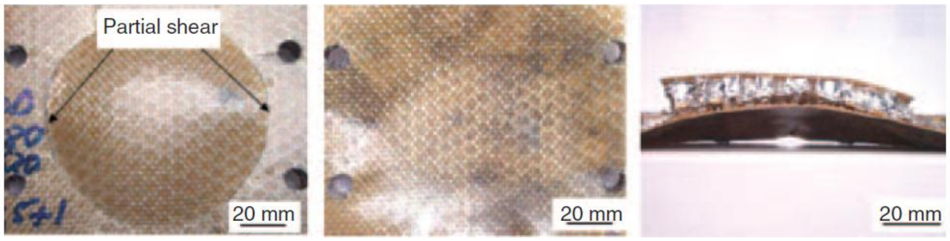

(a) (b) (c)

Fig.2.4 The 13mm thick core sandwich panel with composite face sheets, impulse = 4.7 Ns , (a) back face deformation, (b) front face view, and (c) cross-section (Langdon et al. 2010).

Hassan et al. (2012) investigated the density of *PVC* foam core effect on the response of aluminum alloy face sheets sandwich panels under blast loading. Mechanical properties of the foam have been characterized by compression, bending and shear static tests. Experimental ballistic pendulum tests and finite element analysis were used for the investigation. It was concluded that more than 50% of total energy is absorbed by the core.

Borbón and Ambrosini (2013) conducted an experimental investigation on the dynamic response of aluminum square sheets and inner epoxy resin Carbon Nanotubes (*CNT*) sandwich plates under blast loading. The epoxy resin matrix with 5% in weight of *CNT* core were compared with plates having neat epoxy resin core. Different charges of plastic explosive were used to show the change in response of the sandwich plates under both uniform and localized blast loading. The results showed that permanent deformation is larger in the plates with a *CNT* core under both localized and uniform blast loading. However, it showed better energy dissipation than neat epoxy specimens.

Sousa-Martins et al. (2013) used a four cable ballistic pendulum to evaluate the response of aluminum alloy face sheets and a cork core sandwich panel under blast loads. Cork is a natural material with a cellular structure, which could be efficiently used for energy absorption, and it has a microstructure that can be seen by scanning electron microscopy (*SEM*) images. Two micro-agglomerated cork (*MAC*) cores with different thicknesses were considered as inner filling between 5754-H2 aluminum alloy face sheets. Detonation of 30g of high explosive (*C4*) charge at constant stand-off distance 300 mm was used. The impulse transmitted to the back face sheet reduced by increasing the core thickness. The lower density core specimens exhibited higher deflection values than higher density core specimens. Deformation was mainly due to bending, while stretching effect was negligible.

2.6 Composite Sandwich Panels

Composite sandwich panels are defined here as panels with both face sheets and the core formed from composite material. Composite material is a combination of fiber reinforcement and resin. Usually fiber reinforced polymer (*FRP*), carbon fiber reinforced polymer (*CFRP*) and glass reinforced polymer (*GRP*) are used in blast related investigations. With the increasing use of composite materials in many applications, numerous studies have focused on the dynamic behavior of composite panels under blast loading.

Jiang et al. (2007) developed a composite design for blast protection, which can efficiently protect army vehicles and occupants. This work integrated three major technologies; a landmine-soil composite interaction model; an advanced design methodology, called Function-Oriented Material Design (*FOMD*); and novel patent composite material concept, called Biomimetic Tendon-Reinforced (*BTR*). Fig. 2.5 illustrates the configuration of the proposed *BTR* material.

The *BTR* composite was analyzed numerically under blast loading to predict and design the composite structure for a wide range of blast scenarios. It was found that *BTR* composite can protect structures and has the ability to undergo large deformations without severe damage. The foam composite matrix layer exhibited energy absorption and reduced the transmitted force to the main structure.

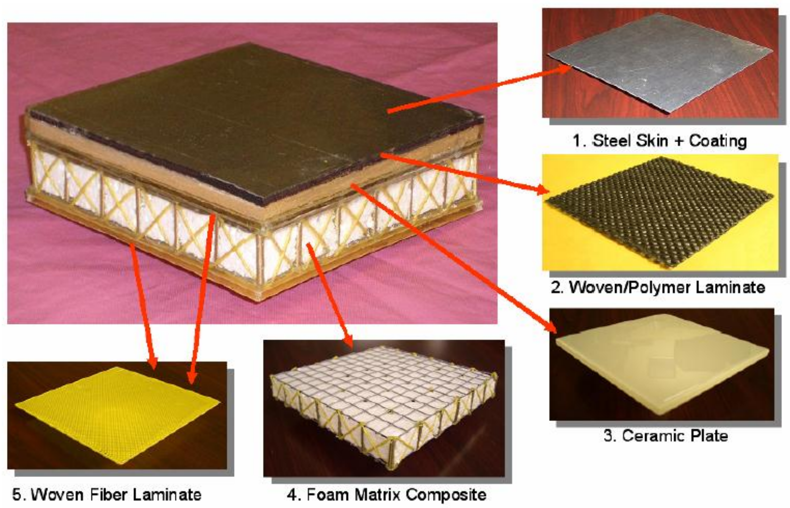

Fig.2.5 Example configuration of the proposed *BTR* material (Jiang et al. 2007).

Bahei-El-Dien and Dvorak (2008) proposed three modified designs to enhance the blast resistance of composite sandwich panels. The panels consist of composite laminate face sheets and a structural foam core. Ductile interlayers are placed between the core and face sheets to absorb incident energy and reduce the crushing of the foam core. *FEM* was employed to analyze the sandwich panels with the elastomeric foam and polyurethane interlayers under the effect of blast loading. The results showed that the maximum kinetic energy and compression of the core were reduced by more than 50 %, and the maximum deflection was reduced by 15 %.

Andrews and Moussa (2009) developed failure mode maps for sandwich panels with E-glass composite face sheets and a PVC foam or balsa wood core subjected to air blast loading. The failure mode maps were based on a single degree of freedom (*SDOF*) model, which was used to determine maximum deformation of panel. Good agreement was found between the analytical to experimental results.

Wang et al. (2009) investigated the response of stepwise graded core sandwich panels with E-glass vinyl ester (*EVE*) face sheets. The experimental tests are conducted using a shock tube. Two configurations of graded density styrene foam were proposed. The first was composed of low/middle/ higher core, while the second composed of middle/low/high foam core. It was found that the first configuration performed better due to the efficient integration between core layers in transmitting the imparted load on the front face to the back-face of the sandwich panels, nonetheless the computed absorbed energy for the second configuration was higher.

Icardi and Ferreo (2009) performed an optimization study to minimize the inter laminar stresses of face sheet layers of sandwich panels under blast loading. Single, double and triple composite core layers with different fiber orientation were considered. An Euler-Lagrange model was used to predict the response of the panels under a blast load and to identify an optimal reinforcement fiber orientation was identified. In addition, stress concentrations were observed to occur at the interface between face sheets and the core. The stresses the developed in the dual core sandwich panels were found to be lower than the stressed that developed in the single core counterparts.

Kazemahvazi and Zenkert (2009) developed an analytical model for the compressive and shear response of solid and hierarchical corrugated composite cores. Bending, shear and stretching deformation contributions were considered in the stiffness model. The analytical results were compared to *FEM* and to experimental results. Five different failure mechanisms were used to characterize the core strength as follows: face fracture, core shear failure, general buckling, local buckling/wrinkling, and shear buckling. It was found that initial imperfections affect the deformation shape of a core member, and strength of the structure. Initial imperfections typically reduced the core strength by 20% compared to perfectly straight core panel.

Tekalur et al. (2009) proposed a novel type of sandwich material called Transonite, which is fabricated using 3D woven E-glass fiber stitched to a Trymer foam core, as shown in Fig. 2.6. A shock tube was used to investigate the effect of core stitching density on the response of panels and the transient response and imparted damage were recorded using a high-speed camera. A numerical study was subsequently performed using 3D MOSAIC dynamic analysis code. The numerical results were in excellent agreement with experimental results for the case of high stitching, however, significant discrepancies were observed for the case of unstitched sandwich panels. It was found that the damage type differs for unstitched and stitched sandwiches, and this difference increased with increased stitching density.

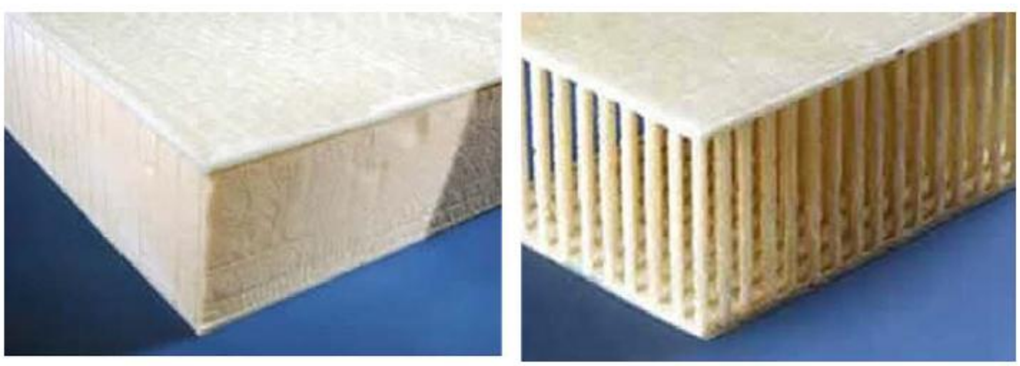

(a) **(b)**

Fig.2.6 Transonite composite sandwich (a) filled core and (b) removed foam.

Yahya et al. (2011) carried out experimental tests using a ballistic pendulum to investigate the dynamic response of carbon fiber reinforced epoxy (*CFRE*) panels. Different fracture mechanisms were defined such as localized delamination, buckling of front face surface fiber, fiber fracture of back face sheet and shear failure along the edges of the panels. Results showed that the impulse required for initiating fracture of back face sheet surface fiber increased by increasing the laminate thickness.

Langdon et al. (2012) conducted preliminary tests to investigate the response of 25 mm thick *PVC* foam core and E-glass fiber reinforced vinyl ester face sheet sandwich panels subjected to localized blast loading. In addition, two different nominal core densities of 200 and 80 kg/m^3 were investigated. Numerical analyses were also carried out to assess the behavior of the sandwich panels and composite only panels (Langdon et al. 2013). Detonation of a plastic explosive disc at a stand-off distance of 50 mm from the panel was used to apply the localized blast loading. Various failure modes were described, including core compression, fragmentation, complete penetration, de-bonding between core and face sheets and delamination between fiber layers. Fig. 2.7 shows the various failure modes of the H200 sandwich panels subjected to different impulse amplitudes. Findings highlighted the superior performance of composite only panels. Furthermore, the higher core density was found to reduce damage and increase the energy absorbed via the core deformation. Minor residual displacements were observed due to elastic nature of the composite panels. The back face sheet experienced permanent deformation and de-bonding from the core at higher impulses.

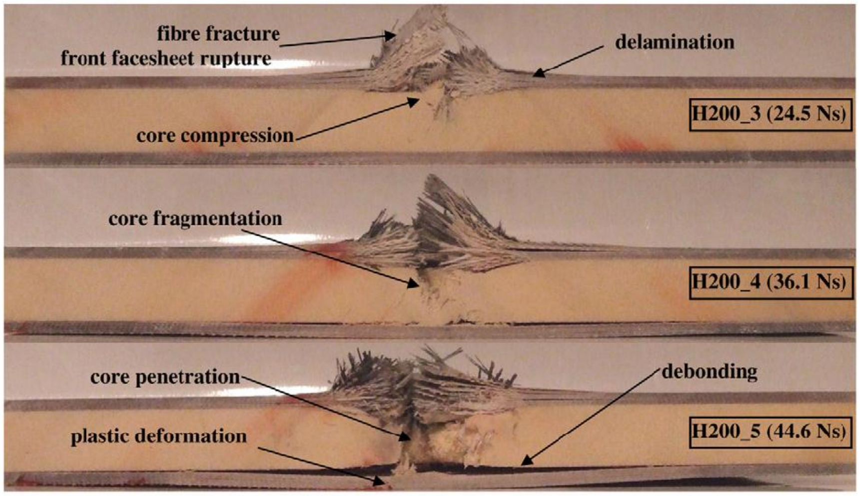

Fig. 2.7 Failure observations for selected H200 sandwich panels under different impulse amplitudes (Langdon et al. 2013).

Schimizze et al. (2013) studied the blast mitigating properties of sandwich structures fabricated from a vinyl-nitrile foam shell filled with different materials such as water, glycerin, glass beads, Aerogel, tuff volcanic rock and expanding foam. The authors compared those structures to both U.S. helmet pad and uniform vinyl nitrile foam. A shock tube was used to apply blast loads on the sandwich panel samples. Results showed the primary importance of density and impedance of materials to mitigate the air shock waves. Lower densities are preferable for helmet padding, such as the U.S. helmet padding and Der-Tex foam. Most of the considered materials were found to attenuate the peak blast pressure.

LeBlanc and Shukla (2011) used experimental testing and numerical analysis to study the response of E-glass vinyl-ester resin curved composite panels under the effect of underwater blast loading. A water filled conical shock tube was used to apply the blast load while a 3D Digital Image Correlation (*DIC*) system was used to measure the transient response of the panel.

The measured velocity and displacement at the center and midway points of the panel were compared to numerically computed values and were found to be in excellent agreement.

Yang et al. (2011) investigated the dynamic response of four different circular sandwich panels subjected to global and local blast loading. The effect of additional sacrificial core interlayers, in order to protect the main core, was studied using *FEM*. *GFRP* face sheets and balsa-wood core was the main structure of the sandwich panel, where an elastomeric layer of polyurea and a compressible Divinycell-H200 foam layer were selected as additional core interlayers. The results showed a reduction in shear failure of the core as a result of adding interlayers and a smoother stress distribution on the sandwich sections.

Panahi et al. (2011) numerically studied the response of submerged cylindrical sandwich panels subjected to underwater shock loading. Fiber reinforced laminates face sheets, with different fiber orientation, and a form core foam core were used to construct the cylinder sandwich panels. Three different types of the Divinycell foam (H100, H160 and H250) were used individually as a core for the sandwich panels. The results showed that core type had major effect on the peak circumferential stress, where maximum circumferential stress exhibited on the outer layer of H100 core panel. It was observed that the magnitude of the circumferential stress was higher in the outer face than the inner face.

Jackson and Shukla (2011) conducted experimental tests to examine the effects of two different types of impact on the blast resistance of sandwich composites. Sequential impact and air blast loading were considered, where impact was applied either by a high velocity projectile or a low velocity drop weight, followed by a secondary blast loading using a shock tube on the same specimens to evaluate the effects of impact damage on the response of the sandwich. Pressure data were measured and high speed images were recorded during the experimental tests. The post-impact observations showed perforation during the high velocity impacts, while the low velocity impact induced confined damage to the impact face and the core. Higher energy absorption was revealed by the sandwich panels during the high velocity impact compared to a lower velocity impact. Finally, the blast resistance of the specimens subjected to high velocity impacts was better than those subjected to low velocity impacts.

Arora et al. (2011) conducted full scale experimental tests to investigate the dynamic performance of glass-fiber reinforced polymer (*GFRP*) sandwich panels and laminate tubes subjected to air blast. A second study considered the response of the sandwich panels under underwater blast loads (2012). *GFRP* sandwich panels with a length of 1.6 m and a width 1.3 m were subjected to the detonation of a 30 kg charge of *C4* explosive in air at stand-off distances 8 and 14 m, while in underwater blast loading 1.0 kg charge was used at stand-off distance 1.0 and1.4 m. High-speed cameras with *DIC* were used to capture the structure performance during the blasts. Nearly 10 times higher pressure was transmitted to the sandwich panels during underwater blast than those in air blast tests. Different failure mechanisms were identified, such as core crushing, skin/core cracking, delamination and fiber breakage. Detailed deformation maps were developed, and observed failure modes during the air blast tests was initiated in the front sheet and shear cracking in the core, while the back face sustained without visible damage. However the results of underwater blasts showed considerable core crushing (up to 50%) and fiber breakage on both face sheet surfaces.

Fatt and Surabhi (2012) used stress wave analysis on a foam core composite sandwich cylindrical shell. The face sheets were made of orthotropic elastic material, while the core was made of elastic-plastic foam materials. Five densities of foam were considered, Divinycell PVC

H30, H100, H200, HCP100 and Klegecell R300. The response of the cylinderical composite sandwich panel was found to be affected by the magnitude and duration of the pressure pulse, and the failure mode was identified as rapture of the outer facing sheet. The energy absorption was found to increase with an increase of the pressure amplitude and the decrease with load duration. The blast resistance was found to be more efficient for lower resistance foam cores, where plastic work dissipation occurs in the core before cylinder failure. Stress wave analysis was found to be an efficient method for composite sandwich analysis, which has been used in number of another studies (Fatt and Palla 2009, Fatt and Sirivolu 2010).

Shukla et al. (2012) conducted experimental tests using a shock tube apparatus to evaluate the blast mitigation of composite sandwich panels with a polyurea layer and graded foam cores (Corecell series A300, A500 and A800). Two configurations were proposed. The first configuration consisted of a polyurea layer that was placed between the core and front face sheet. In the second configuration it was placed between the core and back face sheet. 3D Digital Image Correlation (*DIC*) system was used to record the deformation time history. The results showed that the second configuration exhibited lower energy transfer to the back face compared to the first one, as the maximum values for deflection, strain and velocity of back face sheet were reduced by 35%, 35% and 15%, respectively.

Wang and Shukla (2011) investigated the dynamic behavior of composite sandwich panels subjected to pre-compression and transverse blast loading, using an integrated shock tube facility and a *DIC* system. The sandwich panels consisted of E-glass Vinyl Ester face sheets and a foam core. Three different values of in-plane compression were considered 0, 15, and 25 kN, and the peak incident pressure was 1 MPa for the blast loading. It was found that in-plane compression reduced the blast resistance of the sandwich panels due to local buckling in the front face sheet.

Increasing the in-plane compressive load increased the damage level, deformation, and strain in the sandwich face sheets.

Gupta and Shukla (2012) studied the influence of temperature on the performance of composite sandwich panels using shock tube and digital image correlation (*DIC*) system. The sandwich panels comprised of E-glass Vinyl Ester and a Corcell M100 foam core. Three specimens were tested at three temperatures – low temperature (-40° C), room temperature (22° C) and high temperature (80°C). The blast resistant performance was greatest for room temperature, while in case of high temperature, a fiber breakage and fiber-matrix delamination occurred in the face sheets and maximum core compression failure. In case of low temperature, core cracking and face/core delamination occurred. Finally, the sandwich panels at room and high temperature demonstrated higher shear strain under blast loading than the panels at low temperature.

Kim and Shin (2013) presented a numerical study on the response of a rubber coated plate and a sandwich structure with square and honeycomb cells subjected to underwater explosion. The two structures were proposed to protect the ships from an underwater blast attack. The rubber response exhibited blast mitigation in the elastic regime, while it had a minor effect in the plastic regime. The results highlighted the major effect of number of cells on the response of the sandwich panels, while the core thickness had a secondary effect. The optimum configuration of a sandwich structure was identified through two equations based on the parametric study, where the stress of the plate reduced by nearly 50 %.

The influence of the number of cells was also investigated by Rejab and Cantwell (2013), who carried out a series of experimental tests and numerical analysis for aluminum alloy. Glass fiber reinforced plastic (*GFRP*) and a carbon fiber reinforced plastic (*CFRP*) triangular corrugated core sandwich panels were considered. A hot press molding technique was used to fabricate 45 profiled corrugated cores. It was found that buckling of the cell walls initiated the failure for these corrugated systems, and localized de-bonding between the face sheets and core was observed. The numerical model predictions were in good agreement with the experimental results, while the simple analytical model over-estimated the load bearing capability of the corrugated panels due to the perfect bonding assumption in the model.

Tadepalli and Mantena (2013) developed pressure versus impulse (P-I) curves for composite sandwich panels with a variety of skin and core material combinations. The P-I diagrams were based on experimental data for E-glass and carbon face skin sandwich composite panels with balsa, polyvinyl chloride foam and Tycor cores. The numerical models were used to obtain the strength versus deformation properties of the considered undamaged sandwich composite panels. Good agreement achieved between the model predictions and experimental results for the various composite sandwich panels considered.

2.7 Future work

Sandwich panels have shown their superior ability to resist blast loads. The design could be adapted to efficiently employ the sandwich panels as sacrificial panels or sandwich structures. Energy absorption presented by the front face and the core, accompanied with reducing the transmitted forces to the back face (and to main structure) is a main feature of the sandwich structures in blast applications. The structural geometry preference such as arch, triangle and truss could be employed in different scales (molecular scale up to the main structure scale) in the sandwich panels. Few studies had been performed on the hybrid-metallic sandwich panels under blast loads. Studying the improvement of the bonding between a metallic face sheets and nonmetallic core is still an area of a great challenge. Fragility analysis and optimization techniques remain a challenge for all types of sandwich panels under air/underwater blast loads. Relatively high-cost and complex joining techniques remain a disadvantage for sandwich system. Consequently, there is need for proposing more simple efficient joining techniques with cost-effective materials. It is noticed the lack of published research focusing on the behavior of sandwich panels under confined blast loads, which still need significant efforts of research.

2.8 Conclusion

Sandwich panels can be efficiently used as sacrificial cladding or sandwich structures under air/underwater blast loads. Many studies have shown the preference of sandwich panels to solid plates for blast resistance. There is advantage in using numerical and analytical analysis as it reduces the danger and responsibilities associated with experimental testing, however the experimental testing is still required for validation purposes. The sandwich panels were classified in the presented according to its fabrication material, where three types were identified; Metallic, Hybrid-Metallic and Composite sandwich panels. The presence of manufacture technologies such as selective laser melting and laser cutting allowed the fabrication of complex topologies sandwich panels required for special needs of researchers. There is lack of research focusing on behavior of sandwich panels subjected to confined blast loads. The fracture mechanics modeling of the sandwich panels under blast loads still unwell defined. Furthermore, probabilistic analysis and optimization techniques remain a challenge for all types of sandwich panels under air/underwater blast loads.

2.9 Reference

American Socity of Civil Engineers (ASCE) (2012). "Blast Protection of Buildings." ASCE/SEI 59-11, Reston, Virginia.

Andrews, E. W. and Moussa, N. A. (2009). "Failure Mode Maps for Composite Sandwich Panels Subjected to Air Blast Loading." International Journal of Impact Engineering 36(3): 418-425.

Arora, H., Hooper, P.A., and Dear, J.P. (2011). "Dynamic Response of Full-Scale Sandwich Composite Structures Subject to Air-Blast Loading." Composites Part A: Applied Science and Manufacturing 42(11): 1651-1662.

Arora, H., Hooper, P.A., and Dear, J.P. (2012). "The Effects of Air and Underwater Blast on Composite Sandwich Panels and Tubular Laminate Structures." Experimental Mechanics 52(1): 59-81.

Bahei-El-Din, Y. A. and Dvorak, G. J. (2008). "Enhancement of Blast Resistance of Sandwich Plates." Composites Part B: Engineering 39(1): 120-127.

Biggs, J. M. (1964). "Introduction to Structural Dynamics." New York, USA: McGraw-Hill Inc.

Borbón, F. and Ambrosini, D. (2013). "Dynamic Response of Composites Sandwich Plates with Carbon Nanotubes Subjected to Blast Loading." Composites Part B: Engineering 45(1): 466-473.

Børvik, T., Burbach, A., Langberg, H., and Langseth, M. (2008). "On The Ballistic and Blast Load Response of a 20ft ISO Container Protected with Aluminium Panels Filled with a Local Mass - Phase II: Validation of protective system." Engineering Structures 30(6): 1621-1631.

Børvik, T., Hanssen, A.G., Langseth, M., Olovsson, L. (2009). "Response of Structures to Planar Blast Loads: A Finite Element Engineering Approach." Computers & Structures 87(9-10): 507-520.

Canadian Standards Assiocation (CSA) (2012). "Design and Assessment of Buildings Subjected to Blast Loads." CSA S850-12. Mississauga, Ontario, Canada.

Chen, W. and Hao, H. (2012). "Numerical Study of a New Multi-Arch Double-Layered Blast-Resistance Door Panel." International Journal of Impact Engineering 43: 16-28.

Cui, X., Zhaob, L., Wang, Z., Zhao, H., and Fang, D. (2012). "A Lattice Deformation Based Model of Metallic Lattice Sandwich Plates Subjected to Impulsive Loading." International Journal of Solids and Structures 49(19-20): 2854-2862.

Cui, X., Zhaob, L., Wang, Z., Zhao, H., and Fang, D. (2012). "Dynamic Response of Metallic Lattice Sandwich Structures to Impulsive Loading." International Journal of Impact Engineering 43: 1-5.

Dharmasena,K.P., Queheillalt, D.T., Wadley, H.N, Dudt, P., Chen, Y., Knight, D., Evans, A.G., and Deshpande, V.S. (2010). "Dynamic Compression of Metallic Sandwich Structures During Planar Impulsive Loading in Water." European Journal of Mechanics - A/Solids 29(1): 56-67.

Dharmasena, K.P., Wadley, H.N, Williams, K., Xue, Z., and Hutchinson, J.W. (2011). "Response of Metallic Pyramidal Lattice Core Sandwich Panels to High Intensity Impulsive Loading in Air." International Journal of Impact Engineering 38(5): 275-289.

Ebrahimi, H. and A. Vaziri (2013). "Metallic Sandwich Panels Subjected to Multiple Intense Shocks." International Journal of Solids and Structures 50(7-8): 1164-1176.

Fatt, M. S. and Palla, H. (2009). "Analytical Modeling of Composite Sandwich Panels under Blast Loads." Journal of Sandwich Structures and Materials 11(4): 357-380.

Fatt, M. S. and Sirivolu, D., (2010). "A Wave Propagation Model for The High Velocity Impact Response of a Composite Sandwich Panel." International Journal of Impact Engineering 37(2): 117-130.

Fatt, M. S. and Surabhi, H. (2012). "Blast Resistance and Energy Absorption of Foam-Core Cylindrical Sandwich Shells Under External Blast." Composite Structures 94(11): 3174-3185.

Fleck, N. A. and Deshpande, V. S. (2004). "The Resistance of Clamped Sandwich Beams to Shock Loading." Journal of Applied Mechanics 71(3): 386.

Gopichand, A., Krishnaiah, Dr.G., Krishna, M. B., Reddy D., and Sharma A.V. (2012). "Design and Analysis of Corrugated Steel Sandwich Structures Using Ansys Workbench." International Journal of Engineering Research & Technology 1(8).

Gupta, S. and Shukla, A. (2012). "Blast Performance of Marine Foam Core Sandwich Composites at Extreme Temperatures." Experimental Mechanics 52(9): 1521-1534.

Hanssen, A.G.,Enstock, L., and Langseth, M. (2002). "Close-Range Blast Loading of Aluminium Foam Panels." International Journal of Impact Engineering 27: 593-618.

Hassan, M.Z., Guana, Z.W., Cantwell, W.J., Langdon, G.S., Nurick, G.N. (2012). "The Influence of Core Density on The Blast Resistance of Foam-Based Sandwich Structures." International Journal of Impact Engineering 50: 9-16.

Hyde, D.W. (1990). "Conventional Weapons Effect (ConWep)"Application of TM5-855-1. U.S. Army Engineer Waterways Experiment Station, Vicksburg, USA.

Icardi, U. and Ferrero, L. (2009). "Optimization of Sandwich Panels to Blast Pulse Loading." Journal of Sandwich Structures and Materials 12(5): 521-550.

Jackson, M. and Shukla, A. (2011). "Performance of Sandwich Composites Subjected to Ssequential Impact and Air Blast Loading." Composites Part B: Engineering 42(2): 155-166.

Jiang, D., Liu, Y., Qi, C., Ma, Z. D., Raju, B., and Bryzik, W. (2007). "Innovative Composite Structure Design for Blast Protection."

Karagiozova, D., Nurick, G.N., and Langdon, G.S. (2009). "Behaviour of Sandwich Panels Subject to Intense Air Blasts – Part 2: Numerical Simulation." Composite Structures 91(4): 442-450.

Karagiozova, D., Nurick, G.N., and Langdon, G.S., Yuen, S.C.K., Chi, Y., and Bartle S. (2009). "Response of Flexible Sandwich-Type Panels to Blast Loading." Composites Science and Technology 69(6): 754-763.

Kazemahvazi, S. and Zenkert, D. (2009). "Corrugated All-Composite Sandwich Structures. Part 1: Modeling." Composites Science and Technology 69(7-8): 913-919.

Kim, C. H. and Shin, Y. S. (2013). "Numerical Simulation of Surface Shield Effects to Waterblast Wave." Ocean Engineering 60: 99-114.

Kujala, P. A. (2005). "Steel Sandwich Panels in Marine Applications." Brodogradnja, Vol.56 No.4.

Langdon, G. S., Nurick, G. N., Yahya, A, M. Y., and Cantwell, W. J. (2010). "The Response of Honeycomb Core Sandwich Panels, with Aluminum and Composite Face Sheets, to Blast Loading." Journal of Sandwich Structures and Materials 12(6): 733-754.

Langdon, G. S., Von Klemperer, C.J., Rowland, B.K., and Nurick, G.N.(2012). "The Response of Sandwich Structures with Composite Face Sheets and Polymer Foam Cores to Air-Blast Loading: Preliminary experiments." Engineering Structures 36: 104-112.

Langdon, G. S., Karagiozova, D., von Klemperer, C. J., Nurick, G.N., Ozinsky, A., Pickering, E.G. (2013). "The Air-Blast Response of Sandwich Panels with Composite Face Sheets and Polymer Foam Cores: Experiments and Predictions." International Journal of Impact Engineering 54: 64-82.

LeBlanc, J. and A. Shukla (2011). "Dynamic Response of Curved Composite Panels to Underwater Explosive Loading: Experimental and Computational Comparisons." Composite Structures 93(11): 3072-3081.

Liu, H., Cao , Z.K., Yao, G.C., Luo, H.J., and Zu, G.Y. (2013). "Performance of Aluminum Foam–Steel Panel Sandwich Composites Subjected to Blast Loading." Materials & Design 47: 483-488.

Main, J. A. and G. A. Gazonas (2008). "Uniaxial Crushing of Sandwich Plates Under Air Blast: Influence of Mass Distribution." International Journal of Solids and Structures 45(7-8): 2297-2321.

McShane, G.J., Deshpande, V.S., and Fleck, N.A. (2010). "Underwater Blast Response of Free-Standing Sandwich Plates with Metallic Lattice Cores." International Journal of Impact Engineering 37(11): 1138-1149.

Norris, C., Montague, P., Tan, KH. (1989). "All Steel Structural Panels to Carry Lateral Load: Experimental and Theoretical Behaviour." The Structural Enginee 67(9).

Nurick, G.N., Langdon, G.S., Chi, Y., and Jacob, N. (2009). "Behaviour of Sandwich Panels Subjected to Intense Air Blast – Part 1: Experiments." Composite Structures 91(4): 433-441.

Panahi, B., Ghavanloo, E., and Daneshmand, F. (2011). "Transient Response of a Submerged Cylindrical Foam Core Sandwich Panel Subjected to Shock Loading." Materials & Design 32(5): 2611-2620.

Radford, D.D., McShane G.J.,Deshpande, V.S., and Fleck, N.A. (2006). "The Response of Clamped Sandwich Plates with Metallic Foam Cores to Simulated Blast Loading." International Journal of Solids and Structures 43(7-8): 2243-2259.

Rathbuna, H.J., Radford, D.D., Xue, Z., He, M.Y., Yang, J., Deshpande, V., Fleck, N.A., Hutchinson, J.W., Zok, F.W., and Evans, A.G. (2006). "Performance of Metallic Honeycomb-Core Sandwich Beams Under Shock Loading." International Journal of Solids and Structures 43(6): 1746-1763.

Rejab, M. R. and Cantwell, W. J. (2013). "The Mechanical Behaviour of Corrugated-Core Sandwich Panels." Composites Part B: Engineering 47: 267-277.

Rimoli, J.J., Talamini, B., Wetzel, J.J., Dharmasena, K.P., Radovitzky, R., Wadley, H.N.G. (2011). "Wet-Sand Impulse Loading of Metallic Plates and Corrugated Core Sandwich Panels." International Journal of Impact Engineering 38(10): 837-848.

SANDCORE (2005). " Best Practice Guide for Sandwich Structures in Marine Applications " SAND.CORe, NewRail University of Newcastle upon Tyne.

SANDWICH (2000). "Advancd Composite Sandwich Steel Structures." The European Commission Under 5th Framework Programme Growth KA III.

Schimizze, B., Son, S.F., Goel, R., Vechart, A.P., and Young, L. (2013). "An Experimental and Numerical Study of Blast Induced Shock Wave Mitigation in Sandwich Structures." Applied Acoustics 74(1): 1-9.

Shen, J., Lub, G., Wang, Z., and Zhao, L. (2010). "Experiments on Curved Sandwich Panels Under Blast Loading." International Journal of Impact Engineering 37(9): 960-970.

Sousa-Martins, J., Kakogiannis, J., Coghe, F., Reymen, B., and Teixeira-Dias, F. (2013). "Behaviour of Sandwich Structures with Cork Compound Cores Subjected to Blast Waves." Engineering Structures 46: 140-146.

Tadepalli, T. P. and P. R. Mantena (2013). "Numerical and Experimental Blast Response Characterization of Sandwich Composite Structural Panels." Journal of Sandwich Structures and Materials 15(1): 110-133.

Tekalura, S.A., Bogdanovich, A.E., and Shukla, A. (2009). "Shock Loading Response of Sandwich Panels with 3-D Woven E-glass Composite Skins and Stitched Foam Core." Composites Science and Technology 69(6): 736-753.

Theobald, M. D., and Nurick, G. N. (2007). "Numerical Investigation of The Response of Sandwich-Type Panels Using Thin-Walled Tubes Subject to Blast Loads." International Journal of Impact Engineering 34(1): 134-156.

Theobald, M.D., Langdon, G.S., Nurick, G.N., Pillay, S., Heyns, A., and Merrett, R.P. (2010). "Large Inelastic Response of Unbonded Metallic Foam and Honeycomb Core Sandwich Panels to Blast Loading." Composite Structures 92(10): 2465-2475.

Tilbrook, M.T., Radford, D.D., Deshpande, V.S., and Fleck, N.A. (2007). "Dynamic Crushing of Sandwich Panels with Prismatic Lattice Cores." International Journal of Solids and Structures 44(18-19): 6101-6123.

Wang, E. and Shukla, A. (2011). "Blast Performance of Sandwich Composites with In-Plane Compressive Loading." Experimental Mechanics 52(1): 49-58.

Wang, E., Gardner, N., and Shukla, A. (2009). "The Blast Resistance of Sandwich Composites with Stepwise Graded Cores." International Journal of Solids and Structures 46(18-19): 3492-3502.

Wang, T.J., Ma, M., Yu, W., Dong, S., and Gao, Y. (2011). "Mechanical Response of Square Honeycomb Sandwich Plate with Asymmetric Face Sheet Subjected to Blast Loading." Procedia Engineering 23: 457-463.

Wiernicki, C. J., Liem, F., Woods, G., and Fuorio, A. (1991). "Structural Analysis Methods for Lightweight Metallic Corrugated Core Sandwich Panels Subjected to Blast Loads." Naval Engineers journal 31(3): 192-202.

Xue, Z., and Hutchinson, J. W. (2003). "A comparative studyof impulse-resistant metal sandwich plates." International Journal of Impact Engineering.

Yahya, M.Y., Cantwell, W.J., Langdon, G.S., and Nurick, G. N. (2011). "The blast resistance of a woven carbon fiber-reinforced epoxy composite." Journal of Composite Materials 45(7): 789-801.

Yang, Y., Fallah, A.S., Saunders, M., and Louca, L.A. (2011). "On The Dynamic Response of Sandwich Panels with Different Core Set-ps subject to Global and Local Blast Loads." Engineering Structures 33(10): 2781-2793.

Yuen, S.C.K., Nurick, G.N., Theobald, M.D., and Langdon, G.S. (2010). "Sandwich Panels Subjected to Blast Loading." Dynamic Failure of Materials and Structures: 297-325.

Zhang, J. H., Qin, H.Q., and Wang, T.J. (2011). "Resistance of Metallic Foam-Filled Trapezoidal Plate Core Sandwich Plate to Blast Loading." Materials Research Innovations 15(1): 162-165.

Zhu, F., Wang, Z., Lu, G., and Zhao, L. (2009). "Analytical Investigation and Optimal Design of Sandwich Panels Subjected to Shock Loading." Materials & Design 30(1): 91-100.

Zhu, F., Zhao, L., Lu, G., and Gad, E. (2009). "A Numerical Simulation of The Blast Impact of Square Metallic Sandwich Panels." International Journal of Impact Engineering 36(5): 687-699.

Zhu, F., Zhao, L., Lu, G., and Wang, Z. (2008). "Deformation and Failure of Blast-Loaded Metallic Sandwich Panels: Experimental Investigations." International Journal of Impact Engineering 35(8): 937-951.

CHAPTER 3: BEHAVIOR OF LIGHTWEIGHT METALLIC SANDWICH PANELS UNDER OUT-OF-PLANE LOADING

3.1 ABSTRACT

Sandwich panel systems offer many advantages over typical conventional systems, which facilitate their use in several applications, including aerospace, naval and transportation. The complexity and relatively high cost of sandwich panel system design and fabrication have limited its application in civil engineering applications. In accordance with American (ASCE/SEI 59-11) and Canadian (CSA/ S850-12) standards for blast resistant design of buildings, the dynamic behavior of a system can be predicted using its static resistance function obtained under equivalent uniform loading. The goal of this study is to quantify the quasi-static resistant function of novel cost effective lightweight cold–formed steel sandwich panels to be used in the context of blast resistant structures. An analytical model is introduced to predict the elastic characteristics of the proposed sandwich configurations and to assess the critical failure modes. In addition, an experimental program was performed involving eighteen sandwich panels under uniform quasi-static loading. Different configurations were investigated, including longitudinal and transverse corrugated core sandwich panels, using different deck profiles. The modes of failure experienced by the test panels were assessed and discussed and were found to be consistent with the predicted analytical failure modes. The quasi-static resistance functions for the proposed sandwich panel configurations were characterized in terms of yield loads and ultimate capacities and the corresponding displacement values. Analytically predicted values were compared to the experimental findings and found to be in a good agreement. The influence of sandwich panel core configuration and core sheet thickness on the behavior of the sandwich panels was examined, considering energy absorption and ductility. The results of the current study will serve the future development of cost–effective sandwich panels, to be used as sacrificial cladding for the blast protection of structures.

KEYWORDS: Cold-formed steel; Energy absorption; Lightweight structure; Resistance function; Sandwich panel; Uniform loading.

3.2 INTRODUCTION

Structural sandwich systems can be constructed by separating two relatively thin face sheets made of stiff and strong material by a lower stiffness core. This separation increases the distance between the center of gravity of the face sheets and the neutral axis of the section. This results in an increase in the second moment of area of the sandwich section, which is defined as the sandwich effect. Due to the significant increase in stiffness with only a minor increase in weight, sandwich panel systems are used extensively in aerospace, marine and transportation applications. For example, sandwich panels were used in the construction of antenna platforms on U.S. Navy battleships (Kujala 2005).

The core configuration of a sandwich panel affects its behavior. As such, a large number of researchers have investigated various core configurations, including the prismatic core, honeycomb core, and truss core (Valdevit et al. 2004, Valdevit et al. 2006).

The American ASCE/SEI 59-11 (ASCE 2011) and Canadian CSA/ S850-12 (CSA 2012) codes for blast resistant design of buildings present a dynamic analysis model to evaluate structural component response under blast loading. This dynamic model employs a static resistance function, which was first presented in (Biggs 1964)**.** This type of resistance function is utilized as blast design may allow the structural component to experience non-elastic deformations according to the damage level defined in the design standard.

Typically, Euler-Bernoulli and Timoshenko beam theories, and homogenization hypotheses are considered adequate to describe the elastic structural behavior of sandwich panels (Norris 1989, Romanoff et al. 2007), however, these theories are not valid in the nonlinear response regime. For simplicity, a simply supported sandwich panel can be treated as a beam. The application of a uniformly distributed load on the panel will result in the development of compression and tensile normal stresses in the front face and the back face of the panel, respectively; while the core acts as the shear force-transmitting element in the sandwich system (Allen 1969). In some cases, in order to obtain an accurate description of the resistance function of a structural component beyond the elastic response range experimental testing maybe required.

The objective of this study is to quantify and compare the resistance functions of different cost effective lightweight sandwich panels, which can be used later as sacrificial cladding for blast applications. Sacrificial cladding is typically employed to act as physical barrier between a vulnerable structure element and an explosive charge. Off-the-shelf (readily available) galvanized cold-formed steel corrugated sheets in North America are used in the study to form the core of the proposed sandwich panels. This type of corrugated sheeting is commonly used in building floor/deck and roof systems. Different corrugation profiles, such as *B* and *V* deck profiles, were used in the preliminary design stage of the sandwich panel systems. The study focuses on six different panel types, representing different three core configurations, as shown in Fig. 3.1. All sandwich panels comprised of a single layer corrugated core with a core depth of 38 mm (1.5 in).

3.3 EXPERIMENTAL PROGRAM

Novel sandwich panels that have different core configurations is an example where accurately determining the resistance function beyond the elastic response range would be challenging to do without experimental testing. As a result, an experimental setup had been designed and used to obtain the load-displacement relationships and the static capacities for the proposed sandwich panels under a uniformly distributed load applied and simply supported boundary conditions.

3.3.1. Test Setup & Instrumentation

Quasi-static experimental testing of the sandwich panel specimens was performed using the test setup shown in Fig. 3.2. Each tested panel specimen was simply supported by a pin and a roller at the upper and lower sides of the sandwich panel, respectively. Four load cells were fixed on the test frame to measure the reaction forces at either end of the sandwich panel specimen (see Fig. 3.2).

The face sheet of the sandwich panel facing the load is defined as the front face, while the rear side face is defined as the back face, as shown in Fig 3.2. A uniform distributed load was applied to the front face of the sandwich panel using an airbag with an overall length of 935 mm. The applied pressure rate was regulated using a pressure control valve, while the pressure in the airbag was monitored using a pressure gauge. The airbag was located between the sandwich panel specimen and a stiff self-reacting wall (see Fig. 3.2)

A total of four linear displacement potentiometers were used to measure the deflection of the back face of the test specimen. Fig. 3.2 shows the supporting dimensions of the panels that were tested and the spacing of the potentiometers along the back face of the sandwich panel. Two potentiometers were used to measure the mid-span displacement and two potentiometers were used to measure the displacement at the quarter span of each sandwich panel specimen.

3.3.2. Test matrix and Specimen fabrication

In order to design inexpensive cold-formed steel sandwich panels to be used as sacrificial cladding in blast applications, available off-the-shelf galvanized cold-formed steel profiles of deck sheets in North America, such as *B* and *V* deck profiles were used for the core for the sandwich panels (see Fig. 3.3). A total of eighteen sandwich panels were tested, representing three different core configurations, *V-S*, *B-S* and *V-ST*, respectively and two different core sheet thicknesses. The test matrix was determined in order to study the effect of both the core sheet thickness and the core configuration on the behavior of the sandwich panels. All the tested sandwich panels had approximately the same weight, and had the same dimensions of 305 mm (1 ft) width, 914 mm (3 ft) length and 38 mm (1.5 in) core depth. The nomenclature used to identify the test specimens and the corrugated sheet profile parameters are shown in Fig. 3.3a and Fig. 3.3b, respectively. The parameter ($\bar{B}$) represents the total width of the corrugated core, which had an approximate value of 301 mm, while (d) represent the depth of the corrugated sheet and (θ) is the angle of corrugation. The corresponding values of these parameters defining the different profiles used in the test matrix are presented in Table 3.1. As a preliminary estimate, in order to achieve an efficient sandwich section the face sheet thickness should be selected to be approximately twice the core sheet thickness (SANDCORE 2005, Valdevit et al. 2006). The thickness of the corrugated sheet profiles used in the test matrix varied between 0.9 mm to 1.2 mm (G20, 0.036 in to G18, 0.048 in), while a constant value for the face sheet thickness of 2.0 mm (G14, 0.08 in) was considered.

Metal Inert Gas (MIG) welding was utilized, where both plug and fillet welds were used to join the sandwich panel layers according to the selected configuration. The welds were designed to ensure that failure of the tested sandwich panel occurred in the face sheets or the core before weld failure during the testing. The plug welds were designed to have a diameter of 12.5 mm (0.5 in), while the fillet welds had an arc equal to the core sheet thickness and length of 51 mm (2.0 in).

3.3.3. Test procedure

The test procedure employed in the testing program, started with the placement of the sandwich panel specimen in a vertical position and centered along the mid-span of both the pin and roller supports. The specimen was held in place using four clamps, which were connected to the rigid supporting plates. Next, four displacement potentiometers were attached to the back face of the sandwich panel specimen. Finally, the self-reacting back wall was then attached to the test frame and full contact between the air bag and the front face sheet of the sandwich panel was achieved.

A uniform loading pressure was transmitted to the specimen by adding air to the air bag at a low rate. The rate of the pressure was controlled using a digital pressure control valve; the average rate of loading had approximate value of 0.34 kPa/s (0.05 psi/s). The loading pressure was increased until failure of the specimen occurred.

3.3.4. Material

The tested metallic sandwich panels are constructed using cold-formed steel sheets, where the mechanical properties of the sheets materials were needed to perform a primary analysis using a simplified analytical model, and for further analysis of the experimental results. The stress-strain characteristics of all used different sheets were derived from uniaxial tensile tests following the regulations of (ASTM E8/E8M-13a) standard, where five coupons were tested from each sheet type. The corresponding average yield stress and modulus of elasticity values are presented in Table 3.2.

3.4 TEST RESULTS

The tested sandwich panels were carefully examined after each test and the failure modes were identified for each sandwich panel core configuration. In addition, the load-displacement relationship was determined for each tested sandwich panel. The failure mode for each of tested core configurations is presented in detail as follows:

3.4.1. B-S-core

Fig. 3.4 shows the observed and anticipated buckling and web crippling failure modes for *B-S*-core type sandwich panels. The failure of the *B-S*-core sandwich panels was initiated by minor web crippling within the supports zone, followed by flexural induced yielding and subsequent buckling, which is considered the dominant failure mode for this core configuration. A plastic hinge was observed to form near the mid-span, the reason for the shift in the plastic hinge formation location away from the mid-span was postulated to be due to the existence of shear force effects in combination with flexural effects, and imperfections introduced during construction of the sandwich panels. The approximate value of this shift was 84 mm, which was found to occur in either the upper or the lower direction of the sandwich panel. As shown in Fig. 3.4 (a) and (b), reduction of web resistance gradually occurred due to crippling accompanied by a minor rotation at the corner joints of the core corrugation at the back face side of the sandwich panel.

3.4.2. V-S-core

As shown in Fig. 3.5, the governing failure mode for the *V-S*-core sandwich panel specimens was buckling of the front face, similar to that of *B-S*-core type specimens. The location of buckling was found to occur near the mid-span for all tested specimens of this configuration, except for specimen *V-S-G18-3*, which experienced a shift of 83 mm above the mid-span location as shown in Fig. 3.5 (c). The bearing forces resulted in web crippling, which was observed to occur prior to flexural induced buckling failure. The occurred web crippling pattern was found to be in a good agreement with the anticipated web crippling, as seen in Fig. 3.5 (a) and (b).

3.4.3. V-ST-core

V-ST-core sandwich panel specimens exhibited a truss action type behavior, where the webs of the corrugated core represented the diagonal members of a truss, while the front face and the back face of the sandwich panel acted as compression and tension chords, as shown in Fig. 3.6. In this particular configuration failure was governed by buckling of the front face near the mid-span location; where the principal compression force occurs.

Fig. 3.6 (a) shows the anticipated failure mode in *V-ST*-core, where buckling of the front face in compression governed the failure. As expected, the failure occurred in the upper or the lower adjoining compression bay closest to the mid-span.

3.5 ANALYTICAL MODEL

A number of researchers have investigated the elastic behavior of sandwich panels, including the elastic stiffness constants for different core configurations. For example, Libove and Hubka (1951) studied the elastic constants for corrugated core sandwich panels, Fung et al. (1993) and Fung et al. (1994) presented the elastic constants for *Channel* and *Z* core sandwich panels, and Tat-Seng Lok (2000) introduced a closed form solution for the elastic constants for truss core sandwich panels. Although the current study focused on quantifying the resistance function of the tested configurations up to failure, a simplified analytical model is introduced to predict the yield flexural capacity, shear strength, elastic flexural stiffness, critical web crippling load and energy absorption for the proposed configurations. The model is subsequently used to predict the failure mode(s) for each of the core configurations.

At the mid-span section the maximum face and core stresses are obtained as follows (Allen 1969):

$$\sigma_{f(max)} = \pm \frac{ME_{face}}{D} \cdot \frac{h}{2} \quad , \quad \sigma_{c(max)} = \pm \frac{ME_{core}}{D} \cdot \frac{d}{2} \qquad (1)$$

where D is the flexural rigidity, E_{face} and E_{core} are the modulus of elasticity for the face sheet and the core sheet, respectively, h is the section depth, and d is the core depth. The flexure rigidity is the sum of the flexure rigidities of the sandwich layers (i.e two sandwich faces and core), measured about the centroidal axis of the entire section as follows:

$$D = E_{face}\frac{Bt_f^{\,3}}{6} + E_{face}\frac{Bt_f\left(d+0.5t_f\right)^2}{2} + E_{core}I_{core} \qquad (2)$$

where I_c is the second moment of area of the core. The shear stress (τ) in a sandwich sections is presented assuming constant shear stress over the depth of the core:

$$\tau = \frac{Q}{D}\cdot\frac{E_f t_f d}{2} \qquad (3)$$

where Q is the shear force. When the flexure rigidity of the two faces about their own axis is small (i.e if $3\left(\frac{d}{t}\right)^2 > 100$) the local bending stiffness of the faces is neglected and the shear stress expression in the core reduces to:

$$\tau = \frac{Q}{A_{web}} \qquad (4)$$

where A_{web} is the area of the web. The critical web crippling load is calculated using the unified web crippling equation as follows (CSA S136-07 2007, AISI 2001):

$$P_n = Ct^2 f_y(\sin\theta)\left(1 - C_R\sqrt{\frac{R}{t}}\right)\left(1 + C_N\sqrt{\frac{N}{t}}\right)\left(1 - C_H\sqrt{\frac{h}{t}}\right) \qquad (5)$$

where, P_n is the nominal computed web crippling load per web, t is the web thickness, R is the inside bend radius, N is the bearing length, h is the clear distance between the flanges, and (C,C_R,C_N,C_H) are coefficients values that depend on support condition, load case, and location of the reaction (i.e interior reaction or end reaction).

Finally for the V-ST-core, the critical buckling load for the front face was calculated using Euler' formula:

$$F_b = \frac{\pi^2 E_f I}{L^2} \qquad (6)$$

where F_b is the critical buckling load, and L is the buckling length. The predictions of the analytical model will be presented and discussed in the following sections. It should be mentioned that all the predicted critical loads are expressed in terms of an equivalent concentrated load that equals the applied distributed uniform pressure on the front face that induces the concerned failure mode.

3.6 ANALYSIS OF TEST RESULTS

The experimental tests results showed that, in general, the panels experienced failure modes characterized by the formation of a plastic hinge in the mid-span vicinity of the specimens. The failure for *B-S*-core and *V-S*-core panels was governed by buckling near the mid-span of the panels, while the failure for *V-ST*-core sandwich panels was dominated by buckling in the front face.

The maximum normal stress is typically found at the mid-span location of a simply supported sandwich panel, where front face buckling is observed to occur during testing. The initiation of web crippling was also observed to occur due to end reactions; however, it was not the governing failure mode for the tested panels.

Although, the current research mainly focuses on the equivalent concentrated load representing all the applied pressure on the front face of the panels, an example showing the measured applied pressure-displacement relationship can be seen in Fig. 3.7(a) and the measured vertical displacement of the roller support is shown in Fig. 3.7(b).

3.6.1. Nominal Yield & Ultimate Capacity

As the tests were conducted under load control, rapid uncontrolled resistance degradation beyond the failure capacity load occurred. As a result, only the controlled data points up to the failure capacity are presented. As discussed earlier, the different sandwich panel configurations exhibited different inelastic behavior. For this reason a single criterion was used to carry out a comparison between the different configurations, where the behavior of the sandwich panels was assumed to be elastic perfectly-plastic. The idealized model was assumed to have an equal value of energy absorption as the experimental resistant function. Fig. 3.8 shows the parameters that control the idealized model, where (F_{ny}) is the nominal yield load, (F_f) is the failure load, (K) is the elastic stiffness constant and (δ_y) and (δ_f) are the corresponding displacements for the nominal yield load and the failure load, respectively.

The failure load was defined as the last loading value prior to a rapid loss of capacity on the resistance degradation, as shown in Fig. 3.8. The energy absorption up to the failure load value (E_f) was computed for all tested specimens. A nominal yield load (F_{ny}) was computed based on the energy absorption up to the failure load for each of the tested specimens, assuming an idealized elastic perfectly-plastic response representation of the resistance function. The elastic stiffness constant (K) was assumed to have the same value for both experimental and idealized resistance functions, as shown in Fig. 3.8.

As expected, the nominal yield load was found to be dependent on both the core configuration and the core thickness. The analytical and experimental mean computed values of the nominal yield loads and corresponding *COV* values are presented in Table 3.3. The analytical nominal yield loads are calculated assuming yielding of the face sheets or are based on Euler buckling theory (V-ST-core panels). In addition, the total critical web crippling loads F_{cr} are presented in Table 3.3. It can be observed that web crippling was predicted to occur prior to yielding in all configurations except for the V-ST-core, which was consistent with observations during testing. In addition, the nominal yield values from the simplified analytical model were found to be in a good agreement with the measured values, where the maximum difference did not exceed 13%, as shown in Table 3.3.

Increasing the core sheet thickness for the same B-S core configuration from 0.9 mm (*B-S-G20*) to 1.2 mm (*B-S-G18*) was found to increase F_{ny} by 35.6 %. Similarly, an increase in the core sheet thickness for the *V-S*-core configuration resulted in an increase of 1.6% in F_{ny} and a 5.3% increase in F_{ny} for the *V-ST* core configuration.

The influence of core configuration on the nominal yield load can be seen by comparing the different configurations for a given core thickness, as shown in Fig. 3.9(a). For G20 core thickness sandwich panels, the *B-S-G20* was found to have an F_{ny} value 2.8 times greater than *V-ST-G20*, while the *V-S-G20* had F_{ny} value that was 3.6 times greater than *V-ST-G20*. For G18 core thickness sandwich panels, the *B-S-G18* had an F_{ny} value 3.8 times greater than *V-ST-G18*, while the *V-S-G18* had F_{ny} value that was 3.7 times greater than *V-ST-G18,* as shown in Fig. 3.9.

It can be observed from the test results that the *B-S*-core and *V-S* core configurations achieve substantially higher F_{ny} values compared to the *V-ST* core configuration. In addition, although the core sheet thickness had a significant effect for *B-S*-core sandwich panels, it was found to have little effect on the *V-S* and *V-ST*-core sandwich panels.

Table 3.3 shows the mean and *COV* values of the ultimate capacity, F_u, of the tested sandwich panels. The ultimate capacity was also affected by both the core sheet thickness and the core configuration. Increasing the core sheet thickness for the same core configuration from G20 (0.9 mm) to G18 (1.2 mm) was found to increase F_u by 35.6 %, 3.1%, and 1.6% in *B-S*-core, *V-S*-core, and *V-ST*-core sandwich panels respectively. It is also noted that F_u was affected by the same percentage as the nominal yield load (F_{ny}) by the core sheet thickness in the *B-S*-core sandwich panels

Fig. 3.9(b) shows the influence of core configuration on the ultimate capacity. For G20 core sandwich panels, F_u for *B-S-G20* was found to be 2.6 times greater than that for *V-ST-G20*, while the *V-S-G20* obtained a F_u that was 3.5 times greater than that reached by *V-ST-G20*. For G18 core sandwich panels, *B-S-G18* as found to have a F_u value 3.5 times greater than *V-ST-G18*, while *V-S-G18* was found to have a F_u value 3.4 times greater than *V-ST-G18*.

It is concluded that the ultimate capacity is affected in a similar manner as the nominal yield load by both the sheet core thickness and the core configuration. With respect to strength, the *V-S*-core sandwich panels were found to be the most efficient configuration within the tested configurations considered.

3.6.2. Resistance Function

The resistance functions for the various sandwich panel configurations are reported on in this section. It should be noted that the descending branch of each curve is not reported, as the test setup was not designed to capture the post-failure response. When each core configuration is considered separately, the resistance functions associated with specimens featuring the same core are found to be consistent with each other, with the notable exception of specimen (*B-S-G18-3)*, which experienced a weld type failure at 31.1 kN. The analytical (to yielding) and the experimental resistance functions, presented in Fig. 3.10, show the stiffness, ultimate capacity, and the corresponding displacement values for each type of core configuration. No data is available for panel *V-ST-G18-3* due to failure of the instrumentation during testing. The fluctuating behavior present in the inelastic response region for the *V-S*-core and *B-S-G20* is attributed to web crippling, which was observed during testing. Increasing the core sheet thickness from G20 to G18, particular for the *B-S*-core type, eliminated web crippling but resulted in a more brittle type of behavior. In order to directly compare the behavior of different configurations, the resistance functions of the tested core configurations were normalized and are presented in Fig. 3.11. The load was normalized by the nominal yield load (F_{ny}), while the displacement was normalized by the yield displacement (δ_{ny}). It can be observed that the normalized peak loads do not exceed 1.1, which indicates that the tested sandwich panels did not experience significant strength increase after the nominal yield load.

3.6.3. Energy Absorption

The energy absorbed is a function of the specimen cross-section topology, material and applied loading (Tarlochan et al. 2012). It is defined as the area under load-displacement relationship, including the material and geometry nonlinearities up to failure. The energy absorption is an important parameter in many applications, particularly for dynamic loading such as impact, blast and crashworthiness applications (Theobald and Nurick 2010, Fatt and Surabhi 2012, Tarlochan et al. 2012).

Numerical integration of Eq. (1) was carried out in order to compute the energy absorbed (E) of the different sandwich panel configurations investigated

$$E = \int_0^{\delta_{max}} F(\delta) d\delta \qquad (7)$$

where F is the load, δ is the displacement, and δ_{max} is the maximum displacement .

Energy absorption occurs as a result of plastic deformations in the core and the face sheets, where flexural induced buckling and web crippling were observed during experimental testing.

The energy absorption – displacement curves are plotted for different tested specimens in Fig. 3.12, while the mean and *COV* values of the analytical and the experimental absorbed energy are presented in Table 3.4. The difference between the analytical and the experimental calculated energy absorption values (to yielding) was found to be between (-26% to + 29%). Furthermore, the normalized energy absorption $\left(\frac{E}{E_{ny}}\right)$ versus normalized displacement $\left(\frac{\boldsymbol{\delta}}{\boldsymbol{\delta_{ny}}}\right)$ curves for all the tested panels is shown in Fig. 3.13, where the normalized energy absorption is the ratio of energy absorption (E) to nominal yield energy absorption (E_{ny}). It can be observed that for each of the tested groups, and in some cases specimens within a group, exhibit different values of the maximum normalized energy absorption, but all test specimens appear to follow a consistent trend. To further investigate this behavior all of the normalized energy absorption plots for different tested core configurations are plotted together in Fig. 3.14. The normalized plots were found to collapse on to a single line. Subsequently, using nonlinear regression, a polynomial equation was fit to the normalized energy absorption and the following function was obtained:

$$\left(\frac{E}{E_{ny}}\right) = -1.843 * 10^{-1} \left(\frac{\boldsymbol{\delta}}{\boldsymbol{\delta_{ny}}}\right)^3 + 1.076 \left(\frac{\boldsymbol{\delta}}{\boldsymbol{\delta_{ny}}}\right)^2 + 5.41 * 10^{-2} \left(\frac{\boldsymbol{\delta}}{\boldsymbol{\delta_{ny}}}\right) \quad (8)$$

It is observed that the *V-S-G20* sandwich panels achieved the highest energy absorption within a load range up to the nominal yield value, as depicted in Fig. 3.15(a). This is attributed to the profile shape, which allows for more energy absorption through web crippling prior to reaching the flexural yield capacity. It is also found that the *V-ST-G20* sandwich panels exhibited the lowest energy absorption, as failure of this specimen type was governed by buckling of front face at the mid-span, while the core did not significantly contribute to the energy absorption.

3.6.4. Stiffness

The elastic flexure stiffness constants for the core configurations investigated, representing a single layer corrugated core sandwich panels, were quantified analytically and through experimental testing. The mean values for the elastic stiffness and corresponding *COV* values are presented in Table 3.5. It can be observed that the analytical predicted elastic stiffness and experimentally measured values are in good agreement with error between -12% to +17%.

The highest flexure stiffness was achieved by the *B-S*-core sandwich panel configuration. By comparing the values of elastic stiffness, it is found that by increasing the core sheet thickness from 0.9 mm (G20) to 1.2 mm (G18) the stiffness increased by 23 %, 14.6% and 1.3 % in the B-S-core, *V-S*-core and *V-ST*-core sandwich panels, respectively.

Regarding the effect of core configuration on the elastic stiffness, as shown in Fig. 3.15(b), for the 0.9 mm (G20) sandwich panels the elastic stiffness was found to be 3.28 times greater for *B-S-G20* compared to *V-ST-G20*, while the *V-S-G20* was found to be 3.34 times greater than *V-ST-G20*. On the other hand, the elastic stiffness for the *B-S-G18* was found to be 3.23 times greater than the elastic stiffness for *V-ST-G18,* while *V-S-G18* had an elastic stiffness value that was 3.07 times greater than the *V-ST-G18* sandwich panel-type.

3.6.5. Ductility

Ductility (μ) is defined in this study as the ratio of the maximum displacement to the nominal yield displacement (δ_{ny}); the values of ductility for tested panels are shown in Table 3.6. The nominal yield displacement is the displacement associated with the nominal yield load. The analytically predicted yield displacement values and experimentally measured nominal yield displacement values, along with the mean and corresponding *COV* values, for each panel type are also presented in Table 3.6. It can be observed that the predicted yield displacements are in good agreements with the measured nominal yield displacement.

It was found that the nominal yield displacement for tested specimens varied in a relatively narrow band between 10 mm and 13mm. The core sheet thickness was found to affect the ductility for the same core configuration. The ductility was found to decrease by increasing the core sheet thickness from 0.9 mm (G20) to 1.2 mm (G18) in both the *B-S*-core and the *V-ST*-core, while it increased in the *V-ST*-core.

Fig. 3.16(c) shows the configuration effect on the nominal yield displacement by comparing the three different configurations while maintaining the same core thickness. For the 0.9 mm (G20) core sandwich panels, *B-S-G20* had a δ_{ny} of 4.9 % greater than *V-ST-G20*, while the *V-S-G20* had a δ_{ny} that was 33.4 % greater than *V-ST-G20*. For 1.2 mm (G18) core sandwich panels, the *B-S-G20* had a δ_{ny} that was 2.35% greater than *V-ST-G20*, while *V-S-G20* had a δ_{ny} that was 8.3% greater than *V-ST-G20*.

The maximum ductility, which was achieved by the *B-S-G20* sandwich panels, had a value of 2.33. Increasing the core sheet thickness was found to decrease the ductility for both *B-S*-core and *V-ST*-core, which is presumed due to the increase of web crippling resistance and the flexure stiffness, which caused the failure to be more brittle, subsequently decreased the exhibited ductility. On the other hand for the *V-S*-core, the profile of corrugation led to a significant increase in the value of nominal yield displacement (δ_{ny}) for *V-S-G20* than *V-S-G18*. Consequently, even the *V-S-G20* exhibited the largest value of displacement at failure, but it did not show an increase in the ductility rather than the *V-S-G18.*

3.7 CONCLUSIONS

An analytical and experimental investigation focusing on the behavior of galvanized lightweight cold-formed steel sandwich panels subjected to out-of-plane uniform loading has been presented. The static resistance functions for the tested panels were determined, which will be used in a future blast resistance modeling study. A relatively and rapid fabrication technique, using low cost readily available material (deck profiles), was employed to overcome the complexity and high cost of sandwich panels. Different configurations were proposed and tested; the failure modes, load-displacement relationships, energy absorption, ductility, nominal yield and ultimate capacity were presented and discussed.

It is concluded from the study that:

(A) A simplified analytical model, which can be predict the yield load, yield displacement, elastic stiffness, corresponding energy absorption, web crippling load, and buckling load, was introduced. The analytical results were found in a good agreement with the experimental measurements values. The error between the analytical and the experimental results was quantified for each of the presented characteristics.

(B) The core configuration affected the nominal yield and ultimate capacity, as the highest nominal yield load was achieved by using the *V-S*-core configuration, while the transverse orientation of the same deck profile decreased the achieved nominal yield load and ultimate capacity by a ratio of 0.71 relative to the longitudinal orientation.

(C) The core sheet thickness had a significant effect on both the nominal yield load and on the ultimate capacity for *B-S*-core sandwich panels, while it had a less of an effect on the *V-S*-core and minor effect on the *V-ST*-core sandwich panels.

(D) The tested configurations did not possess significant ductility, as the maximum ductility did not exceed a value of 2.33. As a result, these configurations are not recommended where significant ductility is required.

(E) The flexure elastic stiffness was found to be affected by the core configuration, For example, the stiffness of the *B-S*-core was found to be 3.34 times greater than that for the *V-ST*-core. The flexure elastic stiffness was also affected by the core sheet thickness, where the stiffness for the B-S-core configuration increased by 23% when the core sheet thickness increased from 0.9 mm (G20) to 1.2 mm (G18)

(F) The *V-S-G20* sandwich panels were found to absorb the most energy, this is due to the profile shape, which allows more energy absorption through web crippling. An equation is proposed to represent the normalized energy absorption as a function in the ductility for the tested core configurations.

Finally, the presented results and conclusions of the current study will be used in the future development of lightweight cost–effective sandwich panels, to be employed as sacrificial cladding in the context of blast damage mitigation.

3.8 APPENDIX NOTATION

COV = Coefficient of variance

$\bar{B}$ = Corrugated core width

D = Flexural rigidity

d = Corrugated core depth

E= Energy absorption

E_{core} = Modulus of elasticity of core sheet

E_{face} = Modulus of elasticity of face sheet

E_f = Energy absorption up to failure

E_{ny} = Energy absorption up to nominal yield load

F = Applied load

F_u = Ultimate capacity

F_{ny} = Nominal yield load

F_{nya} = Analytical nominal yield load

F_f = Failure load

F_{ny} = Nominal yield load

F_{cr} = total critical load for web crippling

F_f = Failure load

f_y = yield stress

h = Section height.

K = Elastic stiffness

δ = Displacement

δ_{ny} = Nominal yield displacement

δ_f = Displacement corresponding to failure load

θ = Angle of corrugation

μ = Ductility

$\sigma_{f(max)}$ = Maximum normal stress for face sheet

$\sigma_{c(max)}$ = Maximum normal stress for core sheet

3.9 REFERENCES

A.Gopichand , Dr.G.Krishnaiah, B.Mahesh Krishna , Dr.Diwakar Reddy.V, A.V.N.L.Sharma (2012). "Design And Analysis Of Corrugated Steel Sandwich Structures Using Ansys Workbench." International Journal of Engineering Research & Technology, Vol. 1 (8), pp. 2278-0181.

American Socity of Civil Engineers (ASCE) (2012). "Blast Protection of Buildings." ASCE/SEI 59-11, Reston, Virginia.

American Iron and Steel Institute (AISI) (2001). "North American Specification for the Design of Cold-Formed Steel Structural Members". Washington (DC, USA).

Andrews, E. W. and N. A. Moussa (2009). "Failure Mode Maps for Composite Sandwich Panels Ssubjected to Air Blast Loading." International Journal of Impact Engineering, Vol. 36 (3), pp. 418-425.

Biggs, J. M. (1964). "Introduction to Structural Dynamics." New York, USA: McGraw-Hill Inc.

Norris, C., Montague, P., Tan, K.H. (1989). "All Steel Structural Panels to Carry Lateral Load: Experimental and Theoretical Behaviour." Journal of Structural Engineer, Vol. 67(9), pp. 167-176.

Canadian Standards Assiocation (CSA) (2012). "Design and Assessment of Buildings Subjected to Blast Loads." CSA S850-12. Mississauga, Ontario, Canada.

Canadian Standards Assiocation (CSA-S136) (2007). "North American Specification For the Design of Cold-Formed Steel Structural Members." CSA S850-12. Mississauga, Ontario, Canada.

Knox, E. M., Cowling, M. J., Winkle, I.E.(1998). "Adhesively Bonded Steel Corrugated Core Sandwich Construction for Marine Applications." Journal of Marine Structures Vol 11, pp. 185-204.

Allen, H. G. (1969) "Analysis and Design of Structural Sandwich Panels." Pergamon, Press London.

Hoo Fatt, M. S. and Surabhi, H. (2012). "Blast Resistance and Energy Absorption of Foam-Core Cylindrical Sandwich Shells Under External Blast." Journal of Composite Structures, Vol. 94(11), pp. 3174-3185.

Jelovica, J. , Romanoff, J., Ehlers, S., Aromaa, J. (2013). "Ultimate Strength of Corroded Web-Core Sandwich Beams." Journal of Marine Structures, Vol. 31, pp.1-14.

Jelovica, J., Romanoff, J., Ehlers, S., Varsta, P. (2012). "Influence of Weld Stiffness on Buckling Strength of Laser-Welded Web-Core Sandwich Plates." Journal of Constructional Steel Research, Vol. 77, pp. 12-18.

Libove, C., Hubka, R. E. (1951). "Elastic Constants for Corrugated Core Sandwich Plates." National Advisory Committee for Aeronaytics, Technical Note 2289, Washington, USA.

Theobald, M. D. and Nurick, G. N. (2010). "Experimental and Numerical Analysis of Tube-Core Claddings Under Blast Loads." International Journal of Impact Engineering, Vol. 37(3), pp. 333-348.

Marwan T. Shedid, Drysdale, Robert G., El-Dakhakhni, W. W. (2008). "Behavior of Fully Grouted Reinforced Concrete Masonry Shear Walls Failing in Flexure: Experimental Results." Journal of Structural Engineering, Vol. 134, pp. 1754-1767.

Kujala, P. , Klanac, A. (2005). "Steel Sandwich Panels in Marine Applocations." Brodogradnja, Vol.56, pp. 305–314

Houlston, R., Slater, J. E., Pegg, N., Desrochers, C. (1985). "On Analysis of Structural Response of Ship Panels Subjected to Air Blast Loading." Journal of Computers & Structures, Vol. 21 (112), pp. 273-289.

Romanoff, J. and Varsta, P. (2006). "Bending Response of Web-Core Sandwich Beams." Composite Structures, Vol. 73 (4), pp. 478-487.

Romanoff, J. and Varsta, P. (2007). "Bending Response of Web-Core Sandwich Plates." Composite Structures, Vol. 81 (2), pp. 292-302.

Romanoff, J., Varsta, P., and Klanac, A. (2007). "Stress Analysis of Homogenized Web-Core Sandwich Beams." Composite Structures, Vol. 79 (3), pp. 411-422.

Romanoff, J., Varsta, P., and Remes H. (2007). "Laser-Welded Web-Core Sandwich Plates Under Patch Loading." Journal of Marine Structures, Vol. 20 (1-2),pp. 25-48.

SANDCORE (2005). " Best Practice Guide for Sandwich Structures in Marine Applications " SAND.CORe, NewRail University of Newcastle upon Tyne.

SANDWICH (2000). "Advancd Composite Sandwich Steel Structures." The European Commission Under 5th Framework Programme Growth KA III.

Tarlochan, F., Rameshb, S., Harpreet, S. (2012). "Advanced Composite Sandwich Structure Design for Energy Absorption Applications: Blast Protection and Crashworthiness." Composites Part B: Engineering, Vol. 43 (5), pp. 2198-2208.

Lok, T.S., Cheng, Q.H. (2000). "Elastic Stiffness Prorerties and Behavior of Truss-Core Sandwich Panel." Journal of Structural Engineering, Vol. 126. pp. 552-559.

U.S. Army Corps of Engineers, Naval Facilities Engineering Command, and Air Forces Civil Engineer Support Agency (2008), “Structures to Resist the Effect of Accidental Explosions.” Unified Facilities Criteria, UFC 3-340-02.

Valdevit, L., Hutchinson, J.W., and Eyans, A.G.(2004). "Structurally Optimized Sandwich Panels with Prismatic Cores." International Journal of Solids and Structures, Vol. 41(18-19), pp. 5105-5124.

Valdevit, L., Wej, Z., Mercer, C., Zok, F.W., and Eyans, A.G. (2006). "Structural Performance of Near-Optimal Sandwich Panels with Corrugated Cores." International Journal of Solids and Structures, Vol. 43(16), pp. 4888-4905.

Table 3.1 Test Matrix

NO.	Panel Name	No. of samples	Core deck type	Configuration type	Thickness of core sheet *(mm)*	Sample depth *(mm)*	Deck parameters				
							$\bar{B}$ *(mm)*	*D* *(mm)*	b_1 *(mm)*	b_2 *(mm)*	θ°
1	*B-S-G20*	3	*B* - deck	Single Longitudinal	0.91	42.2	304.8	38.1	82.4	42.0	73°
2	*B-S-G18*	3	*B* - deck	Single Longitudinal	1.21	42. 2	304.8	38.1	82.4	42.0	73°
3	*V-S-G20*	3	*V* - deck	Single Longitudinal	0.91	42.2	304.8	38.1	29.2	29.2	45°
4	*V-S-G18*	3	*V* - deck	Single Longitudinal	1.21	42.2	304.8	38.1	29.2	29.2	45°
5	*V-ST-G20*	3	*V* - deck	Single Transverse	0.91	42.2	304.8	38.1	29.2	29.2	45°
6	*V-ST-G18*	3	*V* - deck	Single Transverse	1.21	42.2	304.8	38.1	29.2	29.2	45°

Table 3. 2 Material Properties

NO.	Sheet	Gauge of sheet	Modulus of elasticity (*GPa*)	Yield Stress (*MPa*)
1	*Face flat sheet*	G14	190.49	304.2
2	*B-deck*	G18	180.87	272.8
3	*B-deck*	G20	139.17	274.6
4	*V-deck*	G18	208.63	256.4
5	*V-deck*	G20	173.39	264.2

Table 3.3 Nominal yield loads and Ultimate capacity loads for the tested panels

No.	Panel Type	F_{ny1} (kN)	F_{ny2} (kN)	F_{ny3} (kN)	Mean (kN)	COV	F_{nya} Analytical (kN)	Ratio $F_{nya}/F_{ny(mean)}$	F_{cr} (kN)	F_{u1} (kN)	F_{u2} (kN)	F_{u3} (kN)	Mean (kN)	Standard Deviation	COV
1	*B-S-G18*	46.16	45.95	**	46.05	0.01	44.7	0.97	37.67	47.17	46.56	**	46.86	0.43	0.01
2	*B-S-G20*	34.48	33.56	33.88	33.97	0.01	38.4	1.13	21.85	34.72	34.54	34.46	34.57	0.13	0.004
3	*V-S-G18*	45.85	43.57	45.46	44.96	0.03	41.9	0.93	26.14	48.68	46.34	48.57	47.86	1.32	0.03
4	*V-S-G20*	45.71	40.98	46.08	44.25	0.06	40.3	0.91	15.51	48.50	42.77	47.96	46.41	3.16	0.07
5	*V-ST-G18*	12.63	12.86	N/A	12.74	0.01	11.67 [b]	0.92	-	12.63	14.21	N/A	13.42	1.12	0.08
6	*V-ST-G20*	12.68	11.94	12.05	12.23	0.03	11.67 [b]	0.98	-	14.07	12.69	12.86	13.21	0.75	0.06

** The specimen faced a weld failure, [b] Calculated buckling load.

Table 3.4 Energy absorbed corresponding to idealized yield forces for the tested panels

No.	Panel Type	E_{ny1} $(kN.mm)$	E_{ny2} $(kN.mm)$	E_{ny3} $(kN.mm)$	$E_{ny(mean)}$ $(kN.mm)$	Standard Deviation	*COV*	$E_{ny(analytical)}$ $(kN.mm)$	*Ratio* *Eny(analytical) / Eny(mean)*
1	*B-S-G18*	255.32	285.86	**	270.59	21.59	0.08	241.9	0.89
2	*B-S-G20*	185.47	187.71	158.08	177.09	16.50	0.09	229.3	1.29
3	*V-S-G18*	267.03	247.68	278.24	264.32	15.46	0.06	226.5	0.86
4	*V-S-G20*	312.46	250.79	318.95	294.07	37.62	0.13	217.9	0.74
5	*V-ST-G18*	76.74	63.01	N/A	69.88	9.71	0.14	63.48	0.91
6	*V-ST-G20*	66.46	56.23	59.72	60.80	5.20	0.09	63.48	1.04

** The specimen faced a weld failure.

Table 3.5 Flexure elastic stiffness determined experimentally

No.	Panel Type	K_1 (kN/mm)	K_2 (kN/mm)	K_3 (kN/mm)	$K_{(mean)}$ (kN/mm)	Standard Deviation	COV	$K_{analytical}$ (kN/mm)	Ratio $K_{analytical}/K_{(mean)}$
1	*B-S-G18*	4.13	4.12	3.84	4.03	0.17	0.04	4.14	1.03
2	*B-S-G20*	3.20	3.01	3.63	3.28	0.32	0.09	3.53	1.07
3	*V-S-G18*	3.94	3.83	3.71	3.83	0.11	0.03	3.88	1.01
4	*V-S-G20*	3.34	3.35	3.32	3.34	0.01	0.01	3.73	1.17
5	*V-ST-G18*	1.18	1.31	N/A	1.25	0.09	0.07	1.08	0.86
6	*V-ST-G20*	1.21	1.27	1.21	1.23	0.03	0.03	1.08	0.88

Table 3.6 Nominal yield displacements and Ductility for the tested panels

No.	Panel Type	δ_{ny1} (mm)	δ_{ny2} (mm)	δ_{ny3} (mm)	$\delta_{ny(mean)}$ (mm)	COV	$\delta_{ny(analytical)}$ (mm)	Ratio $\delta_{ny(analytical)}$ / $\delta_{ny(mean)}$	$\mu 1$	$\mu 2$	$\mu 3$	Mean	Standard Deviation	COV
1	*B-S-G18*	11.06	11.15	**	11.10	0.01	10.88	0.98	1.19	1.28	**	1.24	0.06	0.05
2	*B-S-G20*	10.76	11.18	9.33	10.42	0.09	10.88	1.04	2.39	1.95	2.64	2.33	0.35	0.15
3	*V-S-G18*	11.65	11.37	12.24	11.75	0.04	10.88	0.93	1.75	1.81	2.08	1.88	0.17	0.09
4	*V-S-G20*	13.67	12.239	13.84	13.25	0.07	10.88	0.82	1.89	1.69	1.87	1.82	0.11	0.06
5	*V-ST-G18*	11.91	9.79	N/A	10.85	0.14	10.88	1.003	1.05	1.58	N/A	1.31	0.37	0.28
6	*V-ST-G20*	10.48	9.42	9.91	9.94	0.05	10.88	1.09	1.54	2.40	2.55	2.16	0.54	0.25

** The specimen faced a weld failure.

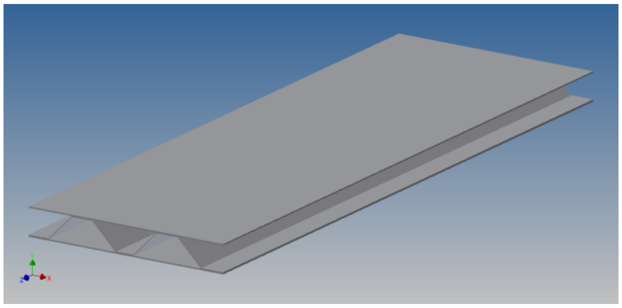

(a)

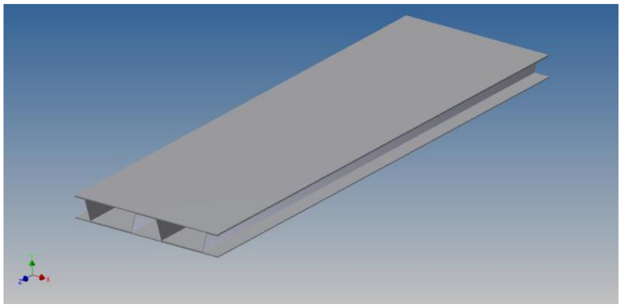

(b)

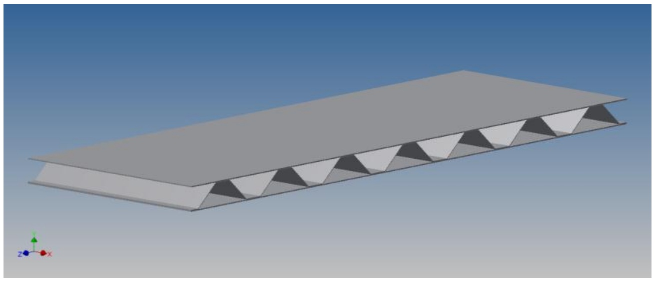

(c)

Fig. 3.1Different tested configurations (a) *V-S*-core, (b) *B-S*-core, and (c) *V-ST*-core

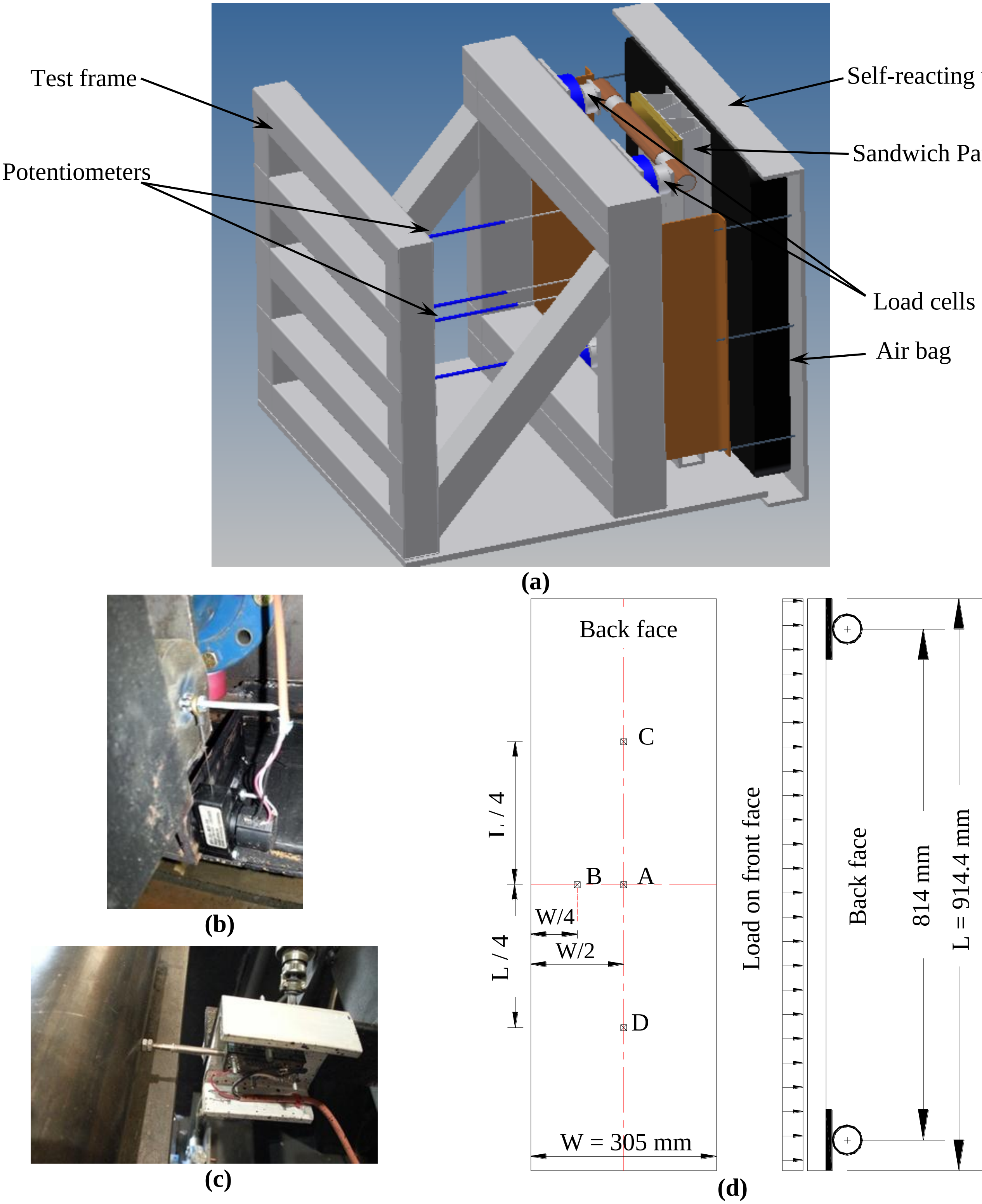

Fig. 3.2 Test setup and instrumentations (a) 3D view for the test setup, (b) String pot at roller support, (c) Potentiometer at pin support, and (d) Panel dimensions and potentiometers location on back face

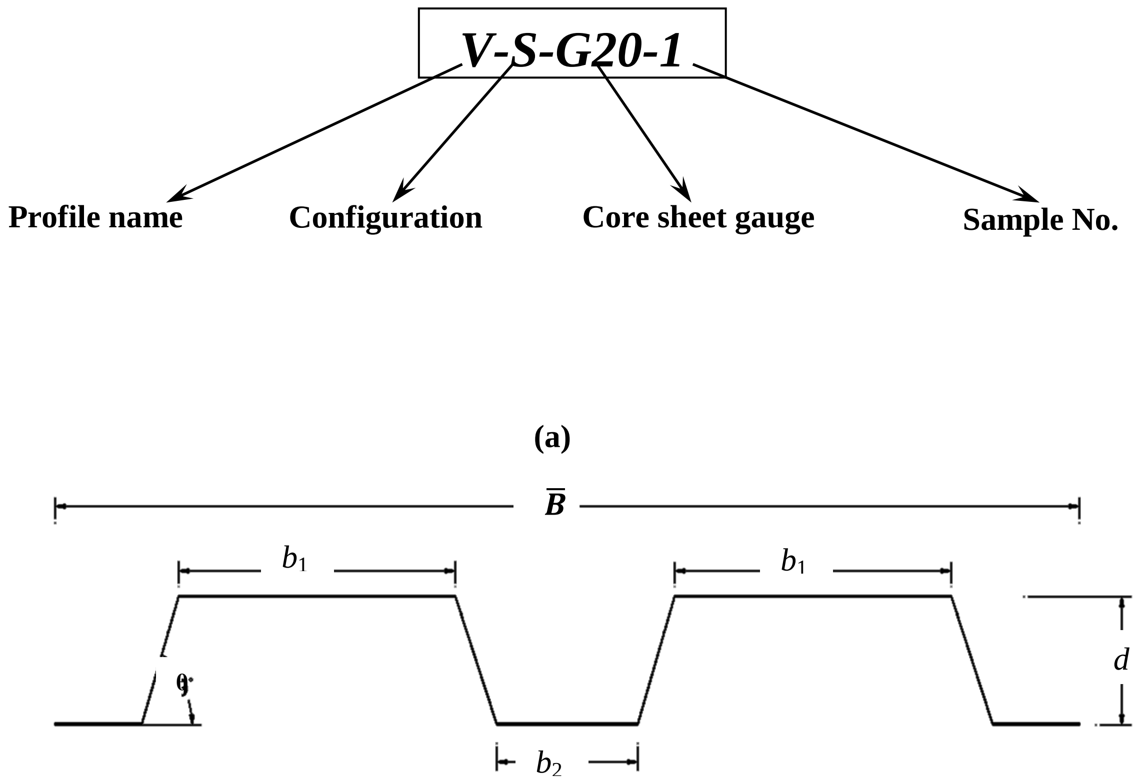

(b)

Fig. 3. 3 (a) The basis of the sample nomenclature, (b) The parameters defining each deck profile.

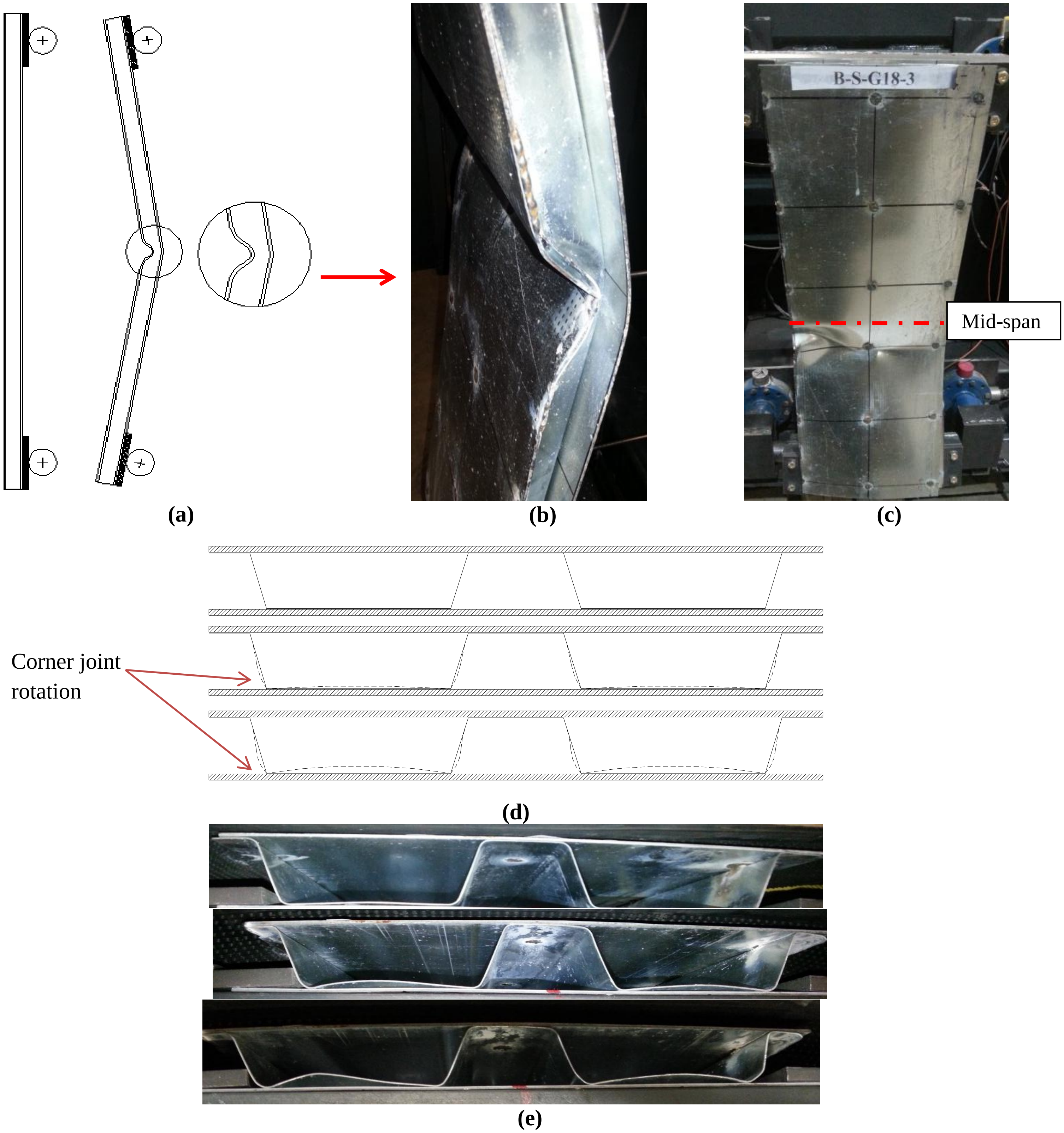

Fig. 3.4 B-S-core sandwich panels, (a) failure mode, (b) observed failure zone, (c) observed failure sample, (d) web crippling, and (e) observed web crippling.

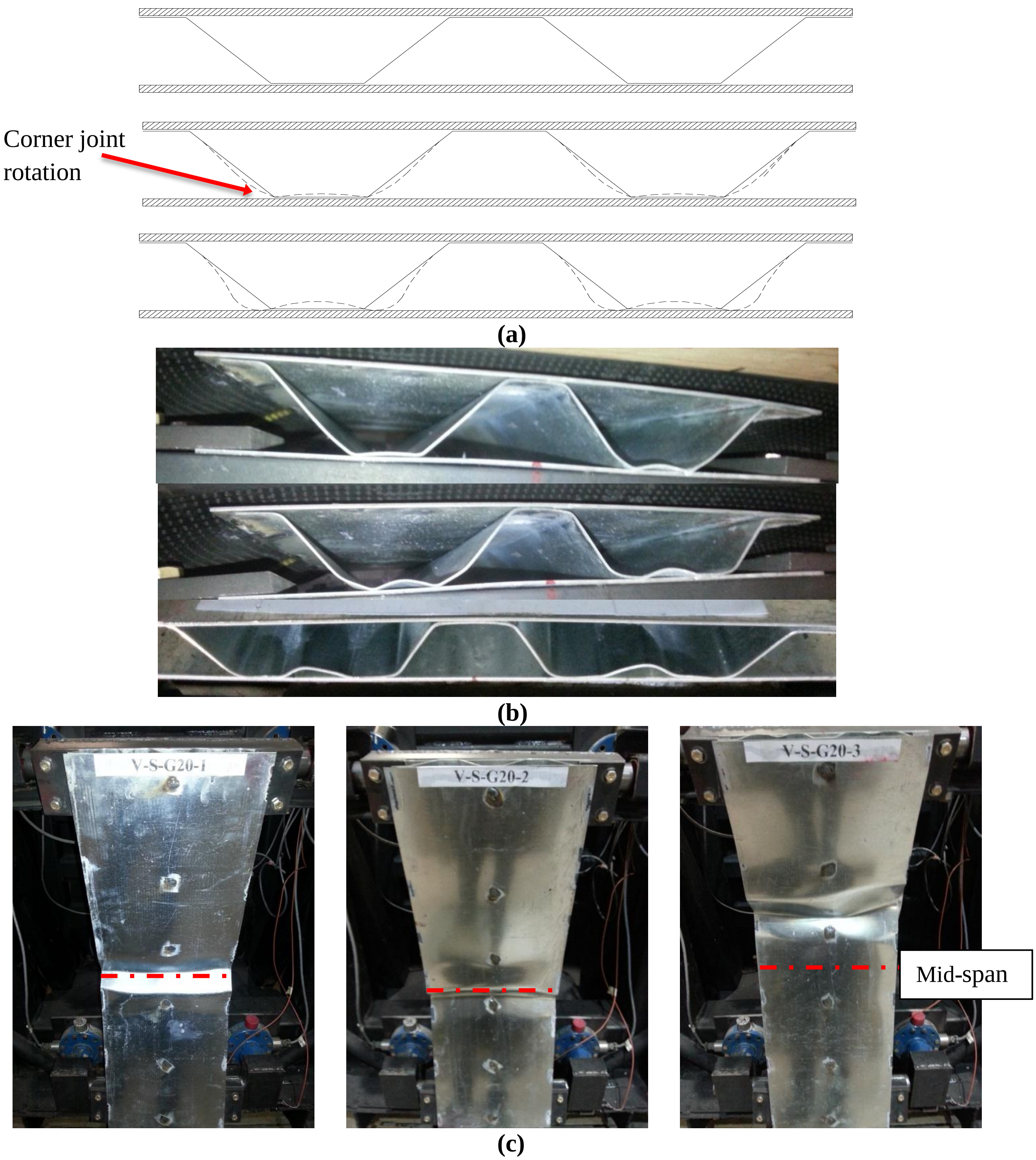

Fig. 3.5 V-S-core sandwich panels, (a) web crippling, (b) observed web crippling, and (c) observed buckling failure.

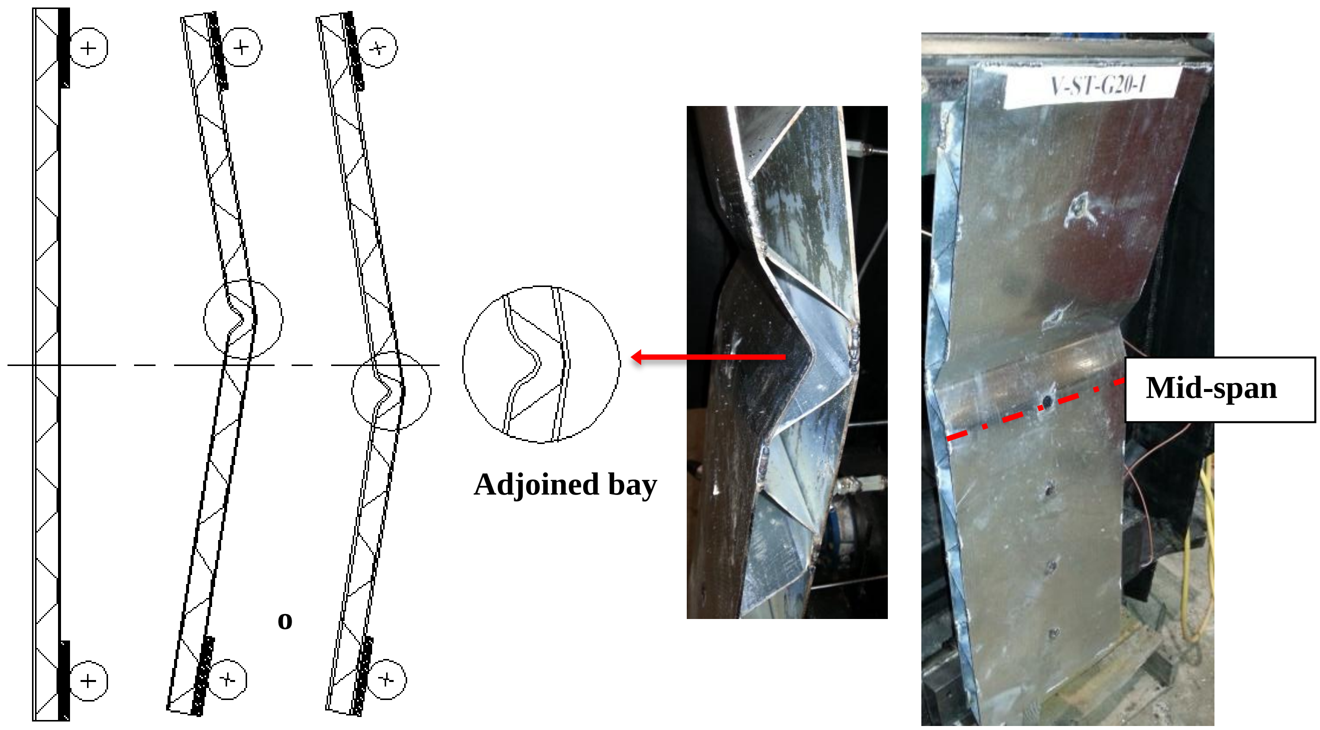

(a) **(b)**

Fig. 3.6 *V-ST*-core sandwich panels (a) compression face buckling, and (b) observed failure

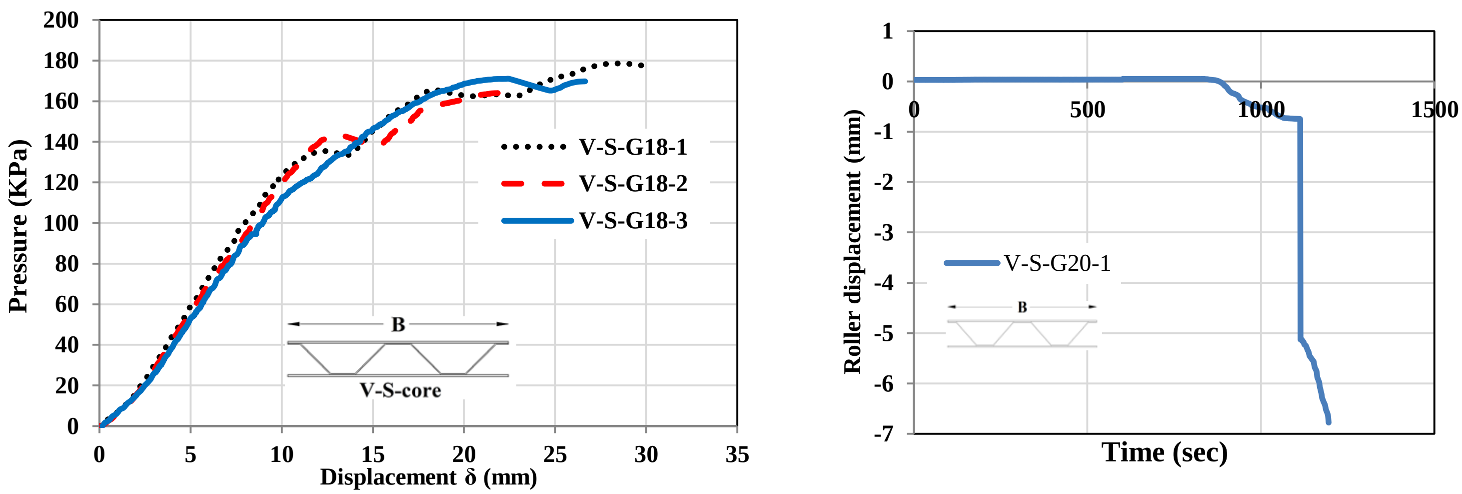

(a) **(b)**

Fig. 3.7 Sample of measured (a) pressure-displacement relationship, and (b) roller displacement.

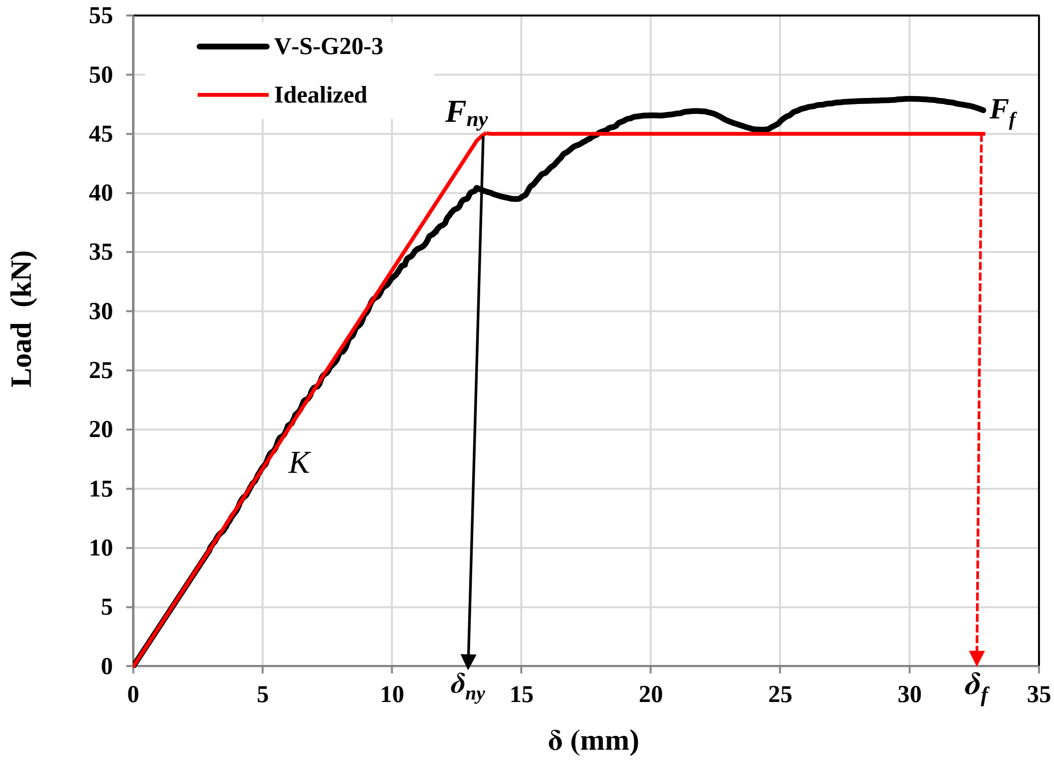

Fig. 3.8 Idealized Load-Displacement

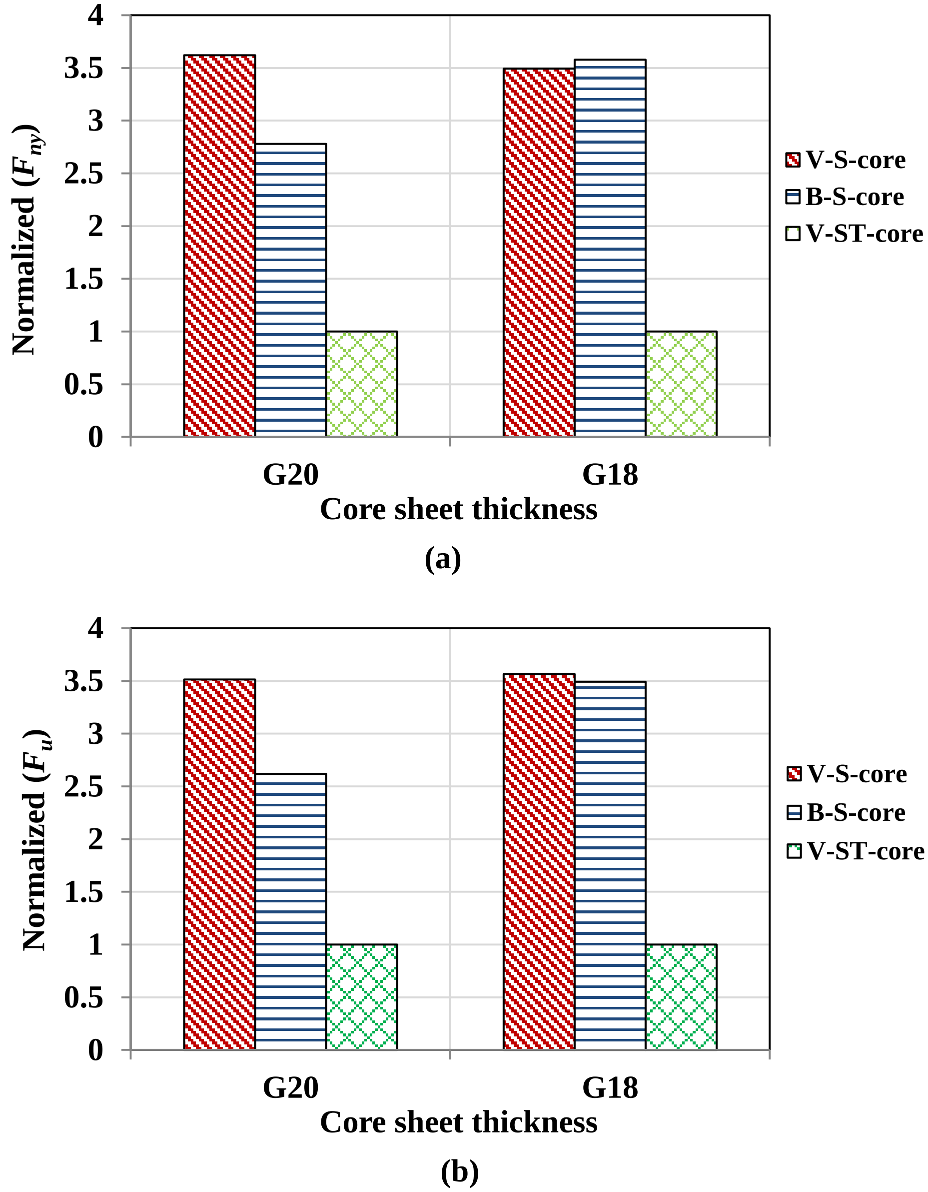

Fig. 3.9 Core configuration effect on nominal yield and ultimate loads

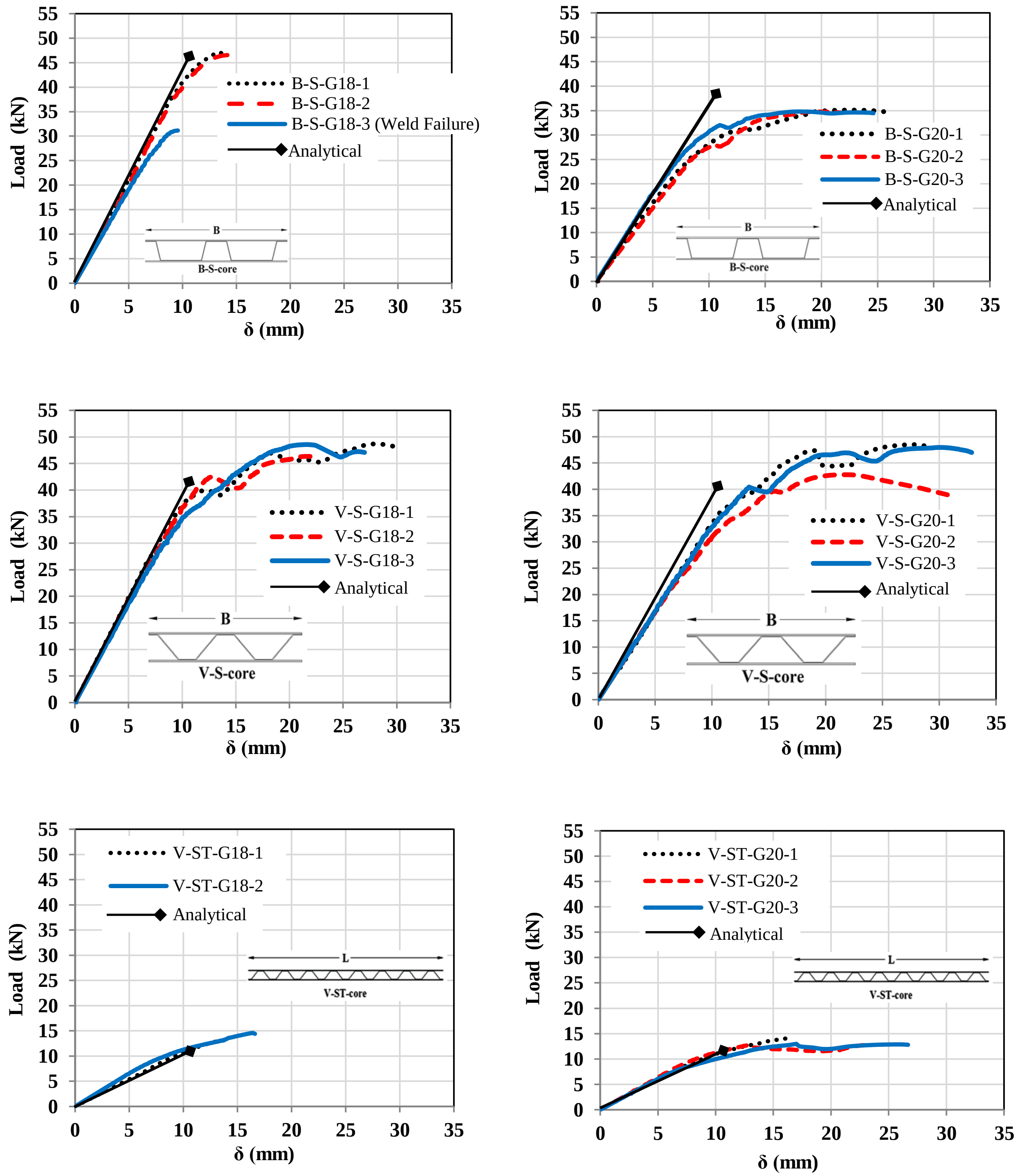

Fig. 3.10 Resistance functions for different core configuration

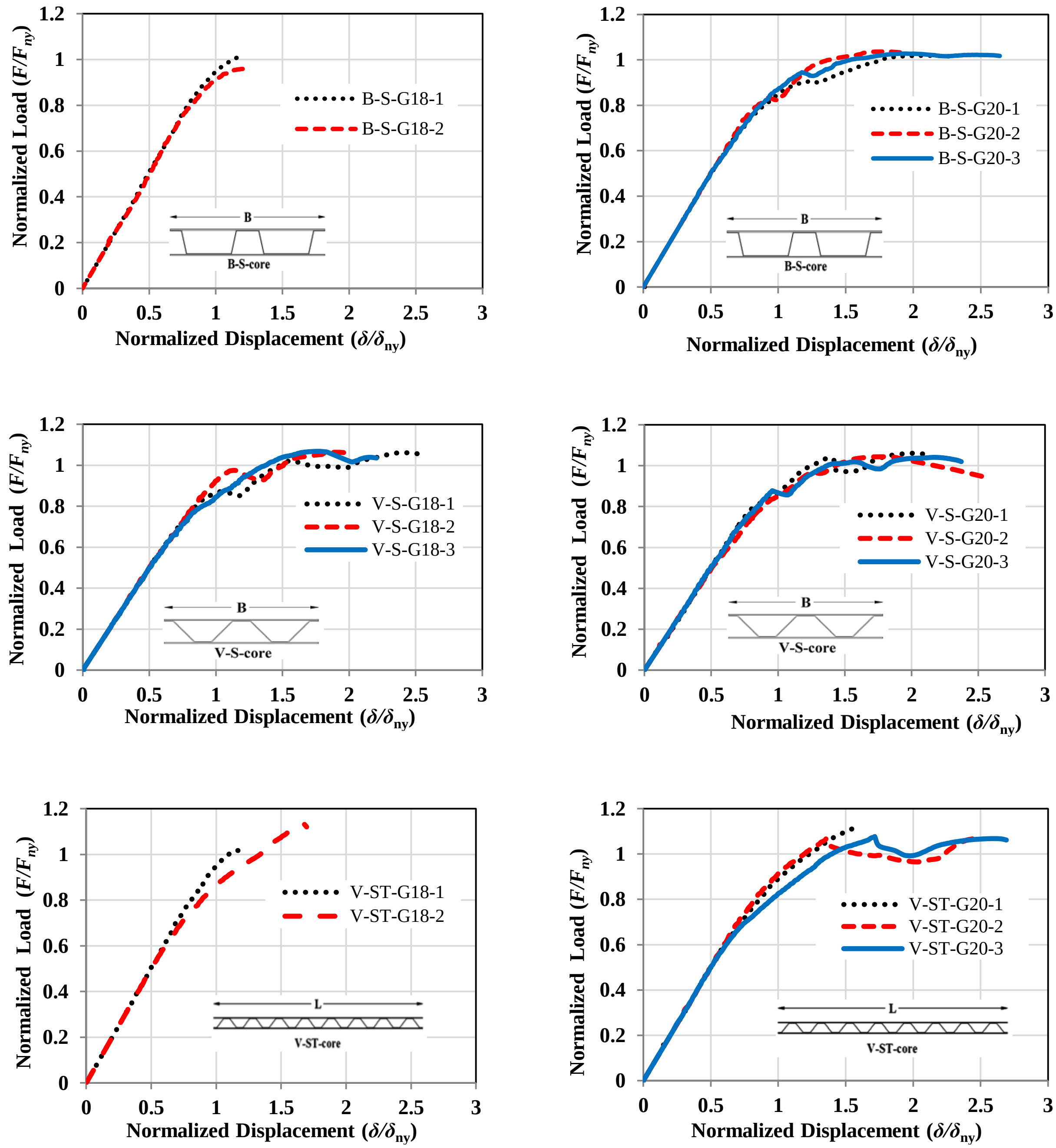

Fig. 3.11 Normalized resistance function

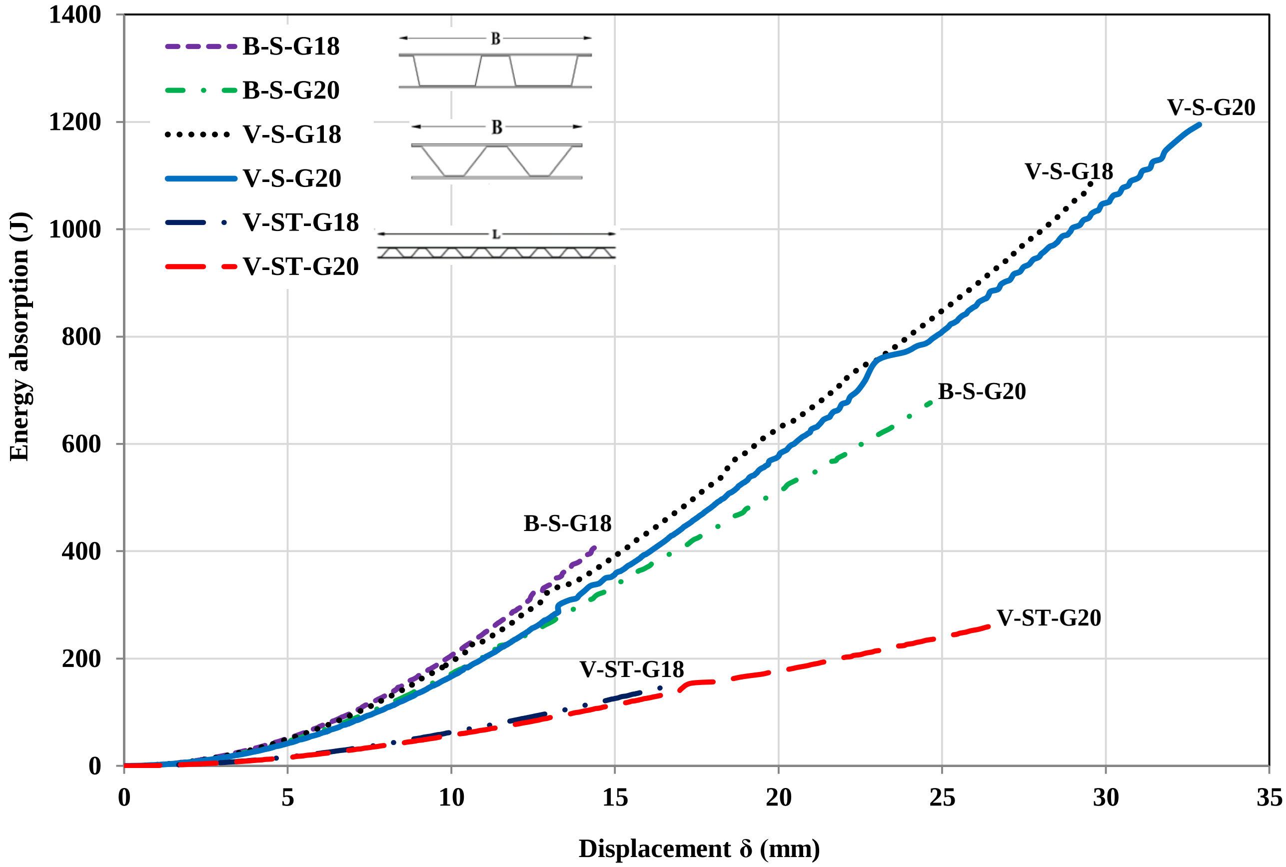

Fig. 3.12 Energy absorption-Displacement relationship

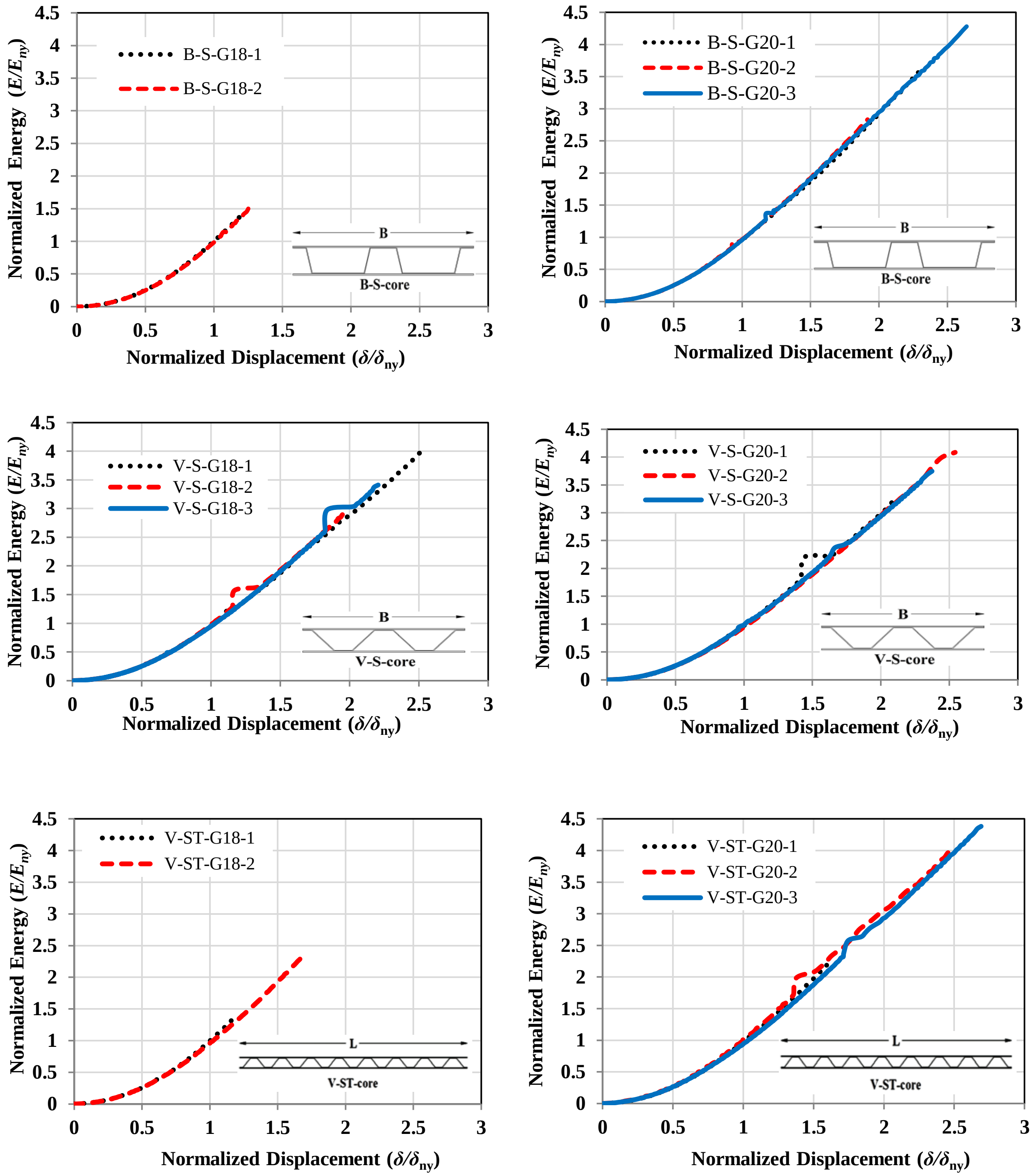

Fig. 3.13 Normalized energy absorption-displacement relationship

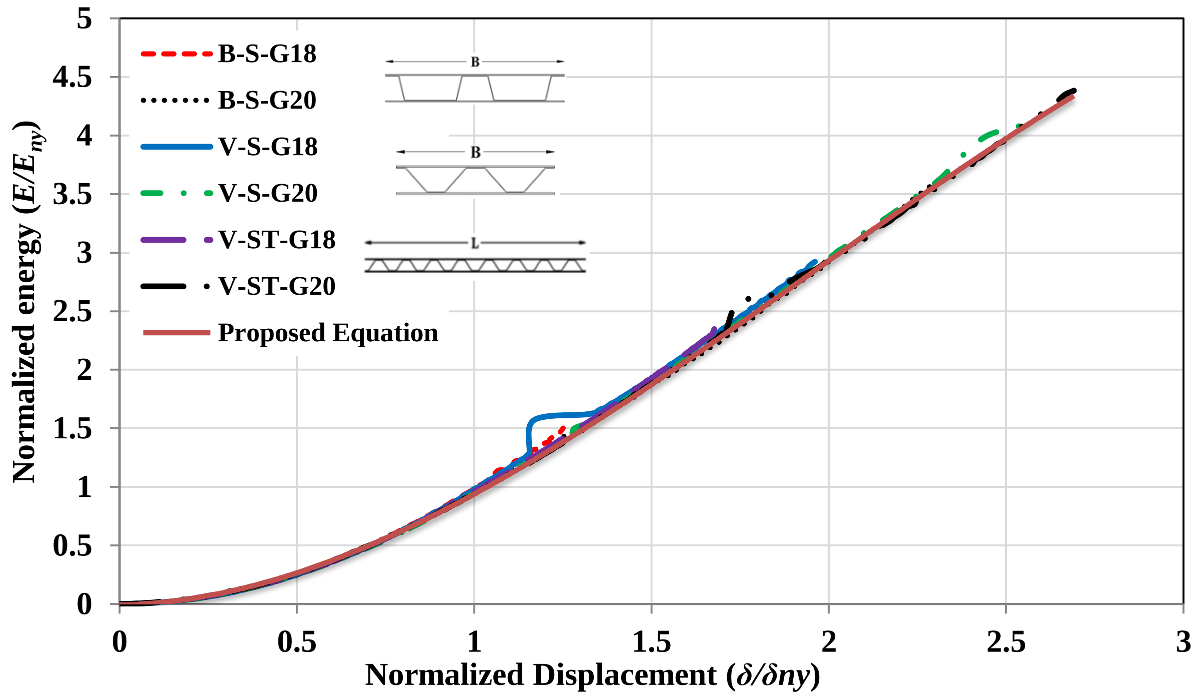

Fig. 3.14 Normalized energy absorption-Normalized displacement relationship

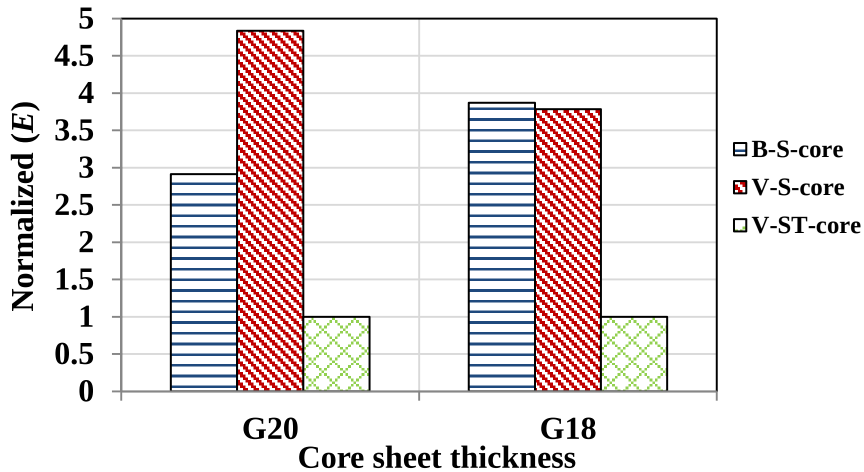

(a)

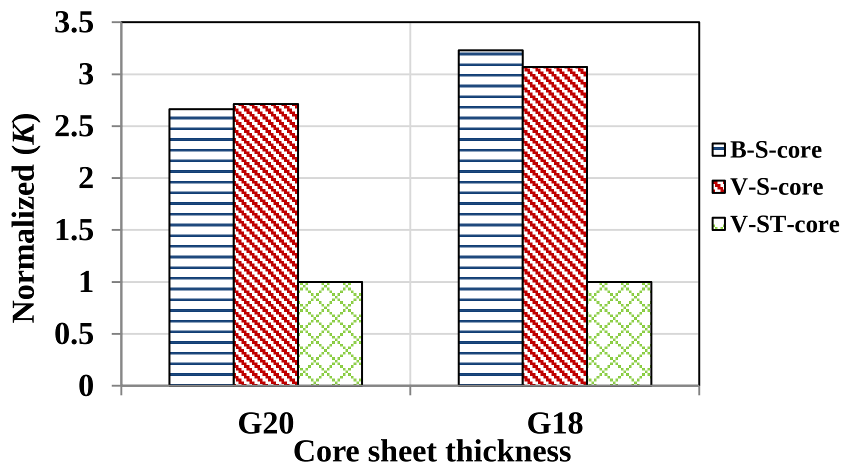

(b)

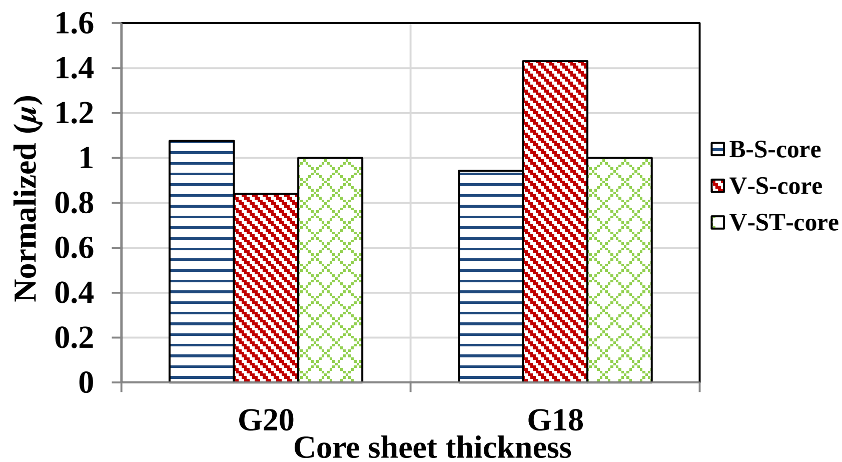

(c)

Fig. 3.15 Core configuration effect on (a) energy absorption, (b) stiffness, (c) ductility

CHAPTER 4: METALLIC SANDWICH PANELS PERFORMANCE ASSESSMENT UNDER QUASI-STATIC LOADING

4.1 ABSTRACT

The current study is part of a larger experimental program investigating the performance of novel lightweight cost effective cold-formed steel sandwich panels with different core configurations under quasi-static out-of-plane loading. In the body of literature addressing sandwich panels, no general methodology is provided to assess their non-elastic behavior under either static or dynamic loading. This study focuses on evaluating the quasi-static resistant function for the proposed sandwich panels to be used later in the context of blast resistant analysis, in compliance with the American (*ASCE/SEI 59-11*) and Canadian (*CSA/ S850-12*) modern design standards for blast resistant design, and is the first step in determining the panel resistance under blast loading. The tests involve twenty-one panels consisting of several configurations, each characterized by different core topology and deck profiles, considering *Uni-directional corrugated*, *Bi-directional corrugated*, and *X-core* sandwich panels. These particular core configurations were proposed to improve the strength, ductility, and energy absorption relative to the panel configurations previously investigated in the first stage of the experimental program. The modes of failure experienced by the test panels are identified and discussed. The load and deflection measurements recorded during the tests allow the characterization of each panel resistance function in terms of yield load, ultimate load, and the corresponding displacements. The influence of core configuration and sheet thickness on the panel ductility and energy absorption capacity is also examined. The conclusions and results of this study will assist the future development of lightweight cost–effective sandwich panels, to be used as sacrificial cladding for the blast protective structures.

KEYWORDS: Cold formed steel; Energy absorption; Flexural stiffness; Lightweight structure; Sandwich panel; Uniform loading.

4.2 INTRODUCTION

The complex design and relatively high fabrication costs of sandwich panel systems have limited their use in civil engineering applications. However, they are commonly used in the aerospace, naval, and transportation industries. Sandwich panels systems are utilized by these industries as a result of their advantages over conventional systems due to the sandwich effect, which results in a significant increase in stiffness with only a minor increase in weight due to separation of the face sheets by the core. As a result, numerous researchers have investigated the behavior of different sandwich panel systems under a variety of loads. The following discussion briefly highlights some of the more pertinent studies.

Libove and Hubka (1951) presented the elastic constants for corrugated-core sandwich plates. Allen (1969) introduced the analysis and design of sandwich systems. Noor (1996) performed an assessment of computational models for sandwich panels and shells and found that the global response can be predicted using a discrete three-layer model, however, for accurate determination of detailed response requires using a higher-order discrete three-layer model or predictor-corrector approaches. (Cheng et al. 2006) presented formulas to estimate the equivalent stiffness of sandwich structures having different core configurations using numerical analysis, (Fung et al. 1993, 1996) presented the elastic constants for C-Channel and Z-Channel core sandwich panels, and Lok et al. 2000) introduced a closed-form solution to evaluate the elastic constants of truss core sandwich panels. The homogenization method was employed for the analysis of corrugated core sandwich panels by Buannic (2003), and by Romanoff et al. (2007) for the analysis of web core sandwich beams. Magnucki (2013) studied the strength and buckling of aluminum alloy sandwich beams with corrugated core beams. Valdevit et al. (2004, 2006) studied prismatic core sandwich panel systems and compared their performance to honeycomb and truss core sandwich panels. In addition, failure maps were presented in order to achieve a near optimum design for a sandwich panel and to control its failure mode. Kujala (2005) presented a review for steel sandwich panels in marine applications, where laser welded sandwich panels offered a 30-50% weight reduction relative to conventional steel systems. (SANDCORE 2005, SANDWICH 2000) projects were conducted by the European Commission in order to develop a practice guide for sandwich structures in marine applications. Later, Romanoff et. al. (2006, 2007) discussed the analytical bending response of web core sandwich beams and plates. Jelovica et al. (2012, 2013) studied the effect of weld stiffness on the buckling strength, and the ultimate strength of corroded web core for the same sandwich panels presented by Romanoff et al. (2006)

4.3 COST EFFECTIVE SANDWICH PANEL SYSTEMS

Although there have been many studies carried out on sandwich panels, the drawback of the high-cost fabrication techniques, such as laser welding and selective laser melting (*SLM*) in addition to the expense of using specialized materials, remain. There is a demand for cost-effective sandwich panels, which use readily available materials and are simple to construct, for use in blast applications as sacrificial cladding. This type of cladding is used as a physical barrier between a non-sacrificial structure and a potential explosion.

The modern standards for blast resistant design of buildings ASCE/SEI 59-11 (ASCE 2011) and CSA/ S850-12 (CSA 2012), present a dynamic analysis model, in compliance with Biggs (1964), to assess the response of a structural component under blast loading. This analysis uses the static resistance of the component of interest and transformation factors, which account for the effect of high strain rate on the actual strength of the material and the dynamic to static strength ratio based on the failure mode (compression, flexure, etc.) in order to predict the dynamic resistance (ASCE 2011, CSA 2012, UFC 2008).

The elastic behavior of sandwich panels was initially investigated, using both Timoshenko and Euler-Bernoulli beam theories, by Allen (1969). Romanoff et al. (2007) subsequently employed the homogenization hypotheses to predict the elastic response. Nevertheless, these theories are not adequate to describe the non-elastic response, which is recommended to be used in the current blast design standards, as the design may rely on energy absorption beyond the elastic region. As such, experimental testing in order to obtain an accurate description of the static resistance of a structural component beyond the elastic response maybe required. Similar approach had been followed in previous studies to investigate related cold-formed steel elements by Salim et al. (2005), Bondok et al. (2013), and Whelan et al. (2015). The attractive characteristics of cold-formed steel in blast applications have been also highlighted in these efforts such as strength, ductility, and energy absorption.

The first stage of a comprehensive investigation on cost effective sandwich panel systems considered single layer corrugated core sandwich panels, in both the longitudinal and transverse direction, using different corrugation profiles (Khalifa et al. 2015a). The results and conclusions from the first stage of the investigation formed the basis for the design of the core configurations presented in this current study, which is focused on cost-effective sandwich panels with enhanced energy absorption and ductility characteristics.

The objective of the current study is to quantify the static resistance functions of various lightweight cost-effective sandwich panels using off-the-shelf (readily available) galvanized cold formed steel corrugated sheets in North America, which are typically used in floor/deck and roof construction. Twenty-one sandwich panels, representing different seven core configurations, *Uni-*

directional (Single) Corrugated, Bi-directional (Two-way) Corrugated and *X-core* sandwich panels were tested as shown in Fig. 4.1. All panels had the same outer dimensions and similar total mass - due to limitations of using off-the-shelf corrugated profiles.

4.4 EXPERIMENTAL PROGRAM AND TEST RESULTS

Currently, no general analytical method is available to accurately evaluate the behavior of sandwich panels beyond the elastic region under either static or dynamic loads. As such, the non-elastic performance of the proposed sandwich panels was evaluated experimentally, until the tested panel reached its maximum capacity.

4.4.1 Test Setup and Instrumentation

Fig. 4.2 shows the test setup used in the quasi-static testing of the proposed sandwich panels under uniform out-of-plane loading. Typically, the front face of a sandwich panel refers to the face sheet facing the load, while the back face refers to the rear face sheet. An air bag with an overall length of 935 mm was positioned between the front face of the sandwich panel specimen and a stiff self-reacting wall. The air bag allowed a uniformly distributed load to be applied to the front face of the sandwich panel, as shown in Fig. 4.2. A pressure control valve was used to regulate the applied pressure to the test specimen, while a pressure gauge was used to measure the pressure in the air bag.

Fig. 4.3a shows the supporting dimensions of the tested panel and the spacing of the four linear displacement potentiometer used to measure the deflection of the back face of the panel, where two potentiometers were used to measure the mid-span deflection at point (A and B), while the other two potentiometers (C and D) were used measure the deflection at the lower and upper quarter span respectively. All the tested panel specimens were simply supported by a pin at the top and a roller at the bottom of the specimen. The reaction forces at either end of panel specimen were measured using a total of four load cells as shown in Fig. 4.3b.

4.4.2 Test Specimens

A total of twenty one cold formed steel sandwich panels were tested in the current stage of the research, representing four different core configurations, as shown previously in Fig. 4.1, and two different core sheet thicknesses, as tabulated in Table 4.1. All investigated core configurations comprised of available off-the-shelf galvanized cold-formed steel corrugated sheets in North America, such as *B*, *V*, and *N* deck profiles, in order to achieve a cost-efficient panel system to be used as sacrificial cladding in blast applications.

The test matrix was designed to investigate the influence of the core configuration and the core sheet thickness on the performance of the sandwich panels. All panels were fabricated using galvanized cold-formed steel with approximately the same mass, and same dimensions of 304.8 mm (1 ft) width and 914 mm (3 ft) length and 76 mm (3 in) core depth. The face sheets had a constant thickness of *G14* (2.0 mm, 0.08 in), while the thickness of the corrugated profiles varied between *G20* (0.9 mm, 0.04 in) and *G18* (1.2 mm, 0.05 in). The corrugated sheets profiles used in the proposed core configurations were *B*, *V* and *N* profiles, where the *B* and *V* profiles had a depth of 38.1 mm (1.5 in) which were used to construct the double layer core for the *Bi-directional (B-T-core)* and *X-core (B-X-core and V-X-core)* sandwich panels, while the *N* profile had a depth of 76.2 mm (3.0 in) and was used in a single layer for the *Uni-directional Corrugated (N-S-core)* panels.

Each of the corrugated sheet profiles is characterized by the parameters shown in Fig. 4.4b, where (d) is the depth, ($\bar{B}$) is the total width, and (θ) is the angle of corrugation. Table 4.1 presents the values of these parameters characterizing the different profiles used. The nomenclature used to identify the tested specimens is shown in Fig. 4.4a.

4.4.3 Fabrication of Specimens

Metal Inert Gas (*MIG*) welding was employed to join the sandwich panel layers, which allowed a continuous weld to be achieved. Both Plug and Fillet welds were used to join the sandwich panel layers according to the core configuration. The welds were designed to ensure that failure of the tested sandwich panel occurred in panel layers prior to the initiation of weld (joint) failure.

The welds were equally spaced in the longitudinal direction at 165 mm (6.5 in) center to center, while the distance from the center of the weld to the edge of the sandwich panel was 44.5 mm (1.75 in). The spacing in the lateral direction varied according to the configuration dimensions and sheets profiles used in the core. Plug welds were designed to have a diameter of 12.5 mm (0.5 in), while the fillet welds were sized to be equal to the core sheet thickness and length of 51 mm (2.0 in).

4.4.4 Test Procedure

Each test started with positioning the panel in a vertical position centered along the mid-span of both supports and fastened by four steel clamps to the supporting plates of the pin and the roller supports. Subsequently, four displacement potentiometers were fixed to the back face of the tested panel specimen.

The air bag was then located between the front face of the panel and the attached self-reacting frame, to achieve continuous contact between the air bag and the front face sheet. A pressure of rate 0.34 kPa/s (0.05 psi/s) was then applied to the tested panel by inflating the air bag using a controlled compressed air supply until the complete failure of the panel.

4.4.5 Material

Cold-formed steel sheets were used in the construction of the sandwich panel specimens. The material properties of the sheets were required as input in an analytical model introduced by Khalifa et al. (2015). The stress-strain relationships for all sheet types considered in this study were obtained from uniaxial tensile tests. Five coupons were obtained from each sheet type and tested, following the regulations of (ASTM E8/E8M-13a) standard. The average values for the yield stresses and elastic modulus are presented in Table 4.2.

4.5 TEST RESULTS

As the proposed test panels are for use as sacrificial cladding systems in blast applications, the purpose of the tests is to evaluate the non-elastic performance of these panels until they reach their maximum load carry capacity, which is defined as the dominant failure. As such, all observed deformations and failure modes up to the dominant failure are discussed in detail.

After each test, the test specimen was examined and the failure mode(s) were identified. No weld failure was observed except for specimen *B-X-G18-1*. Based on the preliminary design, web crippling within the bearing region was expected to be followed by a dominant failure, either flexural (yield) failure or shear failure. The following sections will present the observations and details of failure mode(s) for the different core configurations considered in this study.

4.5.1 V-X-core

Fig. 4.5 shows the failure modes for *V-X*-core sandwich panels, which initiated with web crippling within the support regions (as seen in Fig. 4.5a and 4.5b), followed by flexural induced yielding and subsequent local buckling of the front face sheet, which resulted in the failure of this core configuration. Web crippling was initiated by the onset of buckling in the lower third of the core webs near the support. As the applied load was increased the extent of buckling increased until the web contacted the back face of the sandwich panel. Subsequently, a plastic hinge was observed to form near the mid-span of the specimen, at a distance of approximate 83 mm from the mid-span, as shown in Fig. 4.5c. The shift in the plastic hinge formation location away from the mid-span is in part due to the influence of shear force effects in combination with flexural effects, and imperfections introduced during web crippling of the tested panel. This shift was observed to occur either above or below the mid-span line direction of the tested panels, as shown in Fig 5(c).

4.5.2 B-X-core

The *B*-*X*-core comprised of two layers of *B* corrugated sheet profile forming the *X*-core. The initiation of web crippling was followed by global buckling due to shear failure, as illustrated in Fig. 4.6. It was observed that the initiation of buckling in the lower webs of the *B*-*X*-core resulted in the occurrence of rotations at the core profile corners of the same layer (Fig. 4.6a (i)). Subsequently, the buckled webs then made contact with back face of the sandwich panel (Fig. 4.6a (ii)), while the sides of the core expanded outwards leaving a slightly curved front face, as seen in Fig. 4.6b. The dominant failure for the *B*-*X*-core was shear failure, where global buckling was observed to occur at a distance of approximately (210 mm) from either top or bottom support.

4.5.3 N-S-core

Failure of the *N-S*-core sandwich panels was dominated by shear failure, with the occurrence of web crippling in the bearing regions, where the web crippling progression was found to occur as shown in Fig. 4.7a and Fig. 4.7b. Minor web crippling was initiated due to bearing forces accompanied with small rotations at the back corners of the corrugated core. Furthermore, the web crippling increased in the lower third of the core webs forming a plastic hinge, as shown in Fig. 4.7a (ii), accompanied with the section depth decreasing until the lower buckled length contacted the back face (Fig. 4.7a (iii)). The inner webs formed an interlocking triangular shape, as shown in Fig. 4.7a (iv), which led to an increase in the resistance due to the geometrical non-linearity. As the applied pressure increased, the section exhibited global buckling due to shear within an approximate distance of (110 mm) from the end supported, resulting in the panel failure.

4.5.4 B-T-core

The *Bi-directional* (*B-T*-core) sandwich panels had a two way corrugated core using the *B* deck profile, where the combination of the upper transverse and the lower longitudinal corrugated core layers, resulted in efficient stiffness to be obtained in both directions for this core configuration.

The *B-T*-core sandwich panels experienced local buckling, yielding, and web crippling in a complex manner, as shown in Fig. 4.8. Yielding, resulting in the formation of a plastic hinge was observed at mid-span, which was induced by flexure. Moreover, the tensile diagonals of the upper corrugated layer in the core (see Fig. 4.8b) started to incline outwards from the mid-span line, while the compression diagonals were compressed due to the relative displacement between the layers of the sandwich panel, where an obvious relative displacement occurred between the elastic line of the front and back face sheets. Additionally, web crippling was observed at the support zone in the webs of both the upper and lower layers of the core, as shown in Fig. 4.8c and Fig. 4.8d, which is accompanied by rotations at the corrugated sheet base corners. Local buckling simultaneously occurred in the lower layer webs under the contact points with the compression diagonals of the upper layer from both ends towards the mid-span of the panels in both directions, as shown in Fig. 4.8b.

4.6 ANALYTICAL PREDICTION

An analytical model (Khalifa et al. 2015) is used in the current study to predict the failure mode(s) of the tested core configurations and their elastic properties. It should be noted that the focus of the current study is to quantify the resistance function of the proposed core configurations up to failure. The model accounted for the yield flexural capacity, shear strength, elastic flexure stiffness and critical web crippling loads. The current proposed core configurations were expected to experience significant deformations due to either web crippling (*B*-*X*-core, *V*-*X*-core, and *N*-*S*-core), or compression buckling of the front face (*B*-*T*-core).

The critical web crippling load is calculated using the following equation (CSA S136-07 2007, AISI 2001):

$$P_n = Ct^2 f_y (sin\,\theta)\left(1 - C_R\sqrt{\frac{R}{t}}\right)\left(1 + C_N\sqrt{\frac{N}{t}}\right)\left(1 - C_H\sqrt{\frac{h}{t}}\right) \qquad (1)$$

where, P_n is the nominal computed web crippling load per web, t is the web thickness, R is the inside bend radius, N is the bearing length, h is the clear distance between the flanges, and (C,C_R,C_N,C_H) are coefficients values that depend on support condition, load case, and location of the reaction. The critical buckling load for the front face was calculated using the Euler buckling equation:

$$F_b = \frac{\pi^2 E_f I}{L^2} \qquad (2)$$

where F_b is the critical buckling load, and L is the buckling length. Further details on the model can be found in Khalifa et al. (2015). The main results of the analytical model will be presented and discussed in the following sections, where all the predicted critical loads are expressed as the equivalent concentrated load that equals the uniform distributed pressure on the front face of the panel.

4.7 ANALYSIS OF TEST RESULTS

The experimental results showed, in general, a superior post-elastic performance for the tested configurations compared with that reported previously by Khalifa et al. (2015a). The current specimens showed significant increase in both ductility and energy absorption, while the static resistance function was evaluated for each of the tested core configurations up to the dominant failure. The performance of the panels is described in terms of the yield load, ultimate capacity, ductility, flexure elastic stiffness and energy absorption, as follows:

4.7.1 Yield Load and Ultimate Capacity

The quasi-static resistance functions of all tested core configurations have been assessed, however as discussed previously, different modes of failure were observed for the various core configurations investigated, which was found to be consistent with the analytical predictions. As the non-elastic behavior of the different configurations started due to different critical load cases (i.e web crippling, front face buckling, etc.), a single criterion is introduced and used to compare the different core configurations (Khalifa et al. 2015a). The behavior of the sandwich panels was assumed to be elastic perfectly-plastic with equal energy absorption calculated by integrating the actual load-displacement relationship up to failure point (E_f), as shown in Fig. 4.9. Where, (F_{ny}) is the nominal yield load, which is defined as the load at which the panel begins to deform plastically along the idealized load-displacement relationship, (K) is the elastic stiffness constant, which is determined from the actual load-displacement relationship, (F_f) is the failure load, which is defined as the load prior to the rapid loss of panel capacity (see Fig. 4.9). The rapid loss of capacity occurred as the testing was conducted under load control and the compressibility of the air that used to apply the pressure on the front face of the panel. As a result, the descending branch of each load-displacement relationship is not reported. Finally, (δ_{ny}) and (δ_f) are the corresponding displacements for the nominal yield load and the failure load, respectively. The value of (F_{ny}) was calculated for each of the tested panels, according to its energy absorption up to failure (E_f), presuming an idealized elastic-perfectly plastic resistance function.

The mean and *COV* values for F_{ny} were calculated for the tested configurations and are presented in Table 4.3, in addition to the predicted analytical critical loads. The analytical model results shows a difference than the experimental measured values, which is postulated to be the geometrical nonlinearities exhibited by the panels through the testing, in addition that F_{ny} is computed based on energy dissipation of the resistance function to the complete failure. As expected, (F_{ny}) was found to be dependent on both the core sheet thickness and the core configuration, where the geometrical parameters of the different deck profile contributed to the stiffness and strength of the tested sandwich panels. It was noted that the maximum *COV* value of 5.6 % was found to be for the *N-S-G18* configuration

The core configuration influenced (F_{ny}), as seen in Fig. 4.10a. For the *G20* core sheet thickness panels, the highest mean value for (F_{ny}) was exhibited by the *V-X*-core, followed by the *N-S*-core with a difference of 8.64 %, while the lowest mean value for (F_{ny}) was for the *B-T*-core configuration. Furthermore, the (F_{ny}) values were normalized in order to make comparisons between the different configurations easier, as shown in Fig. 4.10a, where the *V-X-G20* was found to have a (F_{ny}) value that was 2.6 times greater than *B-T-G20*. On the other hand, for *G18*, the highest mean value for (F_{ny}) was achieved by the *B-X-G18* core configuration, which was found to be 1.8 times greater than *B-T-G18* configuration and 1.1 times greater than the *N-S-G18* configuration. It is noticed that, the lowest F_{ny} value was obtained by the *B-T*-core configuration regardless the core sheet thickness.

Increasing the core sheet thickness from 0.9 mm to 1.2 mm resulted in an increase in (F_{ny}) by 68.7%, 45.7% and 13.4 % for the *B-T*-core, *B-X*-core and *N-S*-core configurations, respectively. The increase in (F_{ny}) for the configurations with higher core sheet thickness is related to the contribution of core sheet thickness to the second moment of area.

The ultimate capacity load (F_u) was also affected by both the core configuration and the core sheet thickness. The mean and *COV* values of the ultimate load capacity (F_u) are presented in Table 4.3. Increasing the core sheet thickness for same configuration from 0.9 mm (*G20*) to 1.2 mm (*G18*) was found to increase the mean value of (F_u) by 35.4 %, 59.3% and 23.0 % in the *B-X*-core, *B-T*-core, and *N-S*-core configurations, respectively. The above results indicate that a significant increase in both the nominal yield load and the ultimate capacity for the *B-T*-core configuration can be achieved with a minor increase in the core sheet thickness.

Fig. 4.10b shows the effect of core configuration on the ultimate capacity (F_u). For the *G18* core configurations, the highest (F_u) was achieved by *N-S-G18*, while the lowest (F_u) was obtained for *B-T-G18*. The (F_u) for *N-S-G18* was found to be 1.6 times greater than that for *B-T-G18* and 1.1 times greater than that reached by *B-X-G18*. However, for the *G20* configurations, both *N-S-G20* and *V-X-G20* achieve high values for the ultimate capacity, while the lowest value of (F_u) was obtained for the *B-T*-core. Fig. 4.10b shows that (F_u) for the *N-S-G20* was 2.1 times greater than that for *B-T-G20*, and 1.2 times greater than that for *B-X-G20.*

In general, from a strength perspective, the *N-S*-core exhibited the highest ultimate capacity value, while the *B-T*-core had the lowest value. As such, *V-X*-core and *N-S*-core configurations are recommended for applications where strength is the primary concern.

4.7.2 Measured Load-Displacement Relationship

Fig. 4.11 shows the measured and the analytical load-displacement relationship for all the panel specimens, where good agreement can be seen between the analytical and the experimental relationship (up to yield). The experimental load for each curve was computed by summing the output from the four load cells. The load-displacement curves for a particular core configuration are, in general, found to be in good agreement, with the exception of *B-X-G18-1* (which experienced weld failure) and *N-S-G18-1* (due test equipment related issues).

The performance of the core configurations beyond the elastic region was found to vary substantially. For example, the *Bi-directional* (*B-T*-core) sandwich panels showed a nonlinear hardening plateau beyond slight softening following the elastic limit. Its orthogonal core configuration and the low rate of loading allowed these panels to redistribute the load internally in its layers through failure propagation, until it reached the displacement limit for the test setup.

The *B-X*-core configurations exhibited a hardening plateau with different slopes, which was affected by the core sheet thickness, (as seen in Fig. 4.11), as the post yield stiffness for the *B-X-G18* panels was lower than that exhibited by the *B-X-G20* panels. On the other hand, the *V-X*-core showed increased load capacity after a small initial reduction in force at approximately δ =15 mm due to web crippling, as shown in Fig. 4.11. Subsequently, it experienced a ductile type behavior followed by softening until it reached the failure load.

Finally, the *N-S*-core configuration, which exhibited the highest ultimate capacity, exhibited ductility through various stages of web crippling followed by hardening until reaching the failure load. For further insight into the influence of core configuration, a normalized load-displacement relationship was computed and plotted (see Fig. 4.12) where the load for each panel was normalized by its nominal yield load (F_{ny}), and the displacement was normalized by its nominal yield displacement (δ_{ny}). The *B-T*-core and *N-S*-core configurations reached a maximum normalized load (F_u/F_{ny}) of approximately 1.3 for both *G18* and *G20* core sheet thicknesses, while it was approximately 1.1 for *V-X-G20* and *B-X-G18*, which indicates that the *B-T*-core and *N-S*-core configurations showed a significant increase in strength beyond the nominal yield load until ultimate capacity.

4.7.3 Energy Absorption

The energy absorption is of interest as it plays an important role in determining the efficiency of employing the sandwich panels in dynamic applications, (Kepler and Hansen 2007, Fatt and Surabhi 2012, Tarlochan et al. 2012). The energy absorption is defined as the area under load-displacement curve, considering material and geometric nonlinearities up to the failure point. Energy absorption depends on the cross-section topology, loading and material type (Tarlochan et al. 2012).

Energy absorption occurred due to plastic deformations in the panel layers, where web crippling and global buckling were observed to occur. The total energy absorbed was determined via numerical integration of the experimental load-displacement curves. The mean and *COV* values of energy absorption up to the nominal yield displacement (E_{ny}) are presented in Table 4.4. The maximum *COV* value of (E_{ny}) was found to be 16% for *N-S-G18*, while the minimum value was found to be 2.3% for *B-X-G18*.

The energy absorption – displacement relationship is plotted for various configurations in Fig. 4.13, where all curves had a relatively smooth increasing trend, except for the *N-S*-core configuration, where fluctuations were observed in the energy absorption curves due to web crippling. Furthermore, to express how the panels absorbed energy relative to the nominal yield energy absorption (E_{ny}), the normalized energy absorption was also considered for the tested configurations, as shown in Fig. 4.14. The normalized energy- normalized displacement curves are found to have a consistent trend when each core configuration is considered separately. Subsequently, the normalized energy absorption – normalized displacement relationship for the various configurations is plotted in Fig. 4.15. In addition, a proposed equation was obtained using nonlinear regression to represent the normalized energy as a function in the normalized displacement as follows:

$$\left(\frac{E}{E_{ny}}\right) = 3.5 * 10^{-3} \left(\frac{\delta}{\delta_{ny}}\right)^3 + 1.6 * 10^{-2} \left(\frac{\delta}{\delta_{ny}}\right)^2 + 1.47\left(\frac{\delta}{\delta_{ny}}\right) \quad (3)$$

An increase in core sheet thickness was found to increase the energy absorption value. An increase of 0.3 mm in the core sheet thickness from 0.9 mm to 1.2 mm was found to increase the energy absorption by 24.3%, 72.3%, and 7.2% for *B-X*-core, *B-T*-core, and *N-S*-core sandwich panels, respectively.

4.7.4 Evaluation of Flexure Elastic Stiffness

Increasing the flexure elastic stiffness through a minor increase in the weight of the structural element is an advantageous characteristic of sandwich panel systems. As a result of this particular characteristic it has been the focus of numerous studies, which have included the effect of different core configurations (Fung et al. 1993, Lok et al. 2000).

The elastic flexure stiffness of the proposed core configurations was evaluated using the experimental test results. The elastic flexure stiffness is defined in this study as the slope of the linear portion of the measured load-displacement curve in the elastic region. The mean and corresponding *COV* values for the experimental elastic flexure stiffness, in addition to the analytical values, are presented in Table 4.5, where the maximum *COV* value was found to be 10.5 % for *B-X-G20* configuration, while the minimum value was 1.4 % for *B-T-G18* configuration.

As expected, both of the core sheet thickness and the core configuration were found to influence the elastic flexure stiffness. Increasing the core sheet thickness from *G20* (0.9 mm) to *G18* (1.2 mm) for same core configuration increased the elastic flexure stiffness by 32.9 %, 47.6%, and 12.8% in the *B-X*-core, *B-T*-core, and *N-S*-core configurations, respectively. The largest elastic flexure stiffness value was achieved by *N-S-G18* with a value of (6.34 *kN/mm*), while the lowest value (1.93 *kN/mm*) was obtained by *B-T-G20.*

Fig. 4.16a shows the influence of core configuration on the flexure elastic stiffness. For the *G18* core configurations, the elastic flexure stiffness of *N-S-G18* was found to be 2.2 times greater than the elastic stiffness for *B-T-G18*. For *G20* core configurations, the *N-S*-core attained the highest elastic stiffness value and was found to be 2.9 times greater than the lowest value exhibited by *B-T-G20*. The high elastic stiffness of the *N-S*-core configuration was due to the cross section profile of its core, with webs directly joining the front and back faces and its steep corrugation angle, which results in a higher second moment of area.

4.7.5 Yield Displacement and Ductility

The nominal yield displacement (δ_{ny}) is defined as the displacement related to the nominal yield force in this study. The analytical displacements corresponding to the predicted critical loads and the (δ_{ny}) mean and *COV* values are shown in Table 4.6, where the maximum *COV* was found to be 10.4 % for *B-X-G20*, and the minimum *COV* was found to be 1.4% for *B-T-G18*.

The (δ_{ny}) was also affected by both the core configuration and the core sheet thickness, where an increase of 0.3 mm in the core sheet thickness was found to increase the value of (δ_{ny}) by 14.2% and 14.0% for the *B-X*-core, *B-T*-core panels, respectively, while (δ_{ny}) increased by only 0.6% for the *N-S*-core configuration

The core configuration had an effect on the value of (δ_{ny}), where the maximum mean value for the *G18* core configurations was found to be 11.3 mm exhibited for *B-X-G18*, while the lowest mean value was 7.6 mm for *N-S-G18*. Following the same trend for *G20* configurations, the maximum mean value of (δ_{ny}) was found to be 9.9 mm for *B-X-G20*, while the lowest mean value was 7.57 mm for *N-S-G20*.

Ductility (μ) is defined as the ratio of the maximum displacement at failure (δ_f) to the yield displacement (δ_{ny}). Modern design standards (especially for blast resistance) recognize the importance of ductility as it indicates the ability of the structure element to undergo large deformations before failure.

The mean and *COV* values of ductility for the tested configurations are presented in Table 4.6, where a maximum *COV* for ductility of 15.6% was calculated for *N-S-G20* while *N-S-G18* had the minimum *COV* value of 0.6%. The proposed configurations showed a significant increase in ductility compared to the ductility exhibited by configurations investigated by Khalifa et al.

(2015a), where the maximum value of ductility was 2.3, while the maximum value of ductility exhibited in this study was 14.24 by *B-T-G20* configuration.

Fig. 4.16 (c) shows the influence of core configuration on the ductility exhibited by the test specimens. For the *G18* configurations, the maximum mean value of ductility presented by *B-T-G18* was found to be 2.4 times greater than the value exhibited by *B-X-G18*. For the *G20* configurations, the maximum mean ductility value was also achieved by the *B-T*-core type, which was found to be 4.5 times more than the mean value of ductility developed by *V-X-G20*. It is noted that even with different core sheet thicknesses the *B-T*-core is found to have the most ductile behavior within the proposed core configurations.

Finally, increasing the core sheet thickness was found to have an inversely effect on ductility of the tested panels, where increasing the core sheet thickness from 0.9 mm to 1.2 mm decreased the ductility by 20.2%, 35.3%, and 13.1% for *B-X*-core, *B-T*-core, and *N-S*-core sandwich panels, respectively.

4.8 CONCLUSIONS

The potential use of available (off-the-shelf) deck profiles in the *North America* as the core of sandwich panels has been investigated. A total of twenty one sandwich panels were tested under uniform out-of-plane loading, considering *Uni-directional Corrugated, Bi-directional Corrugated*, and *X-core* configurations and two different core sheet thicknesses. Several of the proposed core configurations exhibited substantial ductility. The failure modes were determined and the details were discussed, and the main findings can be summarized as follows:

A) The sandwich panels can be constructed using a relatively time and cost effective fabrication technique. The welds were sufficient to sustain the loading up to the failure of the sandwich panels without rupture, except for one tested panel.

B) The analytically predicted values were found to be within acceptable agreement with the experimental findings.

C) The dominant failure mode for the tested configurations was shear failure after web crippling occurred, except for the *B-T*-core configuration, which failed by flexure yielding at the mid-span, followed by a complex redistribution to the load through local buckling and web crippling.

D) The nominal yield load (F_{ny}) was affected by both the core configuration and core sheet thickness. The highest mean value for the (F_{ny}) was exhibited by *B-X-G18*, which was found to be 1.8 times greater than the lowest mean value exhibited by *B-T-G18*. Moreover, increasing the core sheet thickness from *G20* to *G18* was found to increase (F_{ny}) by 45.7%, 68.73% and 13.37 % in the *B-X*-core, *B-T*-core and *N-S*-core sandwich panels, respectively.

E) Core sheet thickness also had an influence on the ultimate capacity, where the mean values of (Fu) increased by 35.4 %, 59.3% and 23.0 % in the B-X-core, B-T-core, and N-S-core configurations, respectively, corresponding to the increase of the core sheet thickness from G20 to G18. The ultimate capacity was also influenced by core configuration, which has been illustrated by comparing values for various configurations for a given core sheet thickness. For the G18 core configurations, the highest Fu exhibited by N-S-G18 was found to be 1.6 times greater than the lowest value exhibited by B-T-G18. For the G20 configurations, the highest values for the ultimate capacity (Fu) were achieved by N-S-G20 and V-X-G20, which were found to be 2.1 times greater than lowest value exhibited by B-T-G20.

F) The core configuration had a significant effect on the ductility offered by the different configurations. For the *G20* configurations, the *B-T*-core presented the maximum mean value of ductility and it was found to be 4.5 times greater than that achieved by the *V-X*-core configuration. Increasing the core sheet thickness from 0.9 mm to 1.21mm was found to decrease the ductility by 20.2%, 35.3%, and 13.1% for *B-X*-core, *B-T*-core, and *N-S*-core sandwich panels, respectively.

G) The energy absorption was found to increase by increasing the core sheet thickness, where an increase of 0.3 mm in the core sheet thickness was found to increase the energy absorption by 24.3%, 72.3%, and 7.2% for *B-X*-core, *B-T*-core, and *N-S*-core sandwich panels, respectively.

H) The normalized energy curves were found to be in a good consistency when considering all tested configurations. Subsequently, a proposed equation was obtained to represent the normalized energy as a function in the normalized displacement.

The experimental results and conclusions of this study will be used for the development of lightweight cold-formed steel sandwich panels, to be employed as a sacrificial cladding for blast applications.

4.9 Appendix Notation

COV = Coefficient of variance

$\overline{B}$ = Corrugated core width

d = Corrugated core depth

E= Energy absorption

E_f = Energy absorption up to failure

E_{ny} = Energy absorption up to nominal yield load

F = Applied load

F_u = Ultimate capacity

F_{ny} = Nominal yield load

F_f = Failure load

K = Elastic flexure stiffness

δ = Displacement

δ_{ny} = Nominal yield displacement

δ_f = Displacement corresponding to failure load

θ = Angle of corrugation

μ = Ductility

4.10 REFERENCE

Allen, H.G. and Neal, B. G. (1969) "Analysis and Design of Structural Sandwich Panels." Pergamon, Press London.

American Socity of Civil Engineers (ASCE) (2012). "Blast Protection of Buildings." ASCE/SEI 59-11, Reston, Virginia.

Biggs, J. M. (1964). "Introduction to Structural Dynamics." New York, USA: McGraw-Hill Inc.

Bondok, D., Salim, H., and Agee, B. (2013). “Improved Static Resistance and Failure Mechanisms of Conventional Cold-Formed Steel Stud Walls.” Journal of Performance of Constructed Facilities, 10.1061/(ASCE)CF.1943-5509.0000525,04014069.

Buannic, P. C., and Quesnel, T. (2003). "Homogenization of Corrugated Core Sandwich Panels." Jpurnal of Composite Structures, Vol. 59, pp. 299-312.

Canadian Standards Assiocation (CSA) (2012). "Design and Assessment of Buildings Subjected to Blast Loads." CSA S850-12. Mississauga, Ontario, Canada.

Cheng, Q. H., Lee, H. P., and Lu, C. (2006). "A Numerical Analysis Approach for Evaluating Elastic Constants of Sandwich Structures with Various Cores." Journal of Composite Structures, Vol. 74 (2),pp. 226-236.

Fung, T., Tan, K., and Lok, T. (1994). "Elastic Constants for Z-Core Sandwich Panels." ASCE Journal of Structural Engineering, Vol. 120(10), pp. 3046–3055.

Fung, T., Tan, K., and Lok, T. (1996). "Shear Stiffness D_{Qy} for C-Core Sandwich Panels." ASCE Journal of Structural Engineering, Vol. 122(8), pp. 958–966.

Jelovica, J. , Romanoff, J. ,Ehlers, S. ,and Aromaa, J. (2013). "Ultimate Strength of Corroded Web-Core Sandwich Beams." Journal of Marine Structures, Vol. 31, pp.1-14.

Jelovica, J., Romanoff, J., Ehlers, S. and Varsta, P. (2012). "Influence of Weld Stiffness on Buckling Strength of Laser-Welded Web-Core Sandwich Plates." Journal of Constructional Steel Research, Vol. 77, pp. 12-18.

Kepler, J. A., and Hansen, M. R. (2007). "Numerical Modeling of Sandwich Panel Response to Ballistic Loading Energy Balance for Varying Impactor Geometries." Journal of Sandwich Structures and Materials, Vol. 9 (6), pp. 553-570.

Khalifa, Y. A., Tait, M. J., and El-Dakhakhni, W.W. (2015). "Out-of-plane Behaviour of Lightweight Metallic Sandwich Panels" ASCE Journal of Performance of Constructed Facilities, submitted for publication.

Kujala, P. and Klanac, A. (2005). "Steel Sandwich Panels in Marine Applocations." Brodogradnja, Vol.56, pp. 305–314

Lok, T. and Cheng, Q. (2000). "Elastic Stiffness Prorerties and Behavior of Truss-Core Sandwich Panel." Journal of Structural Engineering, Vol. 126. pp. 552-559.

Libove C., Ralph E. Hubka (1951). "Elastic Constants for Corrugated Core Sandwich Plates." National Advisory Committee for Aeronaytics, Technical Note 2289, Washington, USA.

Magnucki, K., Jasion, P., Krus, M., Kuligowski, P. and Wittenbeck, L. (2013). "Strength and Buckling of Sandwich Beams with Corrugated Core." Journal of Theoretical and Applied, Vol. 51, pp. 15-24.

Noor, A. K. and Burton, W. S. (1996). "Assessment of Computational Models for Sandwich Panels and Shells." Journal of Computer Methods in Applied Mechanics and Engineering, Vol. 124, pp. 125-151.

Hoo-Fatt, M.S. and Surabhi, H. (2012). "Blast Resistance and Energy Absorption of Foam-Core Cylindrical Sandwich Shells Under External Blast." Journal of Composite Structures, Vol. 94(11), pp. 3174-3185.

Romanoff, J. and Varsta, P. (2006). "Bending Response of Web-Core Sandwich Beams." Composite Structures, Vol. 73 (4), pp. 478-487.

Romanoff, J. and Varsta, P. (2007). "Bending Response of Web-Core Sandwich Plates." Composite Structures, Vol. 81 (2), pp. 292-302.

Romanoff, J., Varsta, P., and Klanac, A. (2007). "Stress Analysis of Homogenized Web-Core Sandwich Beams." Composite Structures, Vol. 79 (3), pp. 411-422.

Romanoff, J., Varsta, P., and Remes H. (2007). "Laser-Welded Web-Core Sandwich Plates Under Patch Loading." Journal of Marine Structures, Vol. 20 (1-2),pp. 25-48.

Salim, H. A., Muller, P., and Dinan, R. (2005). “Response of Conventional Steel Stud Wall Systems Under Static and Dynamic Pressure.” Journal of Performance of Constructed Facilities, 10.1061/(ASCE)0887-3828(2005)19:4(267),267–276.

SANDCORE (2005). " Best Practice Guide for Sandwich Structures in Marine Applications " SAND.CORe, NewRail University of Newcastle upon Tyne.

SANDWICH (2000). "Advancd Composite Sandwich Steel Structures." The European Commission Under 5th Framework Programme Growth KA III.

Tarlochan, F., Rameshb, S., and Harpreet, S. (2012). "Advanced Composite Sandwich Structure Design for Energy Absorption Applications: Blast Protection and Crashworthiness." Composites Part B: Engineering, Vol. 43 (5), pp. 2198-2208.

U.S. Army Corps of Engineers, Naval Facilities Engineering Command, and Air Forces Civil Engineer Support Agency (2008), “Structures to Resist the Effect of Accidental Explosions.” Unified Facilities Criteria, UFC 3-340-02.

Valdevit, L., Hutchinson, J.W., Evans, A.G. (2004). "Structurally Optimized Sandwich Panels with Prismatic Cores." International Journal of Solids and Structures, Vol. 41(18-19), pp. 5105-5124.

Valdevit, L., Wei, Z., Mercer, C., Zok, F.W., Evans, A.G. (2006). "Structural Performance of Near-Optimal Sandwich Panels with Corrugated Cores." International Journal of Solids and Structures, Vol. 43(16), pp. 4888-4905.

Whelan, M. J. Ralston, A. D., and Weggel, D. C. (2015). "Blast Testing of Cold-Formed Steel-Stud Wall Panels." Journal of Performance of Constructed Facilities, 10.1061/(ASCE)CF.1943-5509.0000734.

Table 4.1 Test matrix

NO.	Panel name	No. of samples	Core deck type	Configuration type	Thickness of core sheet *(mm)*	Sample depth *(mm)*	Deck parameters				
							$\bar{B}$ *(mm)*	D *(mm)*	b_1 *(mm)*	b_2 *(mm)*	θ°
1	*B-X-G20*	3	*B* - deck	*X-core*	0.91	80.2	304.8	38.1	82.4	42.0	73°
2	*B-X-G18*	3	*B* - deck	*X-core*	1.21	80.2	304.8	38.1	82.4	42.0	73°
3	*V-X-G20*	3	*V* - deck	*X-core*	0.91	80.2	304.8	38.1	29.2	29.2	45°
4	*B-T-G20*	3	*B* - deck	*Bi-directional*	0.91	80.2	304.8	38.1	82.4	42.0	73°
5	*B-T-G18*	3	*B* - deck	*Bi-directional*	1.21	80.2	304.8	38.1	82.4	42.0	73°
6	*N-S-G20*	3	*N* - deck	*Uni-directional*	0.91	80.2	304.8	50.8	95.8	40.3	85°
7	*N-S-G18*	3	*N* - deck	*Uni-directional*	1.21	80.2	304.8	50.8	95.8	40.3	85°

Table 4.2 Material mechanical properties

NO.	Sheet	Gauge of sheet	Modulus of elasticity (*GPa*)	Yield Stress (*MPa*)
1	*Face flat sheet*	G14	191	304
2	*B-deck*	G18	181	273
3	*B-deck*	G20	139	275
4	*V-deck*	G18	209	256
5	*V-deck*	G20	173	264
6	*N-deck*	G18	145	277
7	*N-deck*	G20	175	291

Table 4.3 Nominal yield load and ultimate capacity for the tested panels

No.	Panel type	F_{ny1} (kN)	F_{ny2} (kN)	F_{ny3} (kN)	$F_{ny(mean)}$ (kN)	C.O.V	$F_{CR(analytical)}$ (kN)	F_{u1} (kN)	F_{u2} (kN)	F_{u3} (kN)	$F_{u(mean)}$ (kN)	Standard deviation	C.O.V
1	*B-X-G18*	**	54.3	52.7	53.5	0.021	37.7	**	59.4	57.7	58.5	1.25	0.021
2	*B-X-G20*	36.5	36.5	37.1	36.7	0.009	21.9	41.9	44.8	42.9	43.2	1.43	0.033
3	*V-X-G20*	44.9	45.6	47.9	46.2	0.035	19.3	50.4	51.7	52.1	51.4	0.88	0.017
4	*B-T-G18*	30.4	28.8	29.4	29.5	0.028	25.8 [b]	40.8	36.9	40.4	39.4	2.15	0.055
5	*B-T-G20*	17.2	17.3	17.9	17.5	0.025	14.5 [b]	23.3	29.2	21.7	24.7	3.99	0.161
6	*N-S-G18*	46.9	46.4	51.3	48.2	0.056	40.3	62.6	62.6	65.7	63.6	1.78	0.028
7	*N-S-G20*	41.5	43.2	42.8	42.5	0.021	27.2	52.5	59.7	42.9	51.7	8.36	0.162

** weld failure, [b] calculated buckling load.

Table 4.4 Calculated energy absorption corresponding to nominal yield forces for the tested panels

No.	Panel Type	E_{ny1} *(kN.mm)*	E_{ny2} *(kN.mm)*	E_{ny3} *(kN.mm)*	Mean *(kN.mm)*	Standard Deviation	*C.O.V*
1	*B-X-G18*	**	297.7	307.5	302.7	6.9	0.023
2	*B-X-G20*	159.1	190.4	196.6	182.1	20.1	0.110
3	*V-X-G20*	200.8	226.5	219.2	215.5	13.2	0.061
4	*B-T-G18*	159.8	147.3	151.6	152.9	6.4	0.042
5	*B-T-G20*	76.4	73.9	88.4	79.6	7.7	0.097
6	*N-S-G18*	169.2	165.3	218.1	184.2	29.4	0.160
7	*N-S-G20*	146.6	168.8	167.6	161.0	12.5	0.078

** weld failure.

Table 4.5 Elastic flexure stiffness

No.	**Panel type**	K_1 *(kN/mm)*	K_2 *(kN/mm)*	K_3 *(kN/mm)*	$K_{(mean)}$ *(kN/mm)*	**Standard deviation**	***C.O.V***	$K_{(Analytical)}$ *(kN/mm)*
1	*B-X-G18*	5.39	4.97	4.52	4.96	0.44	0.088	5.20
2	*B-X-G20*	4.18	3.51	3.50	3.73	0.39	0.105	4.81
3	*V-X-G20*	5.02	4.59	5.25	4.95	0.33	0.068	4.32
4	*B-T-G18*	2.89	2.81	2.85	2.85	0.04	0.014	4.39
5	*B-T-G20*	1.93	2.03	1.83	1.93	0.10	0.051	4.19
6	*N-S-G18*	6.50	6.50	6.02	6.34	0.28	0.044	4.79
7	*N-S-G20*	5.86	5.52	5.47	5.62	0.21	0.038	4.49

Table 4.6 Nominal yield displacements and calculated ductility for the tested panels

No.	Panel type	δ_{ny1} (mm)	δ_{ny2} (mm)	δ_{ny3} (mm)	$\delta_{ny(\text{Mean})}$ (mm)	*C.O.V*	$\delta_{cr(\text{Analytical})}$ (mm)	$\mu 1$	$\mu 2$	$\mu 3$	Mean	Standard deviation	*C.O.V*
1	*B-X-G18*	**	10.9	11.	11.3	0.043	7.3	**	4.4	4.2	4.3	0.16	0.036
2	*B-X-G20*	8.7	10.4	10.7	9.9	0.104	4.6	5.8	5.1	4.7	5.2	0.53	0.101
3	*V-X-G20*	8.9	9.9	9.1	9.3	0.056	4.5	3.6	2.9	3.0	3.2	0.34	0.107
4	*B-T-G18*	10.5	10.2	10.3	10.4	0.014	5.9	11.0	10.7	9.8	10.5	0.64	0.061
5	*B-T-G20*	8.9	8.5	9.8	9.1	0.073	3.4	14.3	15.3	13.1	14.2	1.08	0.076
6	*N-S-G18*	7.2	7.1	8.5	7.6	0.102	8.4	N.A.	7.8	7.7	7.8	0.05	0.006
7	*N-S-G20*	7.1	7.8	7.8	7.6	0.057	6.0	8.3	7.9	10.5	8.9	1.39	0.156

** The specimen faced a weld failure.

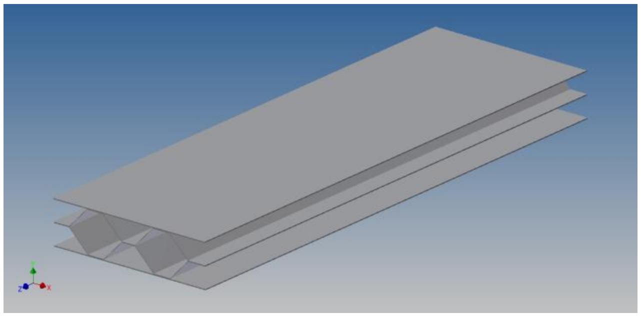

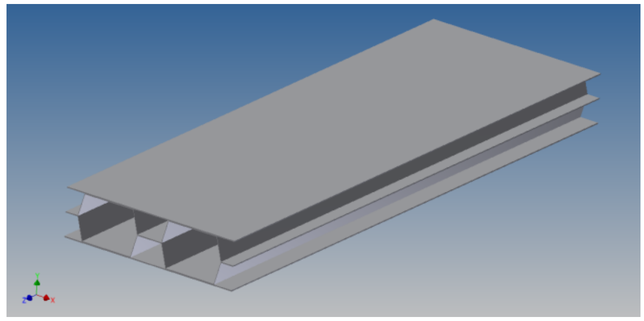

(a) **(b)**

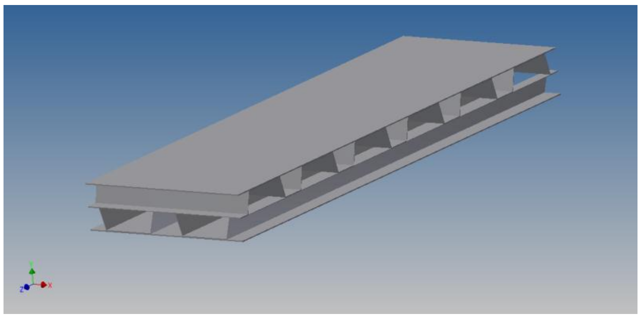

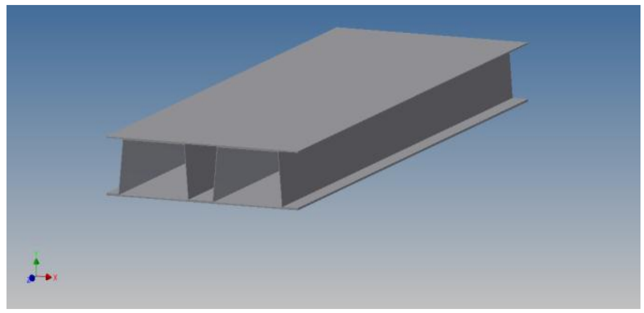

(c) **(d)**

Fig. 4.1 Different configurations tested in the present work, (a) *V*-*X*-core, (b) *B*-*X*-core, (c) *B*-*T*-core and (d) *N*-*S*-core.

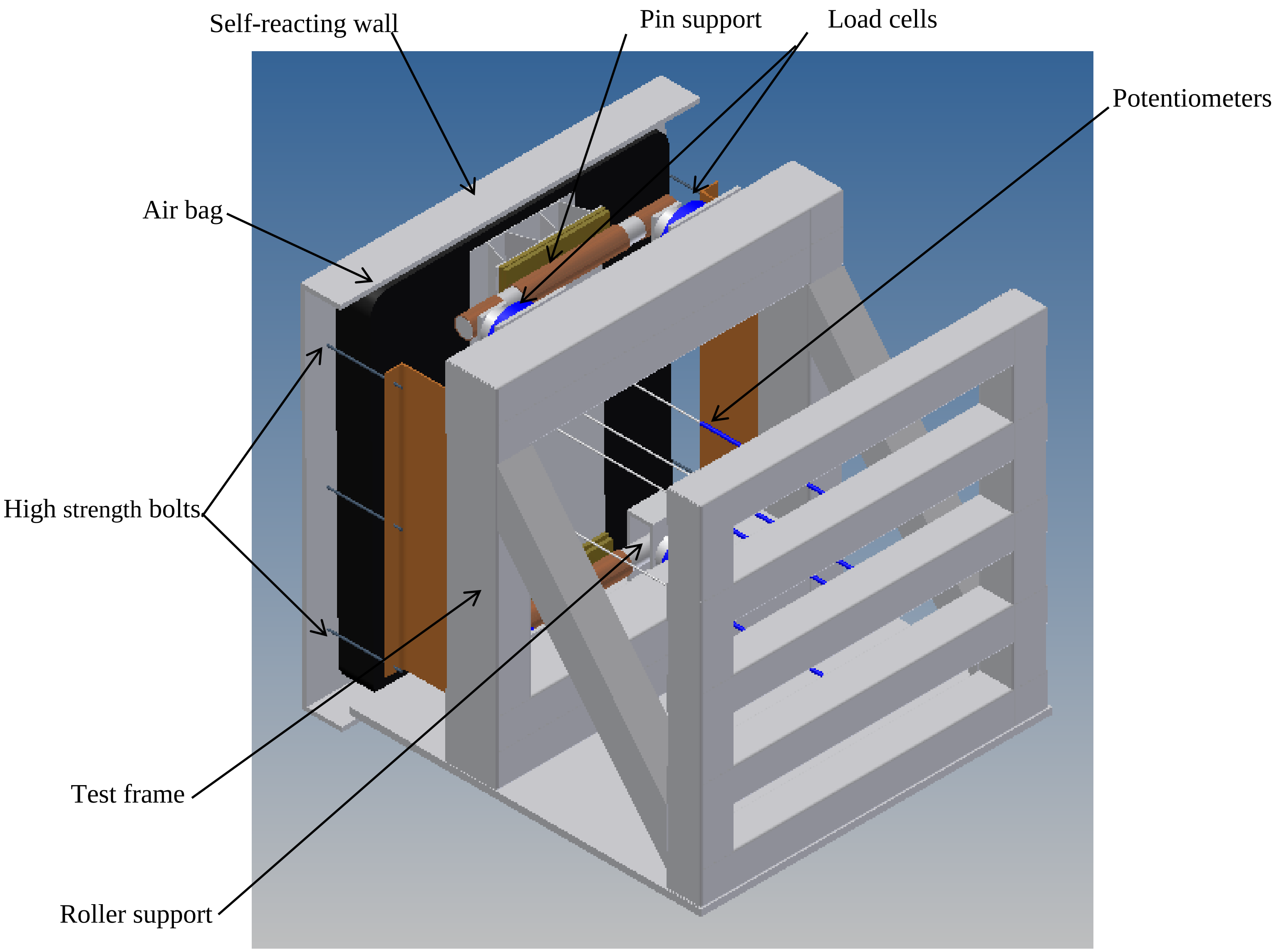

Fig. 4.2 3D view for the test setup and instrumentations

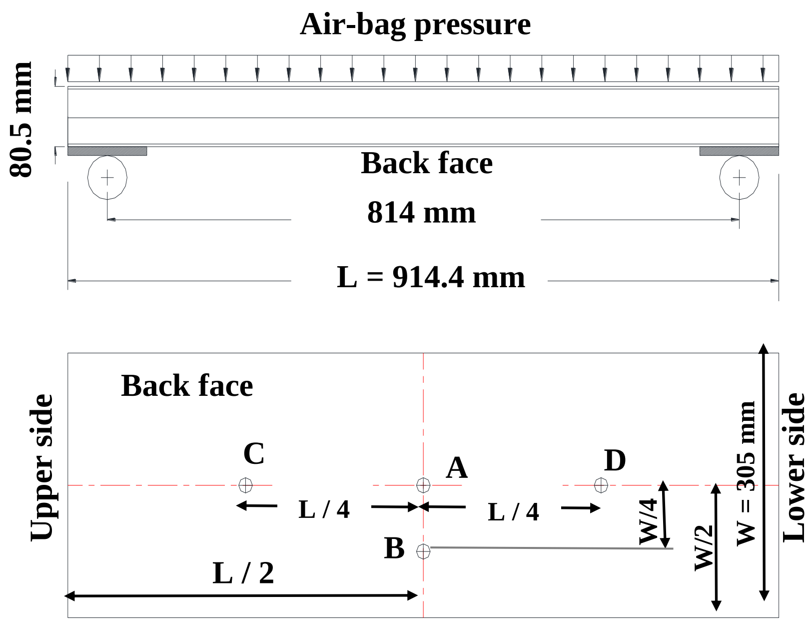

(a)

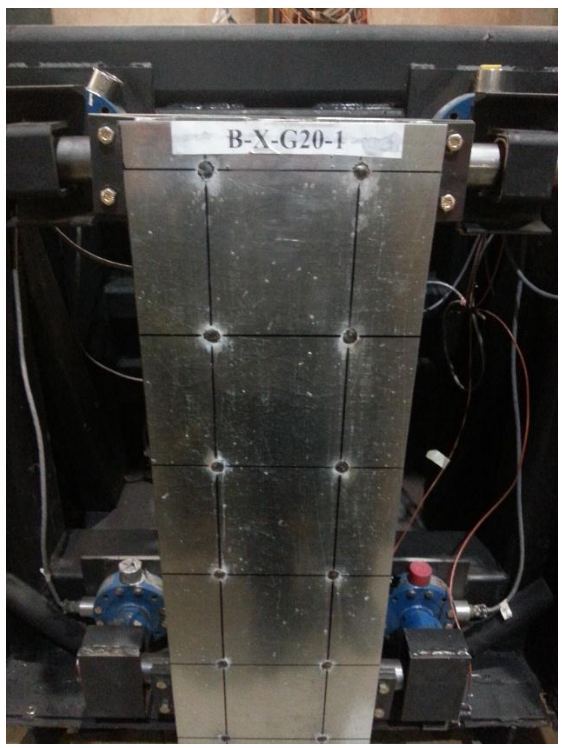

(b)

Fig. 4.3 Test setup and instrumentations (a) panel dimensions and potentiometers location on back face and (b) front view for the test setup.

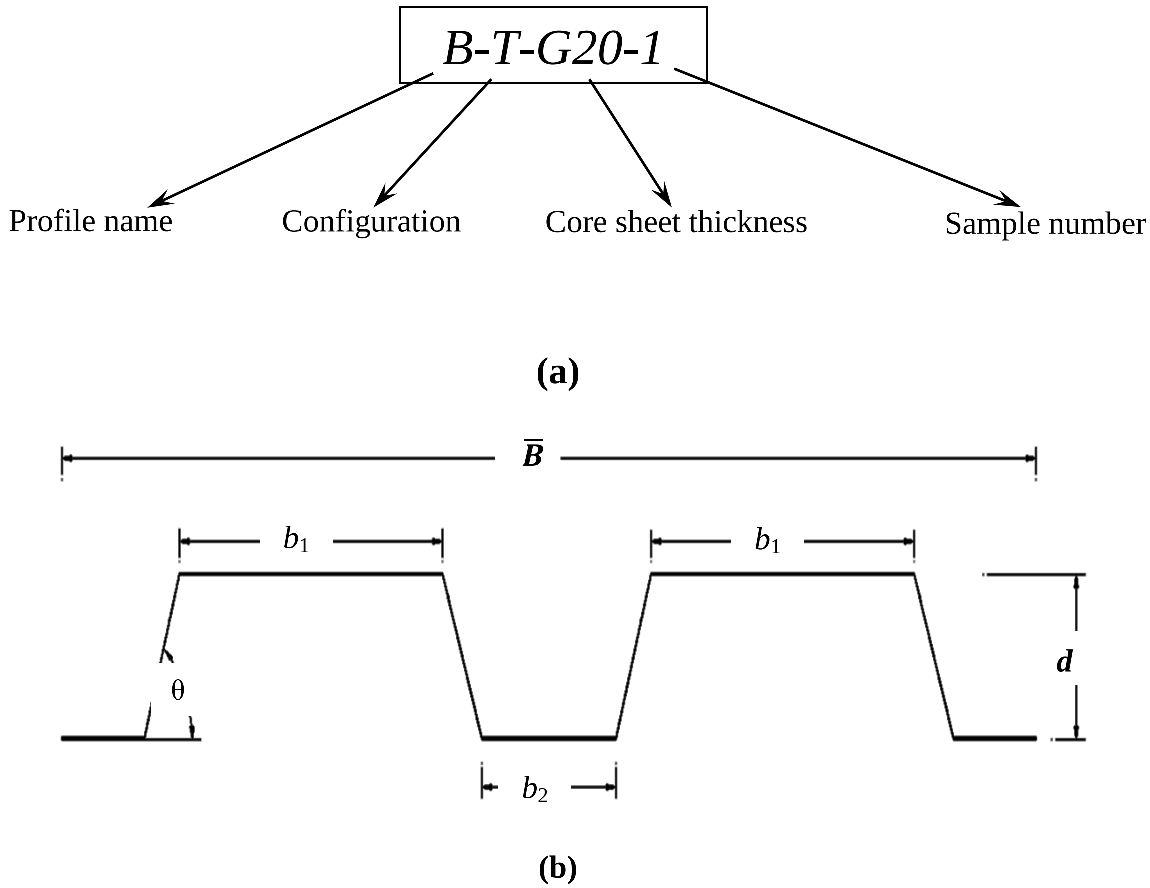

Fig. 4.4 (a) the basis of the sample nomenclature and (b) the parameters defining each deck profile.

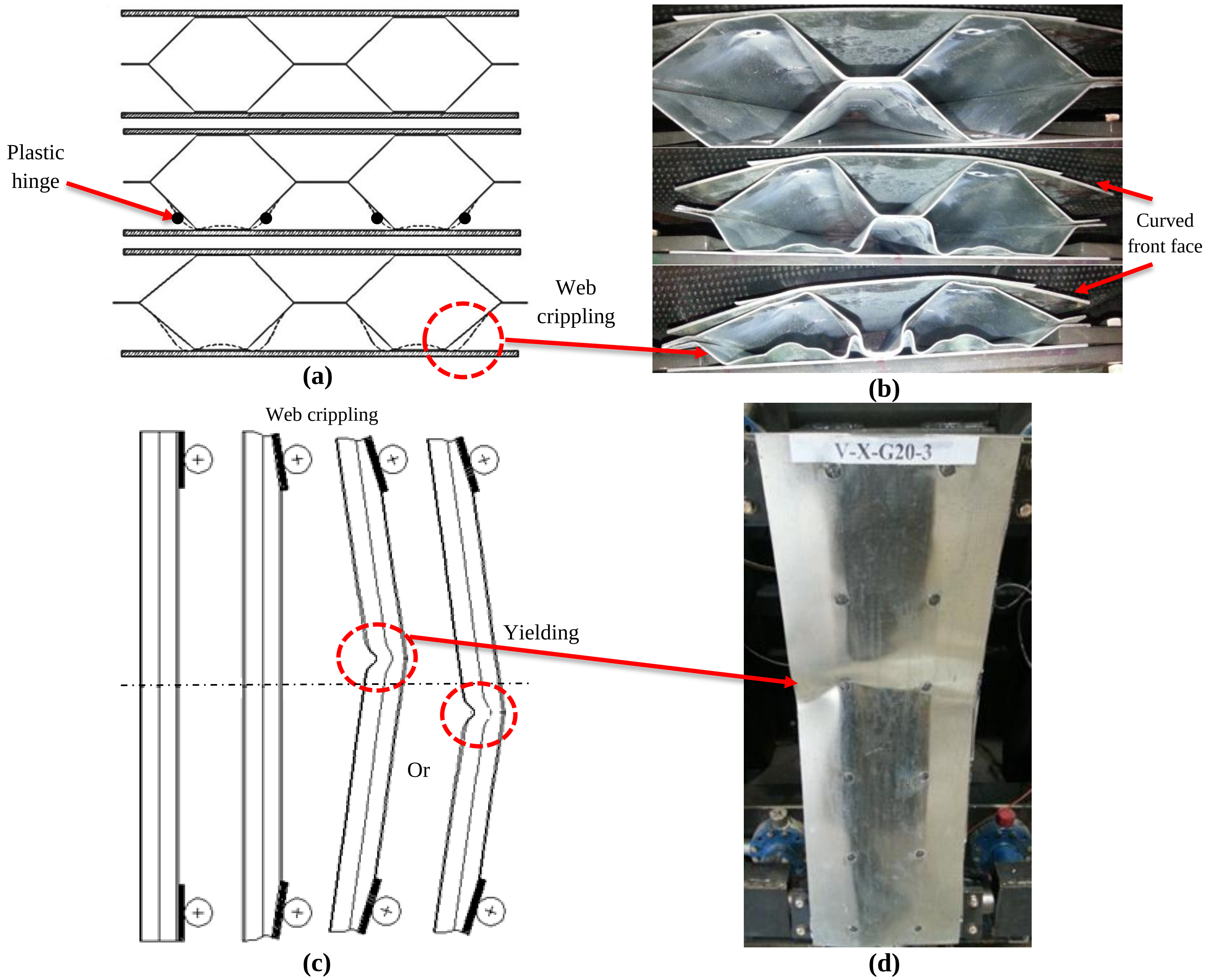

Fig. 4.5 Yielding and web crippling in *V-X*-core sandwich panels, (a) schematic of web crippling propagation, (b) actual web crippling propagation, (c) schematic of failure mode for *V-X*-core sandwich and (d) actual yield failure

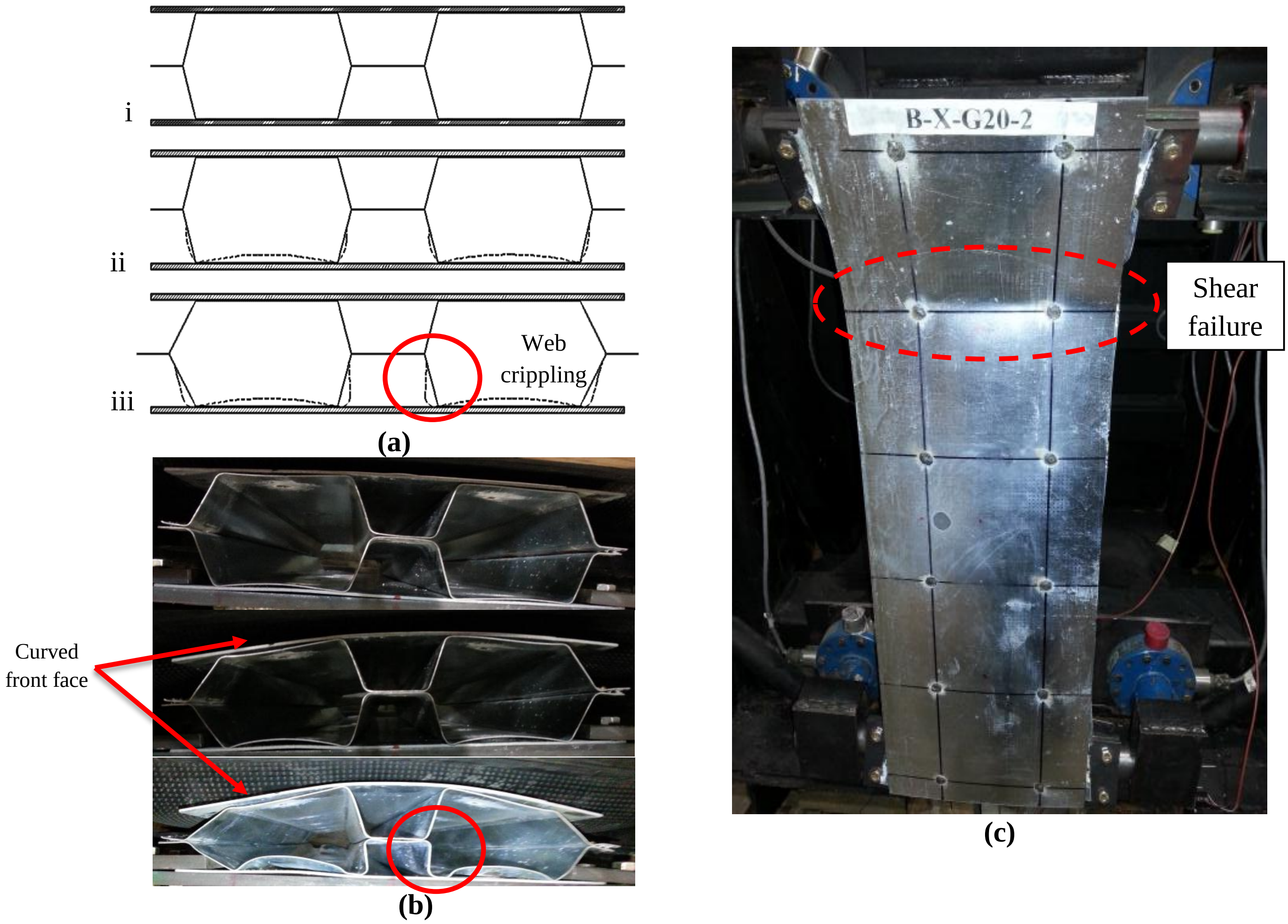

Fig. 4.6 Failure modes for *B*-*X*-core sandwich panels, (a) schematic of web crippling progression, (b) actual web crippling and (c) Shear failure of *B*-*X*-core sandwich panel.

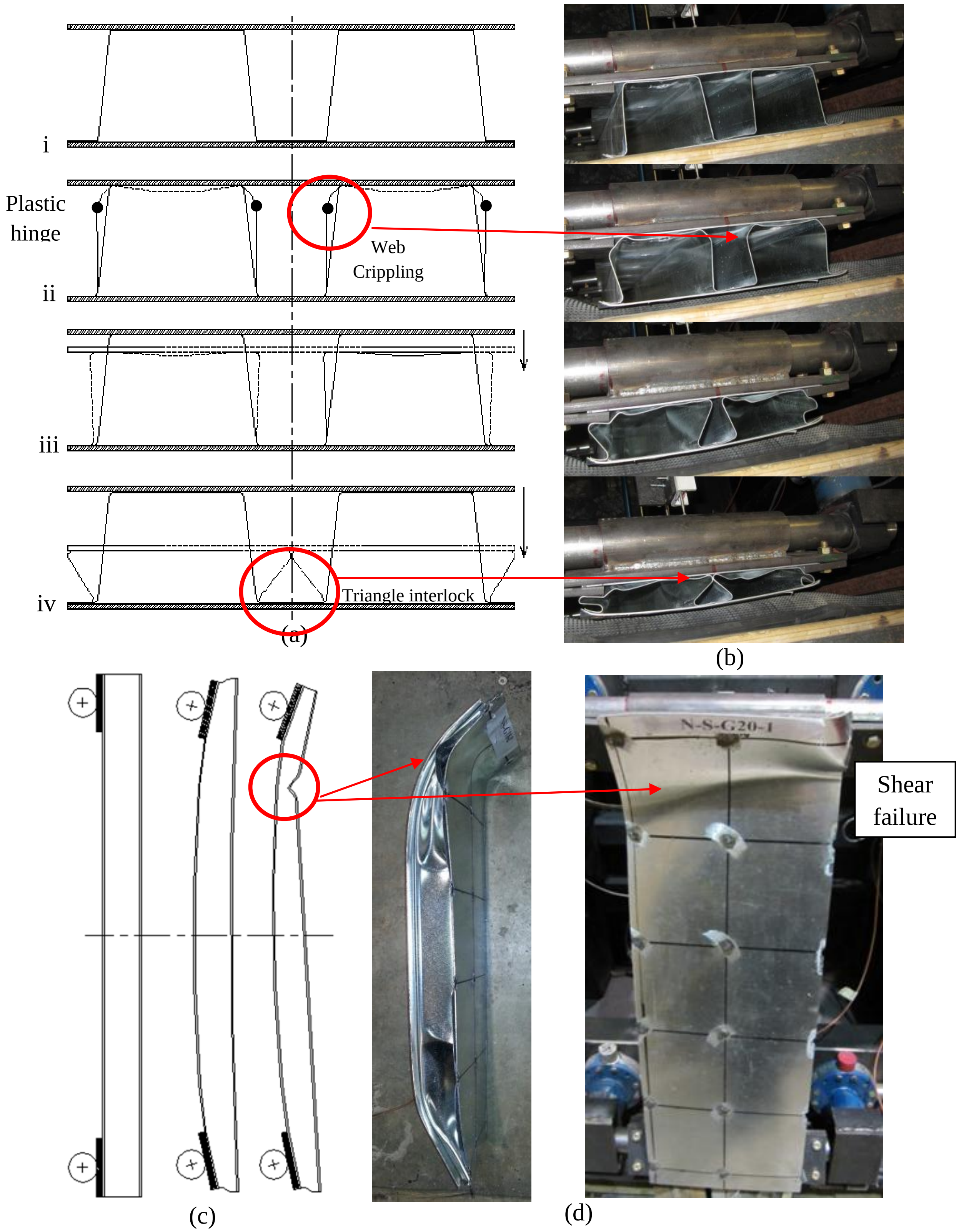

Fig. 4.7 Failure modes for *N-S*-core sandwich panels, (a) schematic of web crippling propagation, (b) actual web crippling, (c) schematic of shear failure and (d) actual shear failure in *N-S*-core.

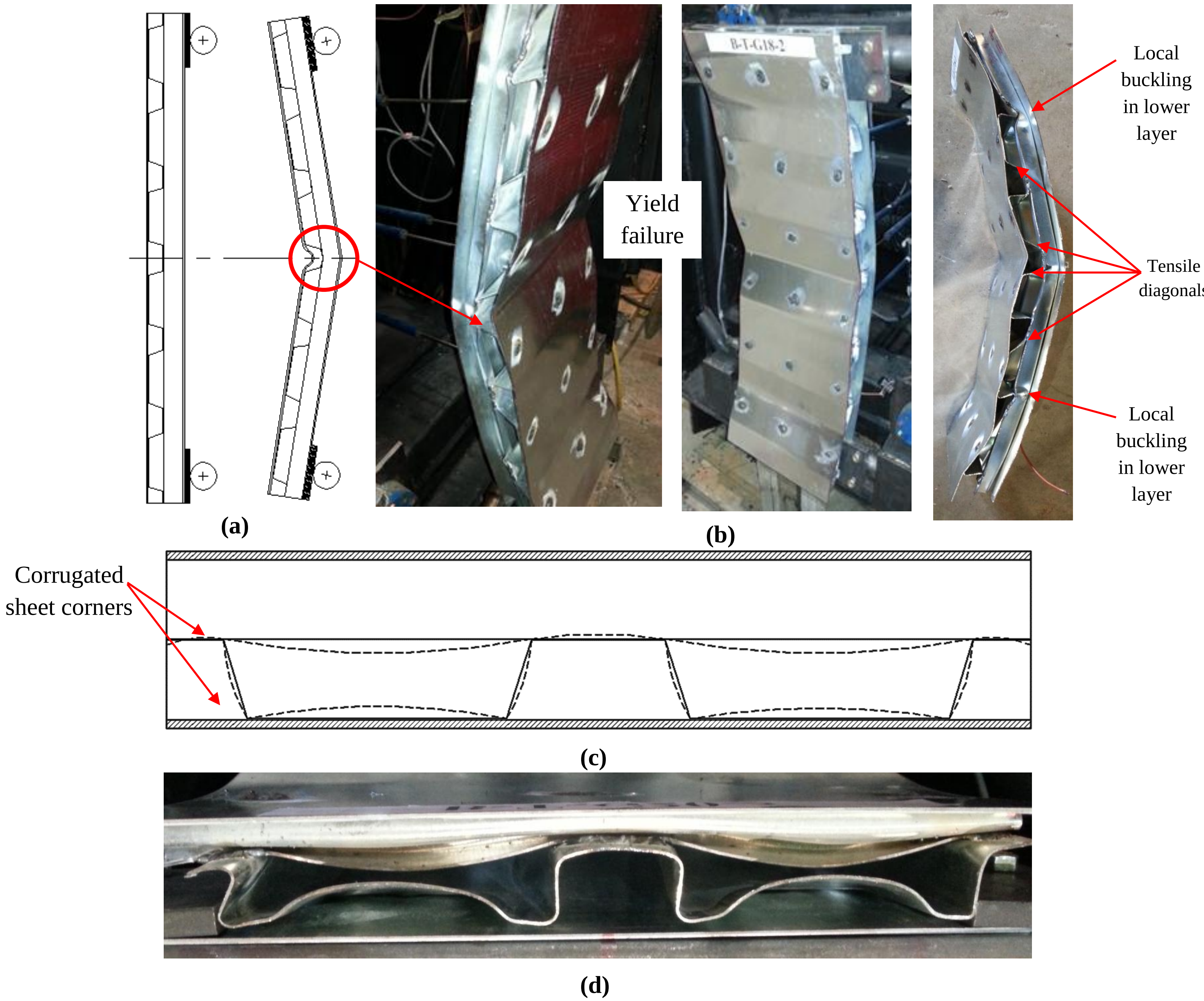

Fig. 4.8 ***B-T*-Core sandwich panels, (a) schematic of yield failure, (b) actual yield failure, (c) schematic of web crippling and (d) actual web crippling.**

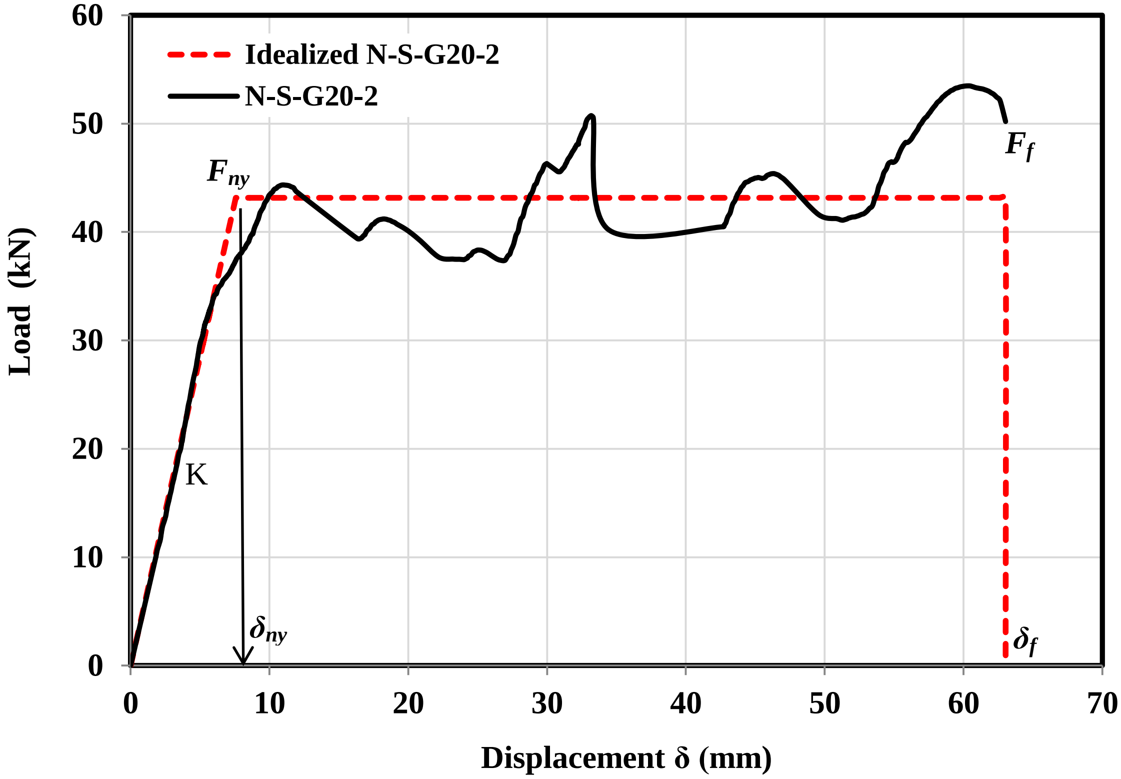

Fig. 4.9 Idealized load-displacement relationship.

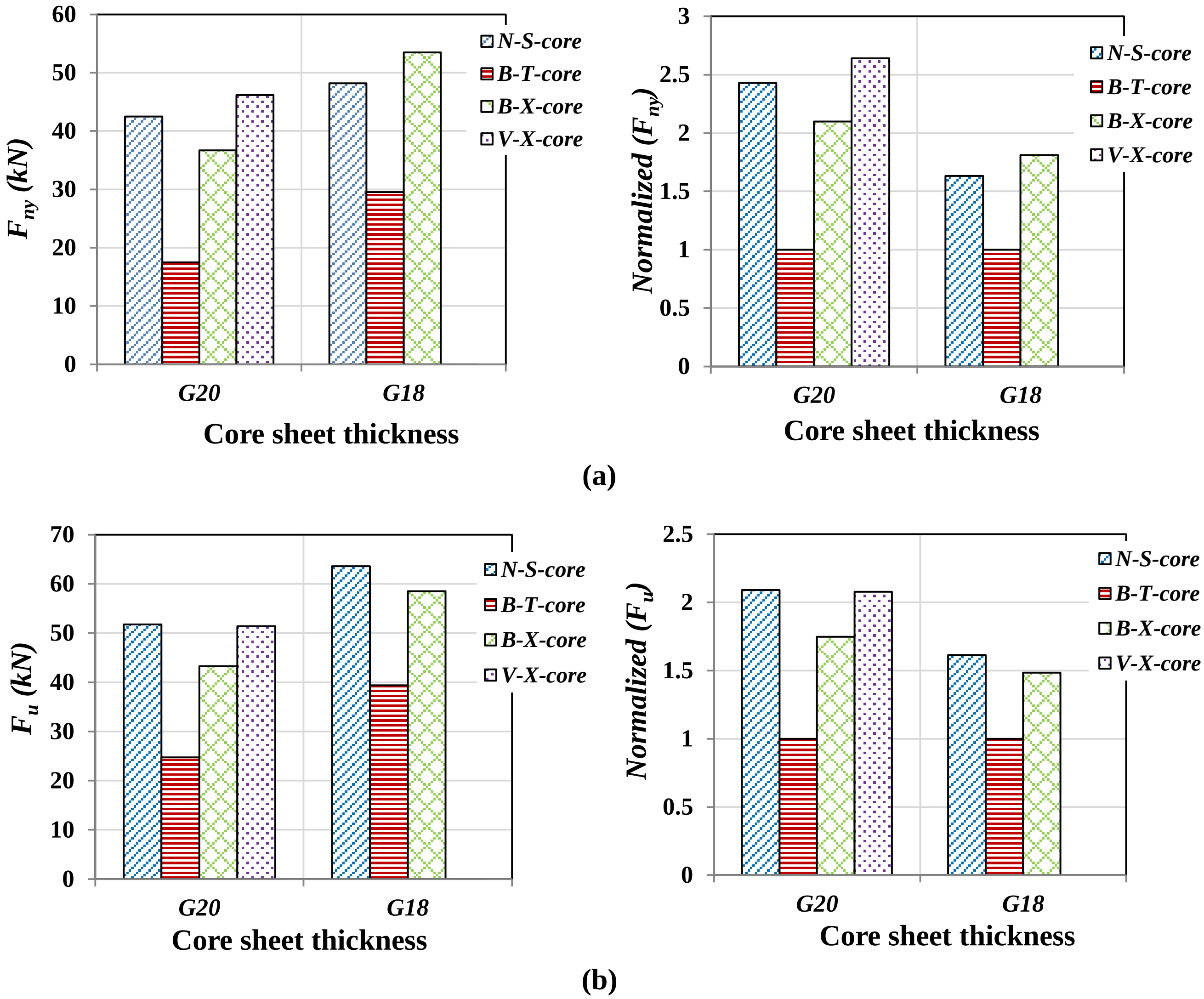

Fig. 4.10 Core configuration effect on: (a) nominal yield load and (b) ultimate load.

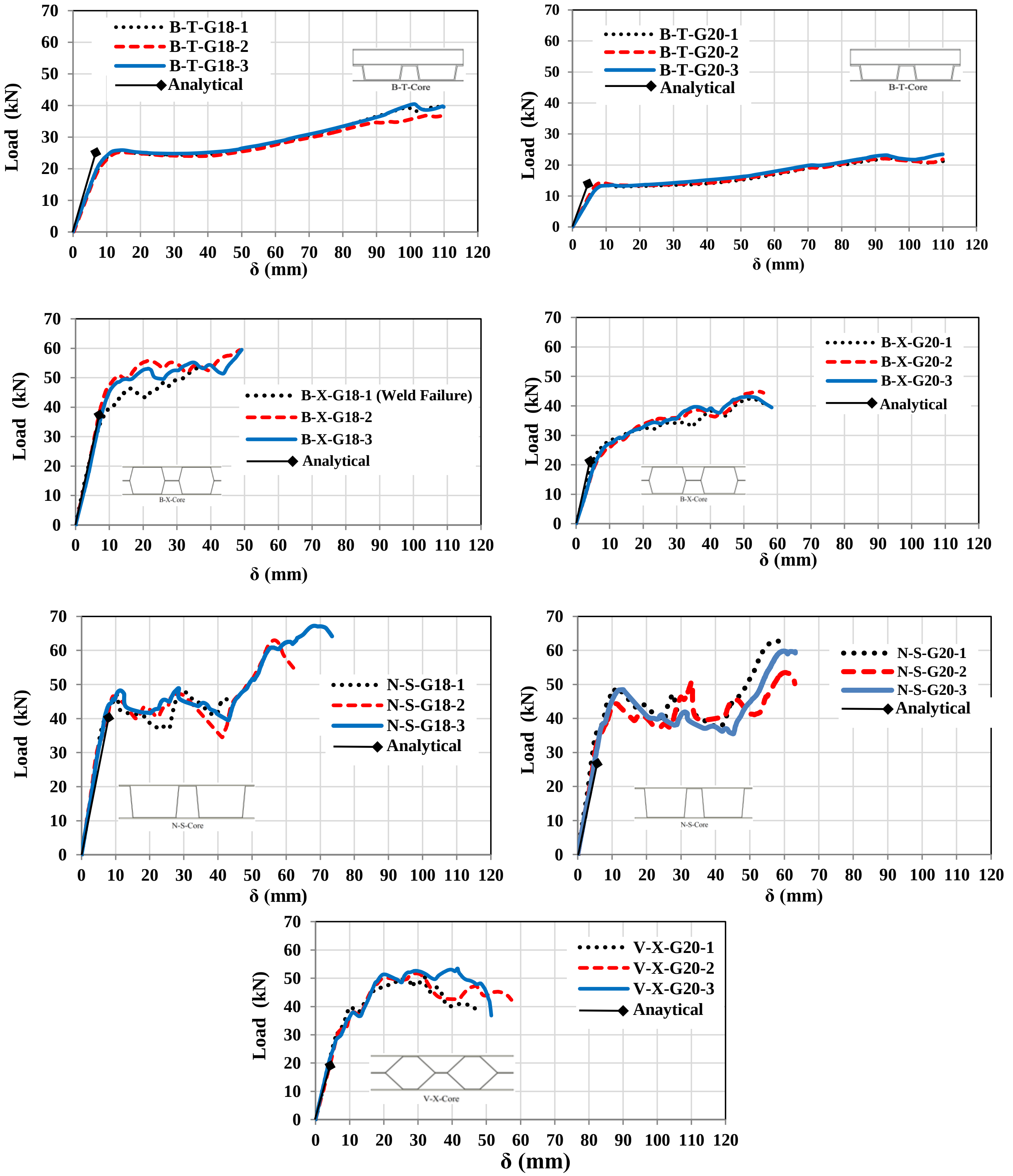

Fig. 4.11 Resistance functions for the tested sandwich panels.

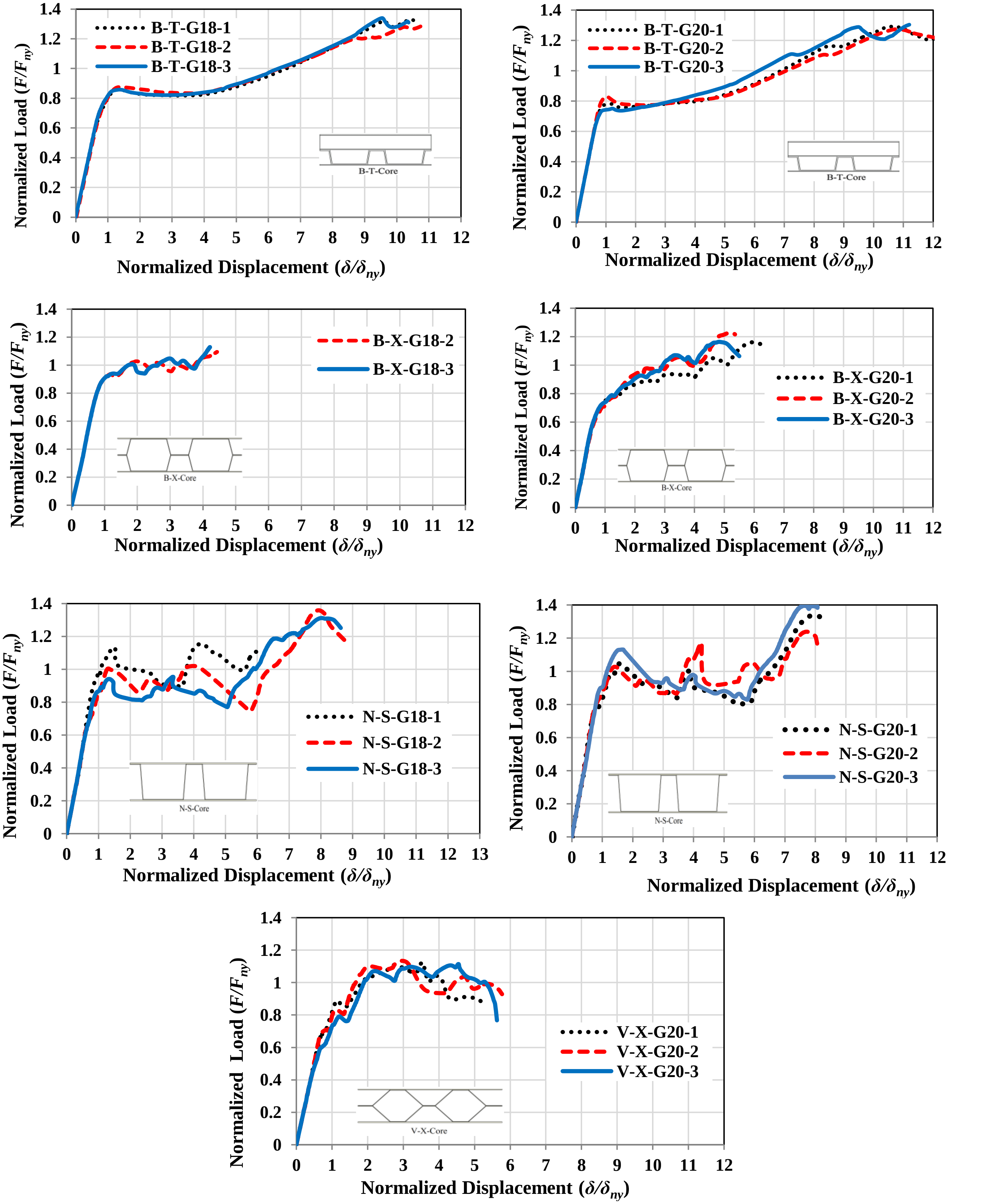

Fig. 4. 12 Normalized load-displacement relationships for tested panels.

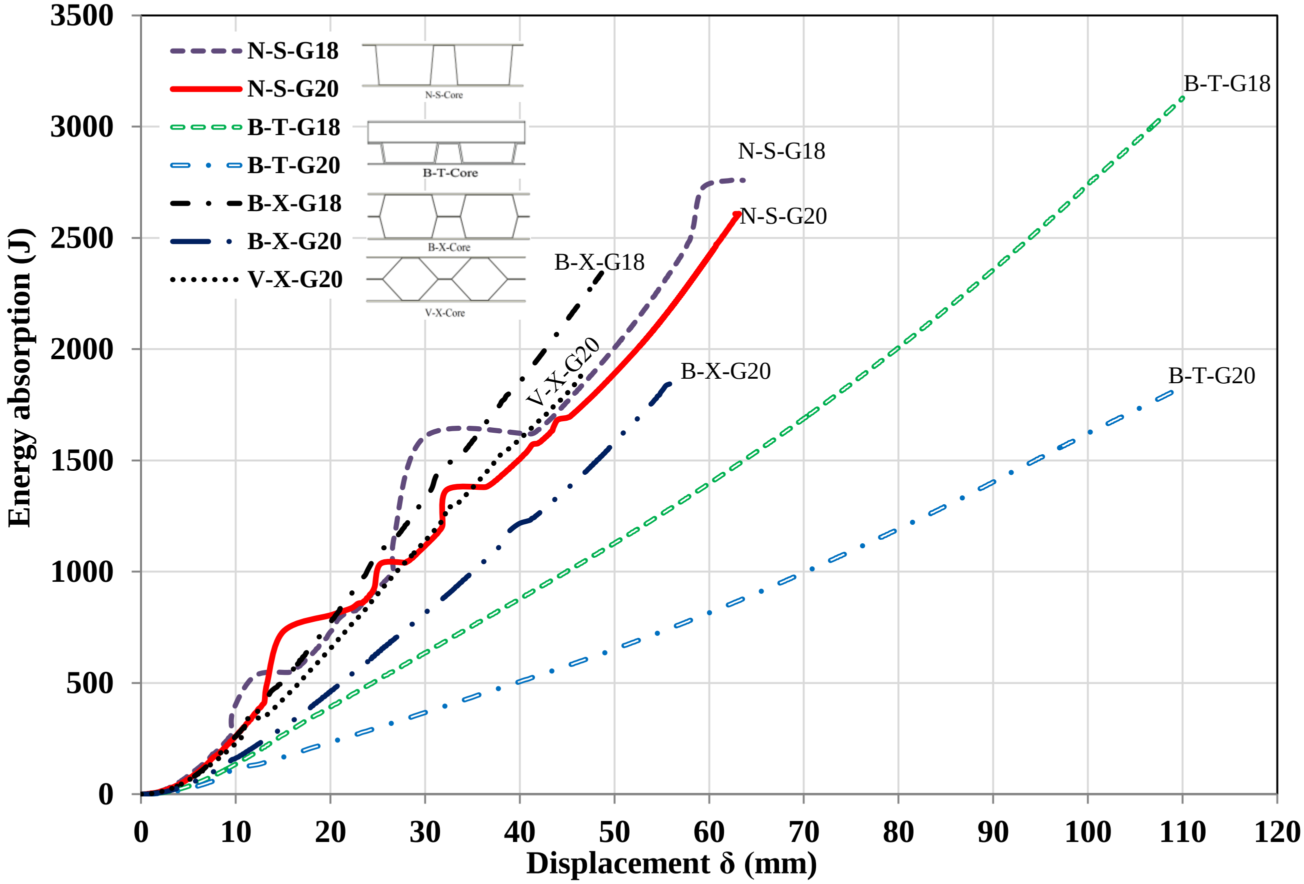

Fig. 4.13 Calculated energy absorption-displacement relationships for different core configurations

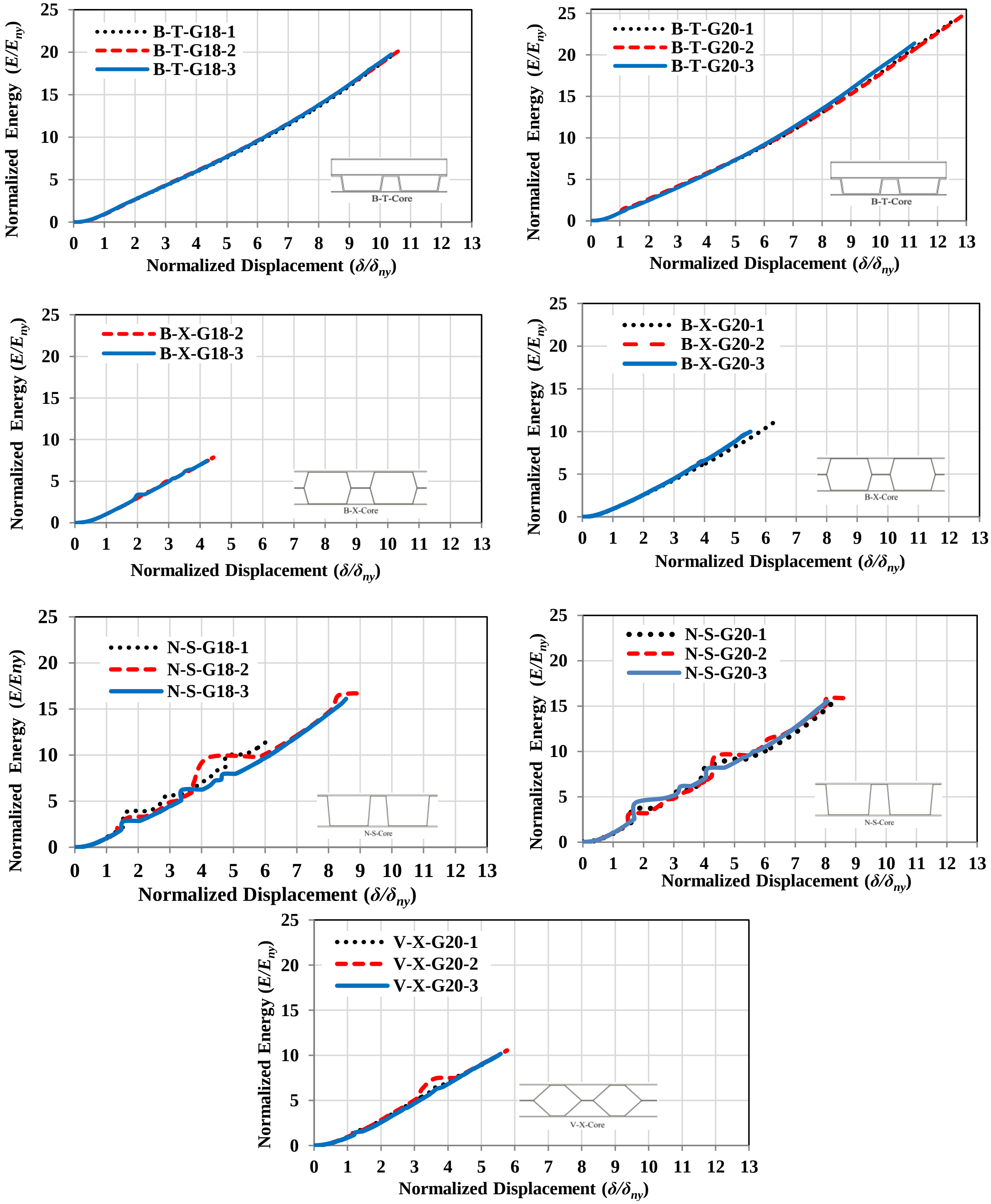

Fig. 4.14 Normalized energy absorption-displacement relationships for all tested panels.

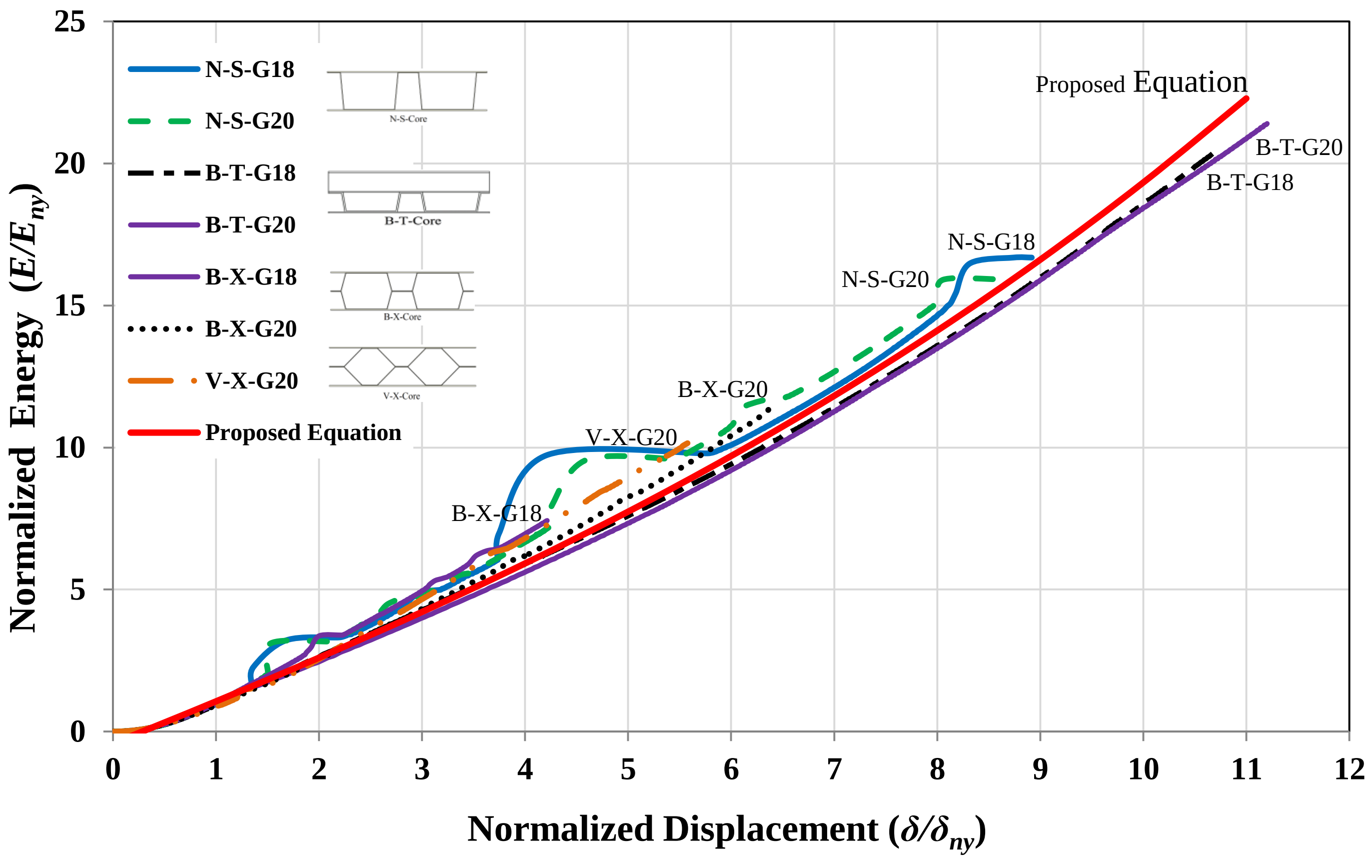

Fig. 4.15 Proposed equation and measured normalized energy absorption-displacement relationships for tested configurations.

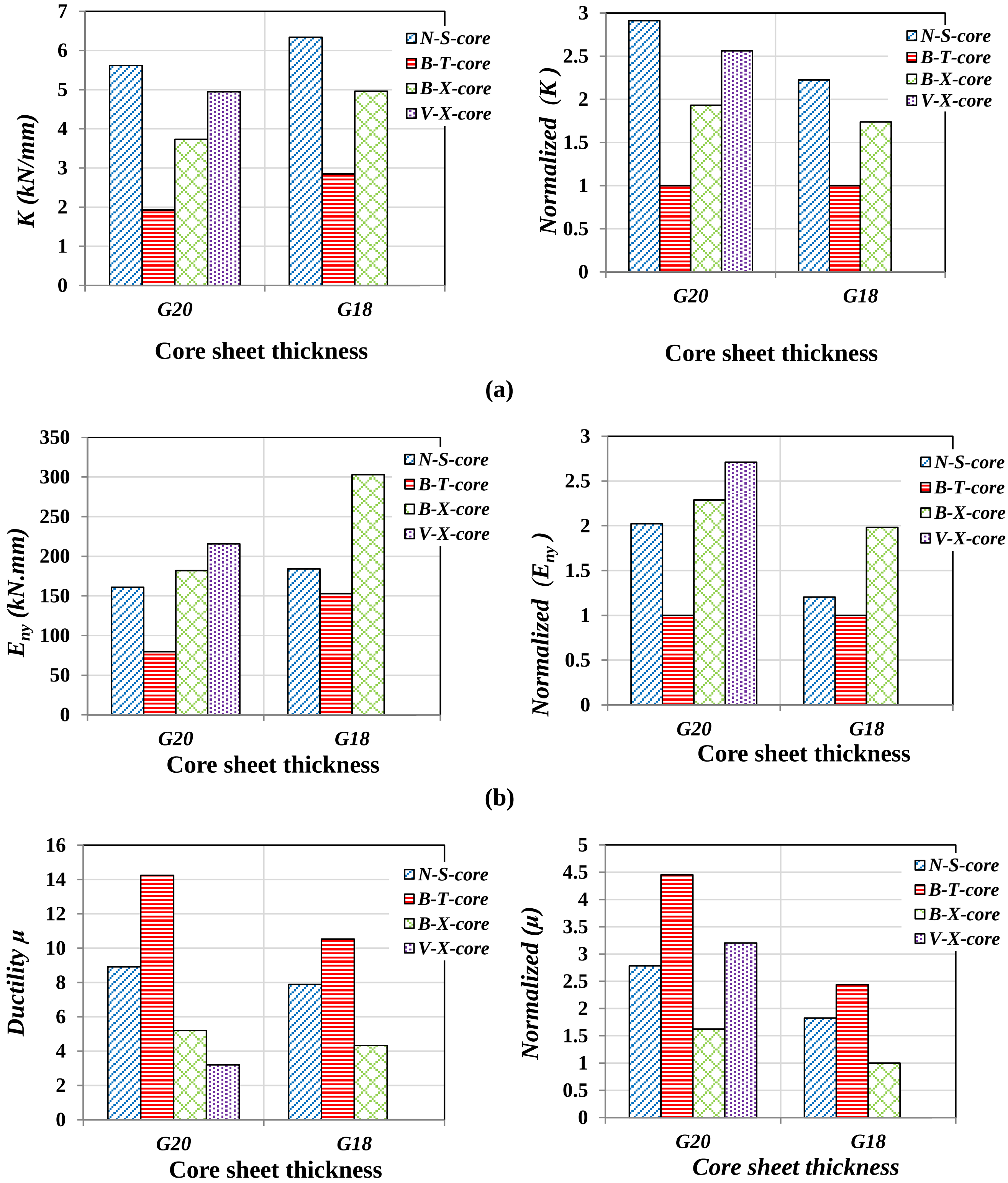

Fig. 4.16 Influence of core configuration on (a) flexure elastic stiffness, (b) energy absorption and (c) ductility.

CHAPTER 5: PERFORMANCE OF LIGHTWEIGHT SACRIFICIAL CLADDING UNDER CONFINED BLAST LOADS

5.1 ABSTRACT

A confined blast scenario inside a critical facility could have devastating consequences as a short-range explosion detonated at a critical location could paralyze all operations within the facility. Lightweight sacrificial cladding can be employed to act as a physical barrier for high importance (i.e. critical) structures that are vulnerable to a potential explosion. A cold-formed steel sandwich panel offers high energy dissipation at a relatively low cost, which qualifies it to be used to construct a sacrificial cladding system within multiple applications and against a range of threat scenarios. An experimental study using live explosives has been carried out to investigate the dynamic response of cold-formed steel sandwich panels with different core configurations. These core configurations were selected based on the results of a previous study on cold-formed steel sandwich panels under quasi-static loading, which was conducted to evaluate their resistance functions and failure modes. The response of each sandwich panel configuration under three different charge weights, at a constant standoff distance is investigated in this paper. The experimental results are presented in terms of modes of failure, peak displacements, and pressure time histories. In addition, the influence of the panel core configuration on the blast resistance was evaluated. Finally, the paper relates different damage levels to corresponding limits specified by the Canadian Standard for the Design and Assessment of Buildings Subjected to Blast Loads CSA/ S850-12, and the American Standard for the Blast Protection of Buildings ASCE/SEI 59-11.

KEYWORDS: Blast load, Cold formed steel, Confined blast, Lightweight structure, Sacrificial cladding, Sandwich Panel.

5.2 INTRODUCTION

An explosion inside a critical facility can lead to more damage than an equivalent explosion occurring in a free air scenario outside the facility, and may completely paralyze all operations within the facility. The presented research focuses on relatively small charge sizes associated with small standoff distances, which can be sustained by the main structure of a facility, but can lead to damage in non-structural components. Such scenarios may occur due to accidental or artificial explosions. According to the risk assessment guide developed by FEMA 452 (2005), although designers may have no control over the charge size, they can dictate the level of protection by introducing sacrificial spaces that provide enhanced protection to both the structure and the people inside.

Lightweight sacrificial cladding can be employed as a physical barrier between a non-sacrificial structure and a blast load. Sacrificial cladding, from a structural perspective can be classified into three types, as shown in Fig. 5.1, (a) continuous contact with main structure (deformations will be due to compression only), (b) simply supported by the main structure (flexural deformations), (c) continuously supported by the main structure. The research presented in this study focuses on the second type, which is simply supported by the structure. In the application for the proposed type of sacrificial cladding, the panels were designed to be lightweight, cost effective, easy to handle and install, and can be employed in multiple applications against a range of threat levels. Cold-formed steel sandwich panels can offer high energy dissipation at a relatively low cost, which qualifies them to be employed in sacrificial cladding systems within multiple applications and against a range of threat levels.

5.2.1 Previous work review

Over the last decades, sandwich panel systems for blast loading applications have been investigated by a number of researchers. This is primarily due to their ability to absorb energy and their high stiffness to weight ratio. Energy is primarily absorbed through the formation and propagation of a failure mechanism(s) through the core. As a result, the influence of core configuration on sandwich panel response has been focus of several research studies. A number of researchers have compared the response of sandwich panels to alternative monolithic solid plates with same material and having the same mass, to highlight the superiority of the sandwich system. For metallic sandwich panels, Xue and Hutchinson (2003) numerically investigated tetragonal truss core sandwich panels and found that they absorb twice the amount of energy as equivalent monolithic plates. Fleck and Deshpande (2004) investigated the dynamic behavior of clamped sandwich panels, considering various topologies of core (pyramidal, diamond-cell, corrugated, metal foam and square honeycomb). The diamond-cell core was found to possess the most desirable blast resistance performance for both water and air blast. Rimoli et al. (2011) investigated the dynamic response of edge-clamped 6061-T6 aluminum corrugated core sandwich panels under the impact of explosively driven wet sand. The sandwich panels exhibited 15-20% lower permanent deformation than those of monolithic plates constructed using same material and having the same mass. McShane et al. (2010) studied the dynamic response of square-honeycomb and corrugated core configurations in stainless steel sandwich panels subjected to water blast loading. The core topology was found to have a strong influence upon the dynamic compressive strength and upon the degree of core compression, but had a minor effect on the total imparted momentum to the sandwich.

Dharmasena et al. (2010) investigated five different core topologies within rigidly supported stainless steel sandwich panels that were subjected to underwater impulsive loading. The core topologies were square-honeycomb, triangular honeycomb, multi-layer pyramidal truss, triangular corrugation and diamond corrugation. All core configurations had a relative density of approximately 5%. The honeycomb configurations exhibited the highest initial peak strength and rapid softening beyond that point, while the truss and corrugated core exhibited lower strength but possessed a hardening plateau beyond yield load.

Cui et al. (2012), and Zhao et al. (2012) both studied the dynamic response of metallic tetrahedral lattice core sandwich panels through experimental testing. Results from these studies highlight the superior performance of tetrahedral lattice sandwich panels relative to honeycomb. These findings were consistent with findings presented by Dharmasena et al. (2011) who investigated on the response of metallic pyramidal lattice subjected to high impulse in air through a series of experimental tests and finite element modeling.

Nurick et al. (2009) investigated the behavior of sandwich panels consisting of an aluminum alloy honeycomb core under the effect of localized and uniform blast loading. The response of the sandwich panel was compared with that of both mild steel plates and air-core sandwich panels. For the case of uniform blast loading, results showed the superior resistance of the honeycomb sandwich panels over mild steel plates for blast loads having an impulse greater than 20 Ns. However, for blast loads having an impulse that was less than 20 Ns impulse the honeycomb sandwich panels showed higher back face deformations than that of the air-core sandwich panels.

The use of aluminum foams (for example, Alporas and Cymat) for the core were studied by Theobald et al. (2010). The Alporas core was found to have higher relative blast resistance with a thicker face sheet, while Cymat core panels did not show any significant increase in behavior over monolithic plates. Liu et al. (2013) conducted a study on blast attenuation ability of sandwich panels having different aluminum foam densities. It was found a lower core density resulted in higher energy dissipation.

Other studies have considered asymmetric face sheet sandwich panels , such that by Wang et al. (2011), who investigated five different thickness ratios of the upper to the lower face sheets considering the peak deflection and energy absorption of the sandwich panels.

Børvik et al. (2008) tested a cost effective and lightweight protection concept for a 20 foot standard ISO container to be used as a shelter in international operations. The work was done in six stages as described in detail in Børvik et al. (2008). The proposed protection system utilized extruded AA6005-T6 aluminum panels filled with granular material to increase its blast load resistance.

Theobald and Nurick (2007, 2010) conducted a series of experimental tests and numerical simulations to investigate the dynamic response of sacrificial cladding sandwich panels subjected to uniform blast loads. The panels consisted of mild steel face sheets, and (annealed mild steel or 6063-T6 aluminum alloy) tube cores, the number of tubes in the core was considered as a parameter, where specimens had four, five or nine tubes. The test was performed with a target impulse of 55 Ns, the lowest stiffness panels showed more deformations and higher energy absorption.

Regarding the response of cold-formed steel members under blast loads, Salim et al. (2005), Bondok et al. (2013), and Whelan et al. (2015) carried out a similar approach to which was used through the current study in order to predict the dynamic response of cold-formed steel studs under blast loads. Moreover, their efforts also highlighted the attractive characteristics of cold-formed steel in blast applications such as strength, ductility, and energy absorption capabilities.

5.2.2 Development of Confined Explosion

An explosion in a confined space produces a complex blast load. Nevertheless, the first positive phase in the shock (blast) wave is similar to either the spherical or hemispherical conditions, characterized by instantaneous high pressure spike (Baker 1983 and Krauthammer 2008), followed by reflected shock waves, which are formed from the surrounding surfaces that make the environment very complicated to define, as shown in Fig. 5.2. Furthermore, a relatively long duration pseudo-static pressure is formed, which decays with time to ambient pressure as a result of gas ventilation from the confined space and/or the cooling of the hot gasses.

There are various scenarios that could involve confined blast loading, such as inside a building or bus or even a tunnel. The severity of damage experienced by critical structures under confined blasts can be much higher than an equivalent open air scenario (Smith 1994). Therefore, the consequences of confined blasts inside a high risk critical facility need to be taken into account through detailed analysis and design of such structures.

Although, the blast load may occur due to different types of explosives such as (*TNT*, Composition *C4*, .etc.), it is convenient to relate the charge mass of the considered explosive to its *TNT* equivalent mass. Many approaches have been presented to convert the explosive weight to equivalent *TNT* weight in order to match the same output parameters such as (pressure and impulse). In the current research, the Composition *C-4* was used as live explosive in the experimental tests. Composition *C-4* has density of (1.59 g/cm^3), detonation velocity of (8.04 km/sec) and it has a *TNT* equivalent weight factor of (1.37) for pressure and (1.19) for impulse (Krauthammer, 2008).

5.2.3 Research Significance

The current research presents the dynamic performance of cold-formed steel *Single-directional (N-S-core)* and *Bi-directional (two-way) (B-T-core)* sandwich panels subjected to confined live explosions, which can be used as sacrificial cladding on a critical facility. The tested configurations were selected based on the results from previous studies that considered seven different core configurations (Khalifa et.al 2015a and 2015b), where ductility and energy absorption were parameters that were investigated. The study employs low-cost lightweight cold formed steel sandwich panels, using off-the-shelf available corrugated sheets in North America, such as the *B* and *N* deck profiles. A blast chamber (see Fig. 5.3) and live explosives (Composition C-4) were used in order to expose the sandwich panels to realistic blast loading. Finally, the presented research investigates the suitability of a single degree of freedom model to predict the dynamic behavior of the proposed sandwich panels under the blast load.

5.3 EXPERIMENTAL INVESTIGATION

5.3.1 Experimental Setup and Instrumentation

The test bunker used in static testing program to determine the resistance functions of the sandwich panels (Khalifa et al. 2015b) was modified to fit in the blast chamber. A stiff door with an opening to fit in the sandwich panel specimens was installed, allowing relatively quick access to the test specimen and the instrumentation. Testing in the blast chamber required that a complete seal be achieved in the test bunker in order to prevent the blast wave from wrapping around the back of the panel (wrap around effect) and to protect the instrumentation. Usually wing walls are used to eliminate the clearing effect in the blast wave loading. Given the space constraints dictated by the size of the blast chamber, curved steel sheets were added to both the sides and the back of the test bunker to decrease pressure concentration effects on the bunker as shown in Fig. 5.4a. The space between the steel sheets and the bunker was subsequently filled with polyurethane foam,.

The reflected pressure were measured using five piezoelectric pressure gauges mounted on circular galvanized steel plates that enabled them to be attached on the stiff door of the test bunker at the holes locations, as shown in Fig. 5.4b. Pressure gauges P_1 to P_5 were Dytran model #2300V6 with sensitivity of (0.5 ± 20% mV/Psi), while incident pressure (*FF*) was measured using PCB model #113A21 with sensitivity of (25 ± 15% mV/Psi). The sandwich panels were simply supported, where the upper side was a pin support and the lower side was a roller support, where four load cells were used to measure the dynamic reactions for both upper (pin support) and lower (roller support) . Four potentiometers were used to measure displacements on the back face of the sandwich panel. Three potentiometers were fixed at equally spacing along the mid-span line of the tested specimen, while the forth potentiometer was fixed at the upper quarter of the specimen in the mid-width location, as shown in Fig. 5.4b. A high-speed data acquisition with a sampling rate of 1 MHz was used to record the output data.

5.3.2 Test Matrix

Eighteen sandwich panels, consisting of *Uni-directional* or *Bi-directional* core configurations were tested in this experimental investigation, as shown in Fig. 5.5. As tabulated in Table 5.1, each core configuration type was tested under three different scaled distances ($Z=SD/W^{1/3}$), which were determined in the primary dynamic analysis to achieve different damage levels according to the American and Canadian standards (ASCE 2012, CSA 2012).

All panels were fabricated using cold formed galvanized steel, which had a 304.8mm (12 in) width, 914.4mm (36 in) length and a 76.2 mm (3 in) core depth. The gauge 20 (0.91mm, 0.036 in) corrugated deck profiles used in the proposed core configurations were *B* and *N* profiles. The *B* profile had a depth of 38.1 mm (1.5 in), which was used for the double layer core in the *Bi-directional* sandwich panels, while the *N* profile had a depth of 76.2 mm (3 in) and was used in the single layer (*Uni-directional)* panels. The face sheets had a constant thickness of gauge14 (2.03 mm, 0.08 in). The panels were fabricated using Metal Inert Gas welding, where Plug and Fillet welding were used according to the core configurations. The welds were designed to exceed the expected strength of the tested panels, as the weld strength was not a concern in the current study. Further details of welding and fabrication of specimens can be found in (Khalifa et. al 2015b).

5.3.3 Test procedure

The blast testing in the blast chamber provided a controlled experimental environment, where many parameters that may affect the quality of recorded data were regulated, such as temperature, and humidity. The sandwich panels were simply supported and held in position using four steel clamps, each of the clamps fixed by two high strength bolts. Once all instrumentation was attached to the sandwich panel the stiff door in the test bunker was closed and held in place using six high strength bolts. The live explosive charge was held in position using a vertically tensioned rope, the detonator was placed in the explosive charge, and then the blast chamber door was closed. The detonation and recording the data was managed from control room.

5.4 TEST RESULTS

5.4.1 Post-Blast Observations

After each test the post-blast damage and mode of failure of each sandwich panel specimen were evaluated. The tested sandwich panels exhibited an elastic type behavior, as no permanent deformations were observed in the core webs or in the face sheets, under the first scaled distance Z_1. As anticipated, increasing permanent deformations were observed for more critical scenarios which were simulated by increasing the scaled distances from Z_2 to Z_4. No weld failure was observed for the eighteen tested sandwich panels, which emphases the ability of the proposed welding technique to withstand the blast loads and to behave according to the preliminary design. The observed dynamic failure modes for the *Uni-directional* and *Bi-directional* core configurations will be discussed in detail and compared with the quasi-static failure modes in the following sections.

5.4.2 Displacement Response History and Deflected shape

Fig. 5.6 shows the measured displacement response history at the mid-span of the back face of selected specimens under different scaled distances. Fig. 5.6a presents the mid-span displacement time history for the *B-T*-core configuration, where increasing maximum displacement can be seen to correspond to a decrease in the scaled distance. The elastic response of the *B-T*-core is observed to occur for the largest scaled distance Z_1, while the maximum deformation was to occur for the lowest scaled distance Z_3. This behavior was in agreement with the preliminary analysis and the design of the test matrix, where different scaled distances were determined to result in different damage levels as defined by the blast design standards.

Similarly, the influence of scaled distance on the maximum displacement experienced by the *N-S*-core can be seen in Fig. 5.6b. *N-S*-core exhibited an elastic response behavior under the Z_1 scaled distance, and as the scaled distance was decreased the maximum deformation was found to increase. From the test results it was observed that the dynamic strength of the *N-S*-core increased as the scaled distance was decreased. For example, the specimen was expected to experience global buckling due to shear under scaled distance Z_4, however this did not occur even when the scaled distance was reduced to Z_6 (reaching by this the maximum limit of charge weight in the blast chamber). It was also observed that the scaled distance was also found to affect the residual displacement. The residual displacement for each of the tested configurations under different scaled distances can be seen in Fig 6a and 6b, and likewise the maximum displacement, the residual displacement was found to increase by the decrease of the scaled distance.

The deflected shapes of the back face for the *N-S*-core and *B-T*-core configurations at different instants of time are shown in Fig. 5.7a and 5.7b, respectively. The elastic behavior is shown in the deformed shape of the *N-S*-core under scaled distance Z_1, while the plastic deformed shapes are shown for *B-T*-core under scaled distance $Z_{2.}$ As expected, the velocity (displacement/time difference) value varied with the different instants of time shown in figure. For example, the velocity values for the *N-S*-core shown in Fig. 5.7a were approximately 1.1, 3.9 and 1.2 mm/ms, which were calculated at 0.5 ms time intervals between 0-0.5, 1-1.5 and 2.0-2.5 ms, respectively.

5.5 ANALYSIS OF TEST RESULTS

5.5.1 Blast versus Quasi-Static Failure Modes

Blast resistant design standards, such as UFC 3-340-02 (2008), utilize the static resistance function in the solution of the equation of motion for the dynamic model of a structural element under blast load, For that, it is important to determine if the failure mode of a particular sandwich panel configuration remains consistent when exposed to different load regimes. This was accomplished by comparing the dynamic failure modes for the *Uni-directional* and *Bi-directional* corrugated core configurations to the quasi-static failure modes described by Khalifa et al. (2015b).

5.5.2 *Uni-directional* core sandwich panel (*N-S-core*)

According to the primary design and the static experimental test results, the *N-S*-core exhibited web crippling within the supports zone, followed by shear failure at higher load levels. Fig. 5.8 shows that the observed blast failure mode was in a good agreement with the static failure mode, although the *Uni-directional* core sandwich panels did not show the global buckling due to shear as expected. However, the occurrence of web crippling under dynamic loading matched that experienced by the test specimens under static testing (Khalifa et.al 2015b).

The *N-S*-core sandwich panels were tested under five different scaled distance scenarios as tabulated in Table 5.1. The first scaled distance Z_1 was meant to show the elastic behavior of the *N-S*-core, while Z_3 up to Z_6 showed different damage levels of web crippling, as shown in Fig. 5.8. Panel deformation was initiated by web crippling accompanied by small rotations at the back corners of the corrugated core. Under lower scaled distances (i.e. higher loads), web buckling was observed to increase in the lower third of the core webs resulting in the formation a plastic hinge. Furthermore, the section depth continued to decrease until the inner web formed an isosceles triangular shape, as shown in Fig. 5.8 (g). Consequently, it can be concluded that the static and dynamic modes of failure for the *N-S*-core panels were found to be consistent, which encouraged using its static resistance for the blast analysis after applying the transformation factors, which will be discussed later in the paper.

5.5.3 *Bi-directional* core sandwich panel (*B-T*-core)

The *Bi-directional* (*B-T*-core) sandwich panels consist of a two-way corrugated core using the galvanized *B* deck profile, which enables redistribution of the load as the core is deformed. Fig. 5.9 shows that the *B-T*-core sandwich panel dynamic response remained elastic, as expected, under the scaled distance Z_1. For more critical blast load scenarios (achieved by increasing the charge weight) the *B*-*T*-core sandwich panel, initiation of a global compression buckling failure in the front face at the mid-span location accompanied with local core buckling was observed. Under quasi-static testing, additional deformations were observed in the core compared to that during the blast testing, which is due to the impulsive loading regime when exposed to the blast loads. Furthermore, the *B*-*T*-core sandwich panel was observed to experience greater permanent deformation when the scaled distance value was decreased from Z_2 to Z_3. Since the *B*-*T*-core was found have same failure mode under both static and dynamic loads, therefore its recorded static resistance function can be used for the blast analysis after considering the dynamic increase effect.

5.5.4 Predicted versus Experimental Blast Wave Parameters

As mentioned, a confined blast is more complex than an equivalent open air blast, particularly after the early time positive phase shock wave. Typically, the damage resulting from a confined blast is expected to be higher than an equivalent open air blast. This is a result of the contribution of the reflected waves, in addition to the existence of the pseudo-static pressure, which is reflected magnifying the peak impulse value.

Fig. 5.10 shows a typical reflected pressure time history, measured at the mid-span of the tested specimen for different scaled distances, and a sample of the dynamic reactions are also presented in Fig. 5.10e. It is observed that for the small weight charge shots with relatively higher scaled distance values, such as the case of (Z_1 = 2.82 m/kg$^{1/3}$), the reflected pressure time history profile shows three positive pressures phases, which agrees with that proposed by Baker (1983). While for relatively lower values of scaled distances, for example Z_2 = 1.48 to Z_6 = 1.09 m/kg$^{1/3}$), the amplitude of the positive phase pressure of the reflected waves decreases as the scaled distance is decreased. It is postulated that this is a result of increasing the amount of released gases relative to the space volume, which resists the reflected pressure wave propagation in the confined space, and aids in building a higher pseudo-static pressure (gas pressure).

The initial positive shock wave of a confined blast can be predicted for spherical or hemispherical conditions (Baker et al. 1983, Krauthammer 2008). Often the positive phase of a spherical condition can be represented by the Friedlander equation. In order to evaluate the first positive phase parameters (peak pressure and impulse), non-linear regression analysis was used to fit the experimental positive pressure profiles with the modified Friedlander equation, expressed as (Baker et al. 1983):

$$P(t) = P_{max}\left(1 - \frac{t}{t_d}\right)\exp\left(-\alpha\frac{t}{t_d}\right) \qquad (1)$$

where $P(t)$ is the pressure, P_{max} is the peak pressure, α is the curve decay factor, t is the time, and t_d is the positive phase duration. Fig. 5.11 shows measured, Friedlander fitted, and ConWep predicted pressure time history profiles for different scaled distance values. The shock wave parameters, such as peak pressure, impulse, and positive phase duration for a spherical condition were predicted using ConWep (Hyde 1990) and compared to the experimental values, as tabulated in Table 5.2, and shown in Fig. 5.11.

As Composition *C-4* was used, conversion factors were employed to calculate the equivalent *TNT* weight either for pressure or impulse. The equivalent *TNT* weight is used to generate the presented blast wave parameters using ConWep in Table 5.2. For pressure values a conversion factor of 1.37 was used, where the ratio maximum reflected pressure of the experimentally fitted to ConWep predicted values was found to be 0.79, 0.67, 0.83, 0.78, 0.79 and 0.59 for the scaled distances Z_1, Z_2, Z_3, Z_4 ,Z_5, and Z_6, respectively, with a maximum error of (- 41 %). Furthermore, the ratio of maximum incident pressure values was found to be 0.75, 0.97, 0.65, 0.73, 1.05, and 0.77 for the scaled distances Z_1 up to Z_6, respectively, with an error that varied between (+5 % to -35 %).

For the impulse value comparison, a conversion factor of 1.19 was used to calculate the equivalent TNT weight. The ratio of the maximum experimentally fitted to ConWep reflected impulse values were found to be 1.01, 0.85, 0.78, 0.9, 1.08, and 1.11 for the scaled distances of distances Z_1, Z_2, Z_3, Z_4 ,Z_5, and Z_6, respectively, where the error varied between (+11% to -22%). In addition, the ratio of the maximum experimentally fitted to ConWep incident impulse values were found to be 0.87, 1.01, 0.71, 0.86, 0.82, and 0.97 for the scaled distances of distances Z_1 up to Z_6, respectively, and the error was found to vary between (+1% to -18%). Even with the typical uncertainties associated with the blast loading (Campidelli et al. 2015) and according to the presented error percentage between the predicted and the recorded values of pressure and impulse values, the prediction values can be considered to be a good agreement with the measured experimental data.

5.5.5 Single Degree of Freedom Model

Dynamic response modeling using a single degree of freedom (*SDOF*) approach is a well established method to predict component behavior in the context of blast resistant desgin standards (UFC-3-340-02 2008, ASCE 2012, CSA 2012). Transformation factors need to be applied to equate the actual deflection at a certain point on the real structural element to that obtained by the *SDOF* model (Biggs 1964). The transformation properties are determined based on the first mode shape of the structural element . The equation of motion for a *SDOF* model is expressed as

$$K_{LM}\, M\, \ddot{\delta} + R(\delta) = P(t) \tag{2}$$

where $\ddot{\delta}$ and δ are the temporal acceleration and displacement values, K_{LM} is the load-mass factor, M is the mass, $R(\delta)$ is the resistance function, and $P(t)$ is the load acting on the structural element.

The maximum displacement typically occurs during the first cycle of the response, and as a result the effect of damping is usually neglected.

The recorded blast pressure-time history is used as the applied load in the nonlinear *SDOF* model. Typically, in the case of an air explosion, only the positive phase of the shock wave profile is considered. However as previously mentioned, the characteristics of a confined blast wave are different, due to the build up of reflected waves. As such, the actual recorded pressure-time history is used to verify the accuracy of *SDOF* model and to predict the dynamic response of the panels.

In the dynamic mode the blast pressure (load) was assumed to act unifromly on the front face of the sandwich panel. According to the US Army Corps of Engineers Protective Design Center Technical Repot (SBEDS 2008), the blast load is representive of a far field explosion when the scaled distance ($Z > 1.2$ m/kg$^{1/3}$), and results in a near uniform pressure distrbution on the structure surface.

The inbound and rebound resistance are defined as the out-of-plane resistance of a structure component against the pressure wave positive (pushing) and negative (suction) phase, respectively. The inbound resistance in this study is computed as the average nonlinear resistance of the experimental quasi-static resistance functions. For the rebound resistance K_r, three different ratio values in terms of the inbound elastic stiffness (K_e) were considered, where values of K_r was assumed to be 0.5 K_e, 0.75 K_e, and 1.0 K_e as a preminallary assessment for the rebound stiffness on the dynamic response of the panels. Nonetheless, as the rebound resistance is beyond the scope of this study and requires further investigation, it was assumed to have a linear slope with a value equal to the elastic stiffness (SBEDS 2008). The mass of the of *N-S*-core sandwich panels was 12.45 kg and that for *B-T*-core sandwich panel was 15.00 kg. the load-mass factor K_{LM} were deterimend by double integrating of the deformed shape function (Biggs 1964), in order to transform the real sandwich panel to an equivilant *SDOF* system.

5.5.6 Static Resistance Function

Khalifa et.al (2015a and 2015b) used an air bag to apply a uniform out-of-plane quasi-static load on the front face of the sandwich panels considered in this study in order to evaluate their static resistance functions. Different configurations were investigated, including *Longitudinal* and *Transverse corrugated* core sandwich panels, in addition to *Uni-directional*, *Bi-directional corrugated* and *X-core* configurations using different deck profiles. The quasi-static resistance functions for the tested sandwich panel configurations were determined in terms of yield and ultimate forces and the corresponding displacements. Based on the results of the static experimental study, the *Uni-directional* and *Bi-directional* core configurations were selected as they exhibited significant ductility and energy absorption. Fig. 5.12 shows the experimental resistance function measured for the three tested samples of each core configuration, in addition to the average mean value of the three curves. Fig. 5.12a shows the resistance functions for the *Bi-directional*-core (*B-T*-core) sandwich panels, and Fig. 5.12b shows the resistance functions for the *Uni-directional* (*N-S*-core) sandwich panels.

5.5.7 Strain rate effect

The response of an element under impulsive or blast type loading can be considerably different than the response exhibited under long duration loading as high strain rates can affect both the response of the material and structure. According to UFC 3-340-02 (2008), the dynamic increase factor

(*DIF)* is applied to the static resistance to predict the dynamic response under blast loads can be estimated by:

$$R_{Dynamic} = DIF * R_{Static} \quad (3)$$

In accordance to the Canadian Standard CSA S850-12 (CSA 2012), *DIF* = 1.1 for cold formed steel. The *DIF* for the yield and ultimate strength of steel reinforcement as a function of the strain rate ($\dot{\varepsilon}$) was presented by (Malvar 1998) and can be calculated as follows

$$DIF_y = \left(\frac{\dot{\varepsilon}}{10^{-4}}\right)^{\alpha_y} \quad (4)$$

$$\alpha_y = 0.074 - 0.04\frac{f_y}{414} \quad (5)$$

where f_y is the tensile yield strength of steel in (MPa).

$$DIF_u = \left(\frac{\dot{\varepsilon}}{10^{-4}}\right)^{\alpha_u} \quad (6)$$

$$\alpha_u = 0.019 - 0.009\frac{f_y}{414} \quad (7)$$

Dynamic modeling using a single degree of freedom (*SDOF*) model could be employed to predict the dynamic behavior of a structure element subjected to blast loading, where the static resistance function is essintial to consider the stiffness corresponds to the displacement (Biggs 1964).

5.5.8 Comparison between predicted and measured maximum ductility

The sandwich panel back face displacement was determined using the mean value of four potentiometers (*A*, *B*, *C*, and *D*). Three potentiometers (A,B,C) were attached equally spaced along the mid span of the sandwich panel (as previously shown in Fig. 5.4), while potentiometer *D* was attached at the upper quarter of the specimen. Fig. 5.13 shows a typical measured displacement response history along with simulated response histories for the proposed sandwich panels exposed to different scaled distances. As previously mentioned, the inbound stiffness was computed as the slope of the static resistance function through each iteration during the analysis, while the rebound stiffness was assumed to be (K_r = 1.0 K_e). Since the American and Canadian standards for blast resistant design (ASCE 2012, CSA 2012) classify the damage state level according to the value of the maximum ductility or the support rotation, a comparison was performed between the predicted analytical and the experimentally recorded maximum ductility, and the ratio of the analytical to experimental maximum ductility was tabulated in Table 5.3. It was found that the most accurate prediction for the maximum ductility was in case of *N-S-*Z_3*-3* with a ratio of 99%, while the least accurate prediction was in case of *B-T-*Z_3*-2* with a ratio of 49 %. The difference in accuracy of the predicted maximum ductility is to some extent a reflection of the variability and uncertainties associated with blast loading.

5.5.9 Experimental versus predicted qualitative damage levels according to ASCE 59-11 and CSA S850-12

The test matrix was designed so that each type of sandwich panel core configuration was subjected to three different scaled distance scenarios. Each scenario is associated with a particular panel performance that corresponds to a damage level according to the blast resistant design standard. The American and Canadian for blast resistant design standards (ASCE 2012, CSA 2012) state the same limitations for defining the damage levels for cold formed steel, which are presented in Table 5.4, where μ_{max} and θ_{max} are the maximum ductility and support rotations, respectively. The Canadian design standard defines five damage levels - superficial damage where there is no feasible permanent damage; moderate damage where repairable permanent deformations exist; heavy damage where un-repairable permanent deformations exist but no failure; hazardous failure where the component failed but no velocities; and finally blowout where the component is overwhelmed by blast load causing debris with significant velocities.

Table 5.5 presents the analytical and experimentally obtained maximum ductility values for each of the tested sandwich panels. The predicted and observed damage levels were determined according to the standards, as previously discussed and tabulated in Table 5.3. According to the qualitative damage descriptions, the damage of N-S-Z_1 (*Uni-directional*-core) and B-T-Z_1 (*Bi-directional*-core) groups fall within the superficial damage level, as none of the sandwich panels in this group exhibited any permanent damage. For N-S-Z_3 group, the sandwich panels experienced permanent deformations due to web crippling and would be classified, according to the maximum ductility achieved, to fall within heavy damage level. Finally, the B-T-Z_3 and N-S-Z_4 groups achieved maximum ductility values that would be classified under the blowout damage level in accordance to *CSA S850-12* (CSA 2012) and *ASCE 59-11* (ASCE 2012). Even though this limit is not permitted in *ASCE 59-11*, according to the static resistance function, especially for the *N-S*-core (*Uni-directional*- core), this sandwich panel configuration can achieve greater resistance prior to reaching complete failure.

5.5.10 Influence of Core Configuration

By the end of the data analysis, the influence of core configuration on the exhibited performance characteristics of the sandwich panels under confined explosion is presented in this section, where it influenced the observed failure modes, as the *Uni-directional*-core panels exhibited web crippling deformations, while the *Bi-directional*-core failed in flexure with a plastic hinge forming near the mid-span. The core configuration also affected the blast resistance of the sandwich panels, where the *Uni-directional*-core (*N-S*-core) panels was found to have higher blast resistance than the *Bi-directional*-core (*B-T*-core) panels as can be seen by comparing the response of each core configuration corresponding to the same scaled distance.

Fig. 5.14 shows the influence of core configuration on the maximum displacement and ductility under different scaled distances. Comparing the maximum ductility (μ_{max}) of the two core configurations at same threat level, for example at a scaled distance (Z_3) scenario, (μ_{max}) was 2.5 for the *Uni-directional*-core and 23.3 for the *Bi-directional*-core panels. The resulting damage level according to the *CSA S850-12* (CSA 2012) is heavy damage for the *Uni-directional*-core panels and blowout damage for the *Bi-directional*-core panels.

5.6 CONCLUSIONS

The performance of lightweight cold formed steel sandwich panels under confined explosion was studied in this paper. Eighteen sandwich panels were subjected to live explosions in a blast chamber. The blast response of the tested configurations was evaluated and findings suggest that:

- It is viable to use the lightweight relatively cost-effective proposed panels as sacrificial cladding for blast risk mitigation.
- Post blast observations were discussed and the failure modes were determined and compared with the static failure modes of a previous study using the same core configurations (Khalifa et al. 2015b), which was found in a good agreement.
- The influence of scaled distance on the performance of the proposed sandwich panels was highlighted, where the tested configurations showed different deformations and damage levels when subjected to different scaled distances.
- The influence of core configuration on peak displacements and mode of failure was evaluated and discussed. Furthermore, supports rotations and ductility exhibited by the

tested panels were computed, and then related to the qualitative damage classification levels defined by the ASCE 59-11 (ASCE 2011) and CSA S850-12 (CSA 2012).

- No weld failure was observed in any of the tested sandwich panels, which agrees with the primary welding design demand to facilitate the welding to sustain until the complete failure of the sandwich panel, and emphasis the efficiency of the proposed welding technique to be suitable for joining the sandwich panels.
- The recorded blast wave parameters for the first positive phase were related to the predicted parameters (pressure and impulse) using the ConWep (Hyde 1990), and acceptable agreement was found. The error in predicting the reflected impulse varied between +11 % to -22%, while the error in predicting the reflected pressure varied between +17% to -33%.
- An explicit nonlinear SDOF model was developed to predict the sandwich panel response under blast loads. In general, the predicted response was in reasonable agreement with the experimental results. For the *Uni-directional*-core sandwich panels the difference in the maximum displacement was found to be between 67% to 99% , while it was between 67% to 98% for the *Bi-directional*-core panels. This SDOF model will be used later for further studies in the context of blast design, considering more parameters in a probabilistic risk assessment.

5.7 NOTATION

DIF = Dynamic increase factor.

f_y = Tensile yield strength in (MPa).

f_u = Ultimate strength in (MPa).

I_r = Reflected impulse in (kPa.msec).

K_{LM} = Load-mass factor.

M = Structre mass.

$P(t)$ = Pressure time history.

P_r = Peak reflected pressure in (kPa).

R = Resistance function.

SD = Stand-off distance.

$SDOF$ = Single degree of freedom.

SIF = Strength increase factor.

S_S = Specified material static strength in (MPa).

S_D = Dynamic material strength in (MPa).

TNT = Trinitrotoluene.

W = TNT charge mass in (kg).

Z = Scaled distance.

$\ddot{\delta}$ = Structure acceleration.

δ = Structure displacement.

$\dot{\varepsilon}$ = Strain rate in (1/sec).

5.8 REFERENCES

American Society of Civil Engineers (ASCE) (2012). "Blast Protection of Buildings." ASCE/SEI 59-11, Reston, Virginia.

Baker, W.E., Cox, P.A., Westine, P.S., Kulesz, J.J., and Strehlow, R.A. (1983). "Explosion Hazard and Evaluation." Oxford, New York, USA: Elservier Scientific Publishing Company.

Biggs, J. M. (1964). "Introduction to Structural Dynamics." New York: McGraw-Hill Inc.

Bondok, D., Salim, H., and Agee, B. (2013). “Improved Static Resistance and Failure Mechanisms of Conventional Cold-Formed Steel Stud Walls.” Journal of Performance of Constructed Facilities, 10.1061/(ASCE)CF.1943-5509.0000525,04014069.

Børvik, T. A. G. H., S. Dey, H. Langberg, M. Langseth (2008). "On The Ballistic and Blast Load Response of a 20 ft ISO Container Protected with Aluminum Panels Filled with a Local Mass-Phase I: Design of protective system." Journal of Engineering Structures, 30(6): 1605-1620.

Campidelli, M., El-Dakhakhni, W. W., Tait, M. J., and Mekky, W. (2015). "Blast Design-Basis Threat Uncertainty and Its Effects on Probabilistic Risk Assessment." ASCE-ASME Journal of Risk Uncertainty Eng. Syst., Part A: Civ. Eng.10.1061/AJRUA6.0000823.

Canadian Standards Association (CSA). (2012). “Design and Assessment of Buildings Subjected to Blast Loads.”, CSA S850-12, Mississauga, Ontario, Canada.

Cui, X., Zhaob, L., Wang, Z., Zhao, H., and Fang, D. (2012). "A Lattice Deformation Based Model of Metallic Lattice Sandwich Plates Subjected to Impulsive Loading." International Journal of Solids and Structures 49(19-20): 2854-2862.

Cui, X., Zhaob, L., Wang, Z., Zhao, H., and Fang, D. (2012). "Dynamic response of metallic lattice sandwich structures to impulsive loading." International Journal of Impact Engineering 43: 1-5.

Dharmasena,K.P., Queheillalt, D.T., Wadley, H.N, Dudt, P., Chen, Y., Knight, D., Evans, A.G., and Deshpande, V.S. (2010). "Dynamic Compression of Metallic Sandwich Structures During Planar Impulsive Loading in Water." European Journal of Mechanics - A/Solids 29(1): 56-67.

Dharmasena, K.P., Wadley, H.N, Williams, K., Xue, Z., and Hutchinson, J.W. (2011). "Response of Metallic Pyramidal Lattice Core Sandwich Panels to High Intensity Impulsive Loading in Air." International Journal of Impact Engineering 38(5): 275-289.

FEMA (2005). "A How-to Guide to Mitigate Potential Terrorist Attacks Against Buildings - FEMA 452 ". Federal Emergency Management Agency (FEMA), Washington, DC.

Fleck, N. A. and Deshpande, V. S. (2004). "The Resistance of Clamped Sandwich Beams to Shock Loading." Journal of Applied Mechanics 71(3): 386.

Hyde, D.W. (1990). "Conventional Weapons Effect (ConWep)." Application of TM5-855-1. US Army Engineer Waterways Experiment Station, Vicksburg, USA.

Jonathon, C. W. D., and Oehlers, D. J. (2013). "Simplification of Fully Confined Blasts for Structural Response Analysis." Engineering Structures 56: 312-326.

Khalifa, Y. A., Tait, M. J., and El-Dakhakhni, W. W. (2015a). "Out-of-Plane Behaviour of Metallic Sandwich Panels." ASCE Journal of Performance of Constructed Facilities, submitted for publication.

Khalifa, Y. A., El-Dakhakhni, W. W., and Tait, M. J. (2015b). "Metallic Sandwich Panels Performance Assessment under Quasi-Static Loading." Journal of Engineering Structures, submitted for publication.

Karagiozova, D., Nurick, G.N., and Langdon, G.S. (2009). "Behaviour of Sandwich Panels Subject to Intense Air Blasts – Part 2: Numerical simulation." Composite Structures 91(4): 442-450.

Krauthammer, T. (2008). "Modern Protective Structures." New York, USA:CRC Press, Taylor & Francis Group.

Liu, H., Cao , Z.K., Yao, G.C., Luo, H.J., and Zu, G.Y. (2013). "Performance of Aluminum Foam–Steel Panel Sandwich Composites Subjected to Blast Loading." Materials & Design 47: 483-488.

Malvar, L. J. (1998). "Review of Static and Dynamic Properties of Steel Reinforcing Bars." ACI MATERIALS JOURNAL.

McShane, G.J., Deshpande, V.S., and Fleck, N.A. (2010). "Underwater Blast Response of Free-Standing Sandwich Plates with Metallic Lattice Cores." International Journal of Impact Engineering 37(11): 1138-1149.

Nurick, G.N., Langdon, G.S., Chi, Y., and Jacob, N. (2009). "Behaviour of Sandwich Panels Subjected to Intense Air Blast – Part 1: Experiments." Composite Structures 91(4): 433-441.

Smith, P. D., and Hetherington, J. G. (1994). "Blast and Ballistic Loading of Structures." Butterworth-Heinemann Ltd.

Rimoli, J. J., Talamini, B., Wetzel, J. J., Dharmasena, K. P., Radovitzky, R., Wadley, H. N. G. (2011). "Wet-Sand Impulse Loading of Metallic Plates and Corrugated Core Sandwich Panels." International Journal of Impact Engineering 38(10): 837-848.

Salim, H. A., Muller, P., and Dinan, R. (2005). “Response of Conventional Steel Stud Wall Systems Under Static and Dynamic pressure.” Journal of Performance of Constructed Facilities, 10.1061/(ASCE)0887-3828(2005)19:4(267),267–276.

SBEDS (2008). "U.S. Army Corps of Engineers, Protective Design Center Technical Report."

Theobald, M.D., Langdon, G.S., Nurick, G.N., Pillay, S., Heyns, A., and Merrett, R.P. (2010). "Large Inelastic Response of Unbonded Metallic Foam and Honeycomb Core Sandwich Panels to Blast Loading." Composite Structures 92(10): 2465-2475.

Theobald, M. D. and Nurick, G. N. (2007). "Numerical Investigation of The Response of Sandwich-Type Panels Using Thin-Walled Tubes Subject to Blast Loads." International Journal of Impact Engineering 34(1): 134-156.

Theobald, M. D. and Nurick, G. N. (2010). "Experimental and Numerical Analysis of Tube-Core Claddings under Blast Loads." International Journal of Impact Engineering 37(3): 333-348.

US Army Corps of Engineers, Naval Facilities Engineering Command, and Air Forces Civil Engineer Support Agency (2008), “Structures to Resist the Effect of Accidental Explosions.” Unified Facilities Criteria, UFC 3-340-02.

Wang, T., Ma, M., Yu, W., Dong, S., and Gao, Y.(2011). "Mechanical Response of Square Honeycomb Sandwich Plate with Asymmetric Face Sheet Subjected to Blast Loading." Procedia Engineering 23: 457-463.

Whelan, M. J. Ralston, A. D., and Weggel, D. C. (2015). "Blast Testing of Cold-Formed Steel-Stud Wall Panels." Journal of Performance of Constructed Facilities, 10.1061/(ASCE)CF.1943-5509.0000734.

Xue, Z. and J. W. Hutchinson (2003). "Preliminary Assessment of Sandwich Plates Subject to Blast Loads." International Journal of Mechanical Sciences 45(4): 687-705.

Table 5.1: Matrix of test specimens

Shot	**Charge mass *C4* (kg)**	**Equivalent to *TNT* for pressure (kg)**	**Stand-off distance (m)**	**Scaled – distance value (m/kg$^{1/3}$)**	**Scaled - distance Z_i**	**Specimen**	**Core configuration**	**Pressures gauges distances from the charge center**					
								Incident pressure transducer *FF* (m)	**Reflected pressure transducer**				
									P_1 (m)	**P_2 (m)**	**P_3 (m)**	**P_4 (m)**	**P_5 (m)**
1	0.11	0.15	1.50	2.82	Z_1	*N-S-Z1-1*	*Uni-directional*	1.00	1.59	1.52	1.51	1.51	1.52
2	0.11	0.15	1.50	2.82	Z_1	*N-S-Z1-2*	*Uni-directional*	1.00	1.59	1.52	1.51	1.51	1.52
3	0.11	0.15	1.50	2.82	Z_1	*N-S-Z1-3*	*Uni-directional*	1.00	1.59	1.52	1.51	1.51	1.52
4	0.11	0.15	1.50	2.82	Z_1	*B-T-Z1-1*	*Bi-directional*	1.00	1.59	1.52	1.51	1.51	1.52
5	0.11	0.15	1.50	2.82	Z_1	*B-T-Z1-2*	*Bi-directional*	1.00	1.59	1.52	1.51	1.51	1.52
6	0.11	0.15	1.50	2.82	Z_1	*B-T-Z1-3*	*Bi-directional*	1.00	1.59	1.52	1.51	1.51	1.52
7	0.77	1.05	1.50	1.48	Z_2	*B-T-Z2-1*	*Bi-directional*	1.00	1.59	1.52	1.51	1.51	1.52
8	0.77	1.05	1.50	1.48	Z_2	*B-T-Z2-2*	*Bi-directional*	1.00	1.59	1.52	1.51	1.51	1.52
9	0.77	1.05	1.50	1.48	Z_2	*B-T-Z2-3*	*Bi-directional*	1.00	1.59	1.52	1.51	1.51	1.52
10	0.94	1.29	1.50	1.38	Z_3	*N-S-Z3-1*	*Uni-directional*	1.00	1.59	1.52	1.51	1.51	1.52
11	0.94	1.29	1.50	1.38	Z_3	*N-S-Z3-2*	*Uni-directional*	1.00	1.59	1.52	1.51	1.51	1.52
12	0.94	1.29	1.50	1.38	Z_3	*N-S-Z3-3*	*Uni-directional*	1.00	1.59	1.52	1.51	1.51	1.52
13	0.94	1.29	1.50	1.38	Z_3	*B-T-Z3-1*	*Bi-directional*	1.00	1.59	1.52	1.51	1.51	1.52
14	0.94	1.29	1.50	1.38	Z_3	*B-T-Z3-2*	*Bi-directional*	1.00	1.59	1.52	1.51	1.51	1.52
15	0.94	1.29	1.50	1.38	Z_3	*B-T-Z3-3*	*Bi-directional*	1.00	1.59	1.52	1.51	1.51	1.52
16	1.39	1.90	1.50	1.21	Z_4	*N-S-Z4-1*	*Uni-directional*	1.00	1.59	1.52	1.51	1.51	1.52
17	1.62	2.22	1.50	1.15	Z_5	*N-S-Z4-2*	*Uni-directional*	1.00	1.59	1.52	1.51	1.51	1.52
18	1.92	2.63	1.50	1.09	Z_6	*N-S-Z4-3*	*Uni-directional*	1.00	1.59	1.52	1.51	1.51	1.52

Table 5.2: Predicted and measured reflected pressure and impulse

Scaled distance (Z_i)	**Data source**	**Conversion factor = 1.37**		**Conversion factor = 1.19**	
		$P_{r\,(max)}$ (kPa)	$P_{so\,(max)}$ (kPa)	I_r (kPa.ms)	I_s (kPa.ms)
Z_1	Experimental	335	179	78	40
	ConWep	242.03	224	75	47
	Fitted	192	167	76	41
	Ratio	0.79	0.75	1.01	0.87
Z_2	Experimental	1571	1247	285	183
	ConWep	1523	973	307	165
	Fitted	1028	942	260	166
	Ratio	0.67	0.97	0.85	1.01
Z_3	Experimental	2226	968	358	136
	ConWep	1874	1126	356	186
	Fitted	1560	727	279	132
	Ratio	0.83	0.65	0.78	0.71
Z_4	Experimental	3171	1207	613	203
	ConWep	2768	1490	476	228
	Fitted	2153	1081	428	195
	Ratio	0.78	0.73	0.90	0.86
Z_5	Experimental	3736	1740	530	248
	ConWep	3232	1662	495	243
	Fitted	2542	1746	535	200
	Ratio	0.79	1.05	1.08	0.82
Z_6	Experimental	4084	1740	779	259
	ConWep	3820	1877	610	248
	Fitted	2241	1436	675	241
	Ratio	0.59	0.77	1.11	0.97

Table 5.3: Analytical (SDOF) and Experimental maximum displacement, ductility, and support rotation

Shot	Scaled distance		Specimen name	Analytical *(SDOF)*			Experimental			Ratio (Analytical / Experimental)
	(Z_i)	**(m/kg$^{1/3}$)**		δ_{amax} (mm)	μ_{amax}	θ_{amax} (rad)	δ_{emax} (mm)	μ_{emax}	θ_{emax} (rad)	μ_{amax}/μ_{emax}
1	Z_1	2.82	*N-S-Z_1-1*	2.2	0.31	0.005	3.3	0.47	0.007	0.67
2	Z_1	2.82	*N-S-Z_1-2*	2.2	0.31	0.005	1.7	0.24	0.004	1.29
3	Z_1	2.82	*N-S-Z_1-3*	2.2	0.31	0.005	2.5	0.36	0.005	0.88
4	Z_1	2.82	*B-T-Z_1-1*	3.03	0.45	0.007	3.7	0.55	0.008	0.82
5	Z_1	2.82	*B-T-Z_1-2*	3.03	0.45	0.007	4.5	0.67	0.010	0.67
6	Z_1	2.82	*B-T-Z_1-3*	3.03	0.45	0.007	3.8	0.57	0.008	0.80
7	Z_2	1.48	*B-T-Z_2-1*	60.5	9.03	0.132	61.2	9.09	0.129	0.98
8	Z_2	1.48	*B-T-Z_2-2*	60.5	9.03	0.132	44.3	6.61	0.097	1.37
9	Z_2	1.48	*B-T-Z_2-3*	60.5	9.03	0.132	80.1	11.96	0.175	0.76
10	Z_3	1.38	*N-S-Z_3-1*	17.3	2.47	0.038	13.1	1.87	0.029	1.32
11	Z_3	1.38	*N-S-Z_3-2*	17.3	2.47	0.038	18.3	2.61	0.040	0.95
12	Z_3	1.38	*N-S-Z_3-3*	17.3	2.47	0.038	17.4	2.49	0.038	0.99
13	Z_3	1.38	*B-T-Z_3-1*	73.8	11.01	0.161	118.3	17.66	0.259	0.62
14	Z_3	1.38	*B-T-Z_3-2*	73.8	11.01	0.161	156.2	23.31	0.342	0.47
15	Z_3	1.38	*B-T-Z_3-3*	73.8	11.01	0.161	150.7	22.49	0.330	0.49
16	Z_4	1.21	*N-S-Z_4*	66.2	9.46	0.145	43.9	6.27	0.10	1.51
17	Z_5	1.15	*N-S-Z_5*	70.9	10.13	0.155	73.5	10.50	0.161	0.96
18	Z_6	1.09	*N-S-Z_6*	77.1	11.01	0.169	N.A.	-	-	-

δa_{max} = Maximum analytical displacement, δe_{max} = Maximum experimental displacement.

μa_{max} = Maximum analytical ductility displacement, μe_{max} = Maximum experimental ductility displacement.

θa_{max} = Maximum analytical support rotation, θe_{max} = Maximum experimental support rotation.

Table 5.4: Response limits for cold-formed steel elements according to ASCE/SEI 59-11 and CSA S850-12 Response Limits*

<table>
<tr><th>Panel damage state</th><th>Superficial damage</th><th colspan="2">Moderate damage</th><th colspan="2">Heavy damage</th><th colspan="2">Hazardous failure</th><th>Blowout</th></tr>
<tr><td rowspan="3">Quantitative damage description</td><td colspan="2">B_1</td><td colspan="2">B_2</td><td colspan="2">B_3</td><td colspan="2">B_4</td></tr>
<tr><td>Ductility μ_{max}</td><td>Support rotation θ_{max}</td><td>Ductility μ_{max}</td><td>Support rotation θ_{max}</td><td>Ductility μ_{max}</td><td>Support rotation θ_{max}</td><td>Ductility μ_{max}</td><td>Support rotation θ_{max}</td></tr>
<tr><td>1</td><td>-</td><td>1.8</td><td>1.3°</td><td>3</td><td>2°</td><td>6</td><td>4°</td></tr>
<tr><td rowspan="2">Qualitative damage description</td><td rowspan="2">The Panel is unlikely to exhibit any feasible permanent damage.</td><td colspan="2" rowspan="2">The Panel shows a repairable permanent deformation.</td><td colspan="2" rowspan="2">The Panel show un-repairable permanent deformations with no failure.</td><td colspan="2">The Panel fails with no significant velocities (CSA S850-12).</td><td>The Panel has overwhelmed by blast causing debris with significant velocities (CSA S850-12).</td></tr>
<tr><td colspan="2">The Panel is likely to fail and produce significant scabbing (ASCE/SEI 59-11).</td><td>N.A (ASCE/SEI 59-11).</td></tr>
<tr><td>Predicted Level of Performance for non-structure building element</td><td>High</td><td colspan="2">Medium</td><td colspan="2">Low</td><td colspan="2">Very Low</td><td>N.A.</td></tr>
<tr><td>Building performance</td><td>Operational</td><td colspan="2">Immediate Occupancy</td><td colspan="2">Life Safety</td><td colspan="2">Collapse Prevention</td><td>N.A.</td></tr>
</table>

*Corrugated one way panel with limited tension membrane in flexure.

Table 5.5: Analytical (SDOF) and Experimental maximum damage level according to (CSA/ S850-12) and (ASCE/SEI 59-11)

Shot	Scaled distance (Z_i)	Scaled distance (m/kg$^{1/3}$)	Specimen name	Analytical SDOF		Experimental	
				μ_{amax}	Damage level	μ_{emax}	Damage level
1	Z_1	2.82	$N\text{-}S\text{-}Z_1\text{-}1$	0.31	Superficial	0.47	Superficial
2	Z_1	2.82	$N\text{-}S\text{-}Z_1\text{-}2$	0.31	Superficial	0.24	Superficial
3	Z_1	2.82	$N\text{-}S\text{-}Z_1\text{-}3$	0.31	Superficial	0.47	Superficial
4	Z_1	2.82	$B\text{-}T\text{-}Z_1\text{-}1$	0.45	Superficial	0.55	Superficial
5	Z_1	2.82	$B\text{-}T\text{-}Z_1\text{-}2$	0.45	Superficial	0.67	Superficial
6	Z_1	2.82	$B\text{-}T\text{-}Z_1\text{-}3$	0.45	Superficial	0.57	Superficial
7	Z_2	1.48	$B\text{-}T\text{-}Z_2\text{-}1$	9.03	Blowout	9.09	Blowout
8	Z_2	1.48	$B\text{-}T\text{-}Z_2\text{-}2$	9.03	Blowout	6.61	Blowout
9	Z_2	1.48	$B\text{-}T\text{-}Z_2\text{-}3$	9.03	Blowout	11.96	Blowout
10	Z_3	1.38	$N\text{-}S\text{-}Z_3\text{-}1$	2.47	Heavy	1.87	Heavy
11	Z_3	1.38	$N\text{-}S\text{-}Z_3\text{-}2$	2.47	Heavy	2.61	Heavy
12	Z_3	1.38	$N\text{-}S\text{-}Z_3\text{-}3$	2.47	Heavy	2.49	Heavy
13	Z_3	1.38	$B\text{-}T\text{-}Z_3\text{-}1$	11.01	Blowout	17.66	Blowout
14	Z_3	1.38	$B\text{-}T\text{-}Z_3\text{-}2$	11.01	Blowout	23.31	Blowout
15	Z_3	1.38	$B\text{-}T\text{-}Z_3\text{-}3$	11.01	Blowout	22.49	Blowout
16	Z_4	1.21	$N\text{-}S\text{-}Z_4$	9.46	Blowout	6.27	Blowout
17	Z_5	1.15	$N\text{-}S\text{-}Z_5$	10.13	Blowout	10.50	Blowout
18	Z_6	1.09	$N\text{-}S\text{-}Z_6$	11.01	Blowout	N.A.	-

μa_{max} = Maximum analytical ductility displacement, μa_{max} = Maximum experimental ductility displacement.

.

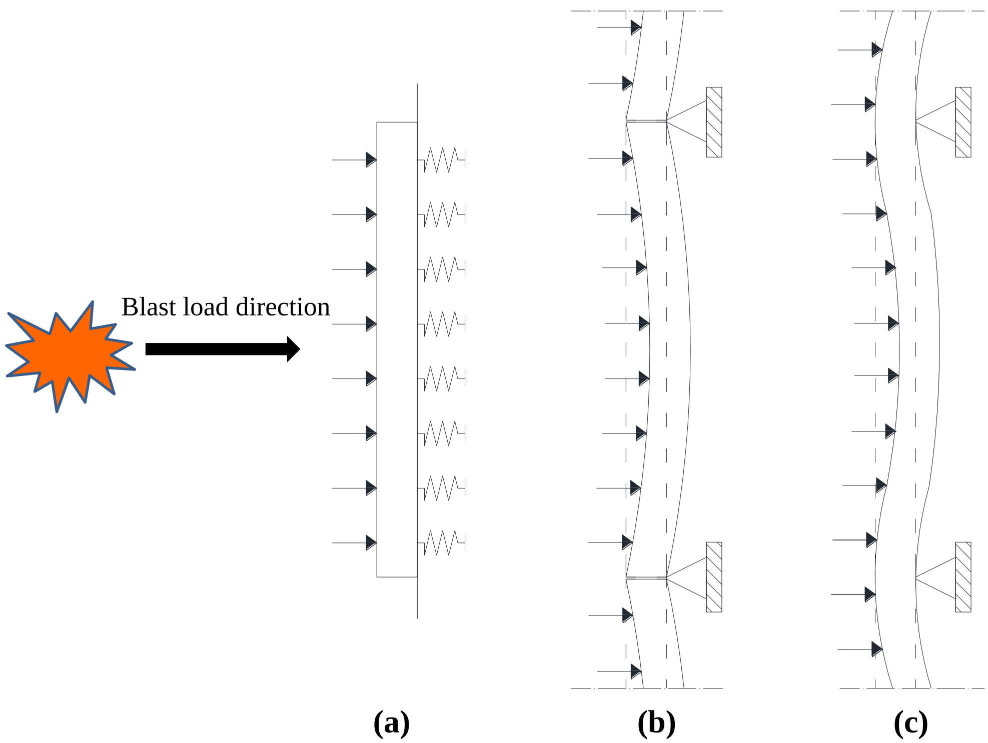

Fig. 5.1 Sacrificial cladding types (a) continuous contact with main structure, (b) simply supported by main structure and (c) continuously supported by main structure.

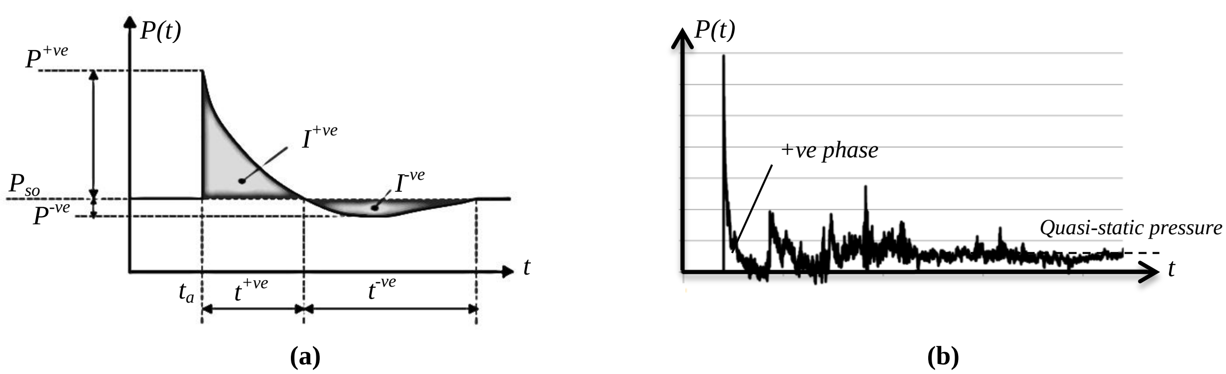

Fig. 5.2Typical blast wave pressure time profile (a) open air blast and (b) confined blast.

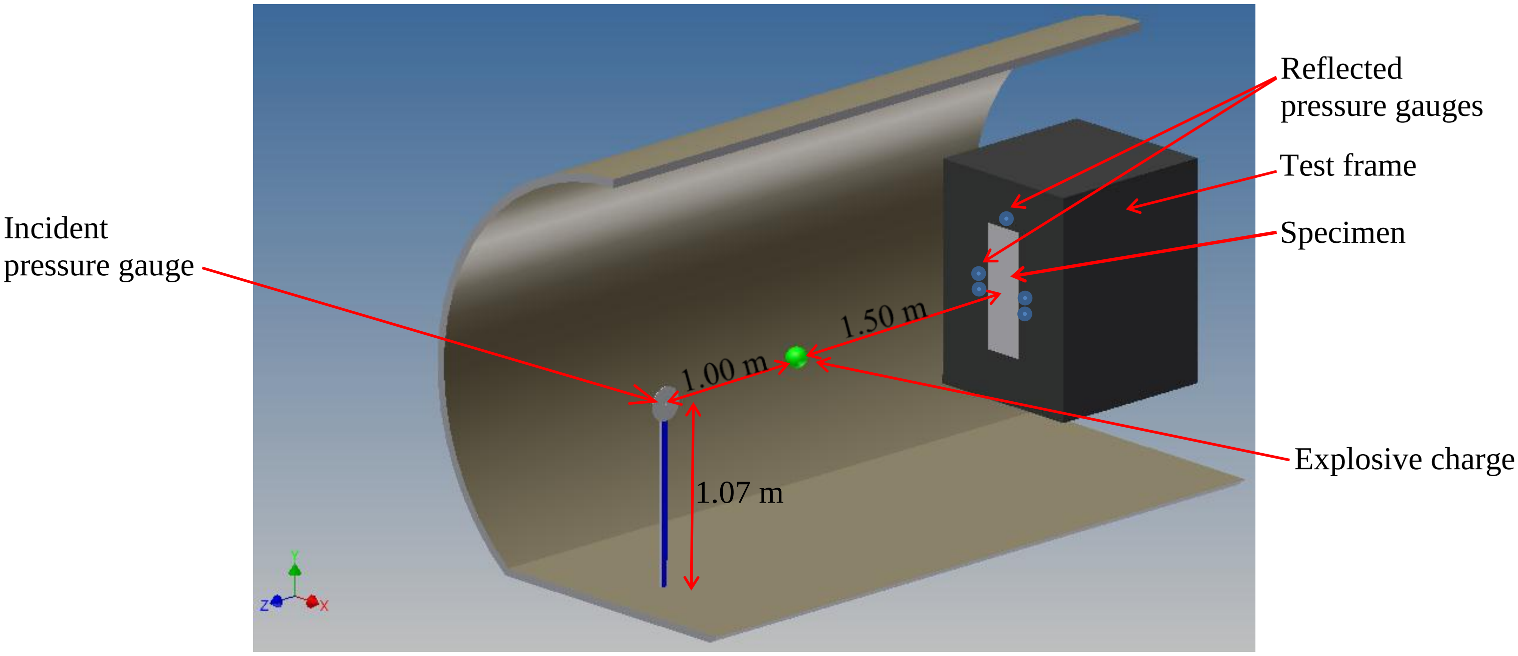

(a)

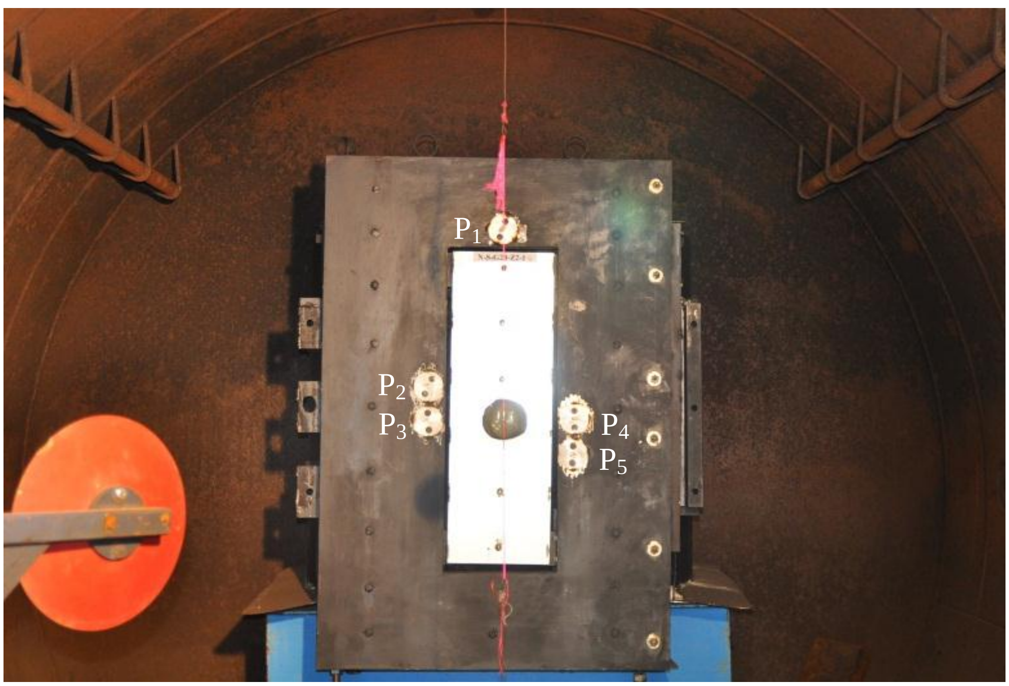

(b)

Fig. 5.3 Test setup and blast chamber (a) 3D schematic view for the test setup and (b) the test setup in the blast chamber.

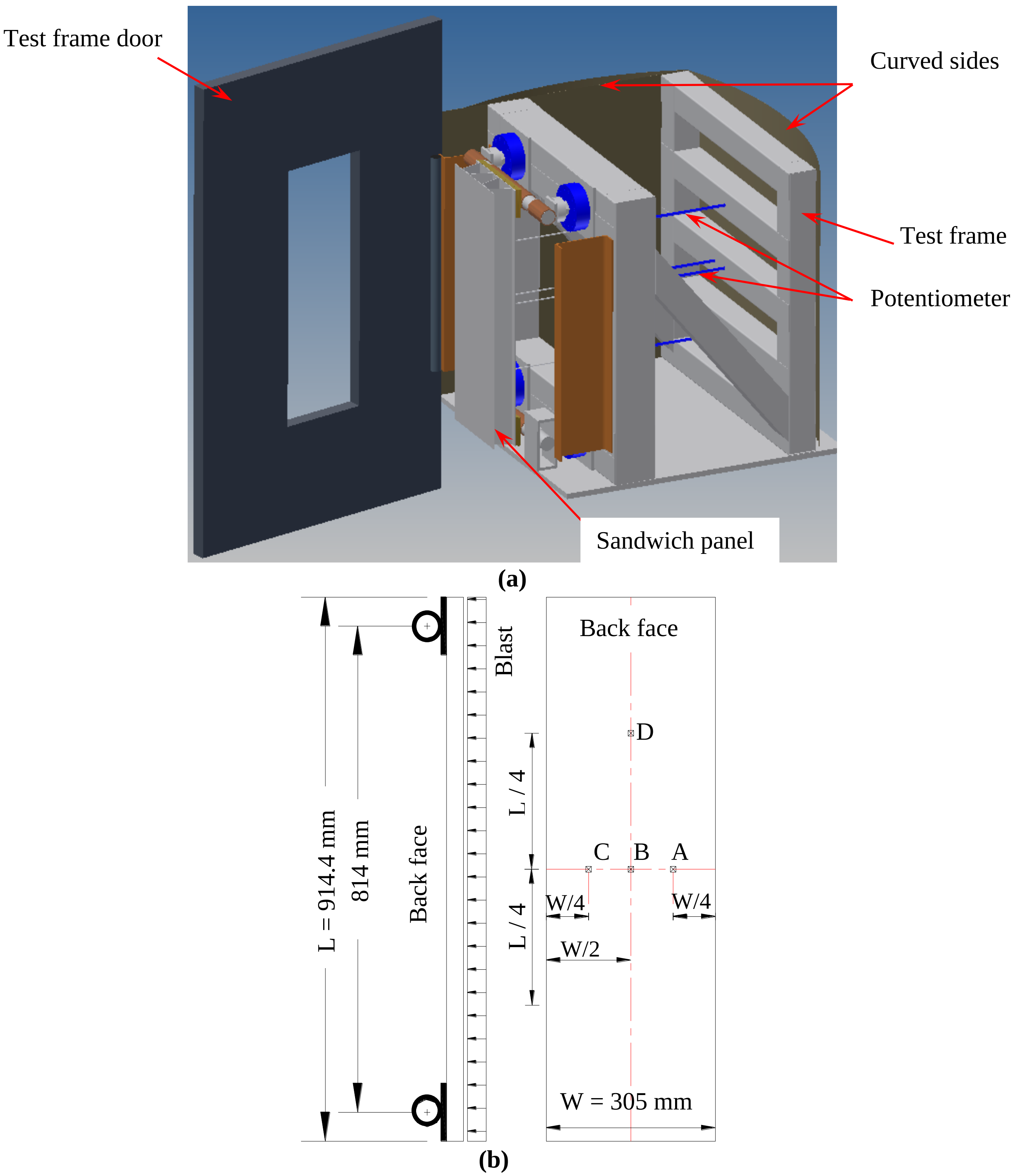

Fig. 5.4 Test setup and instrumentations (a) 3D view for the test setup and (b) Panel dimensions and potentiometers.

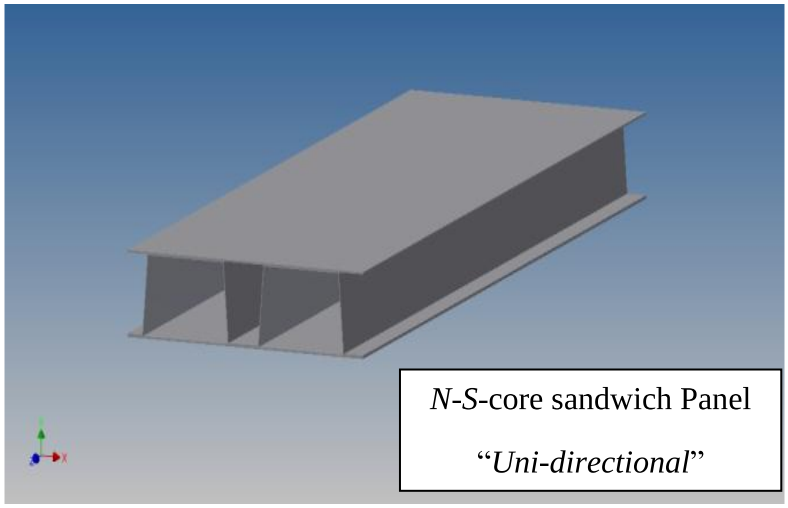

(a)

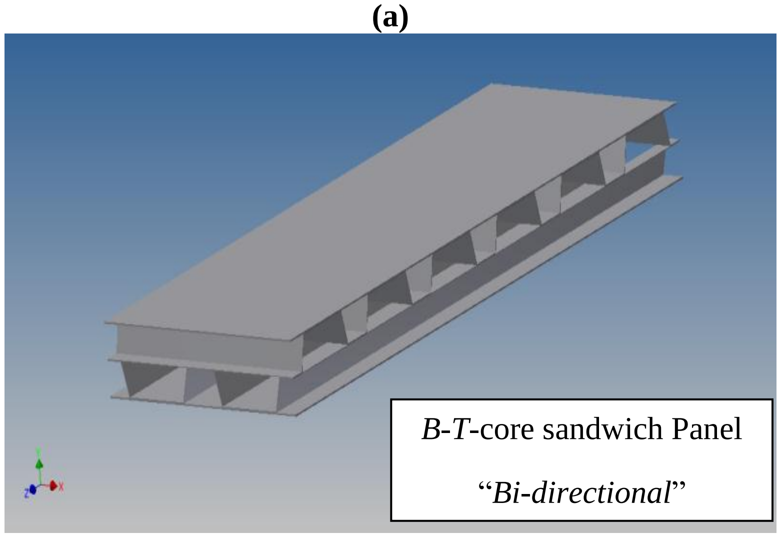

(b)

Fig. 5.5 Proposed sandwich panels core configurations, (a) N-S-core (*Uni-directional*) and (b) B-T-core (*Bi-directional*).

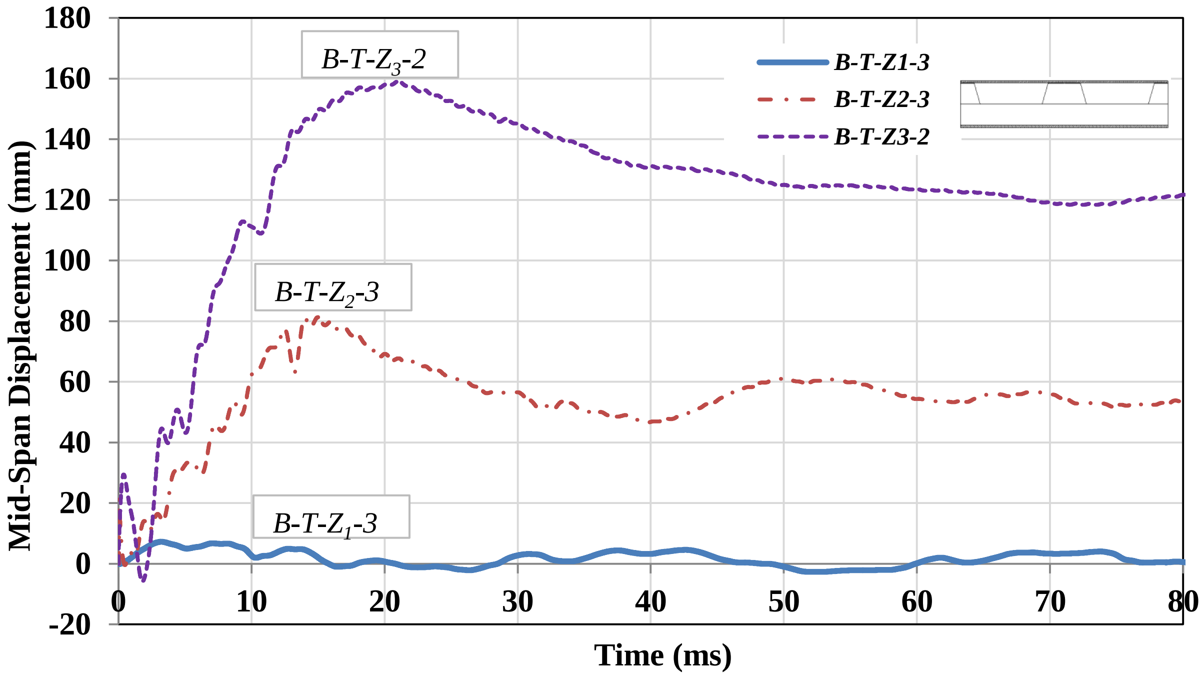

(a)

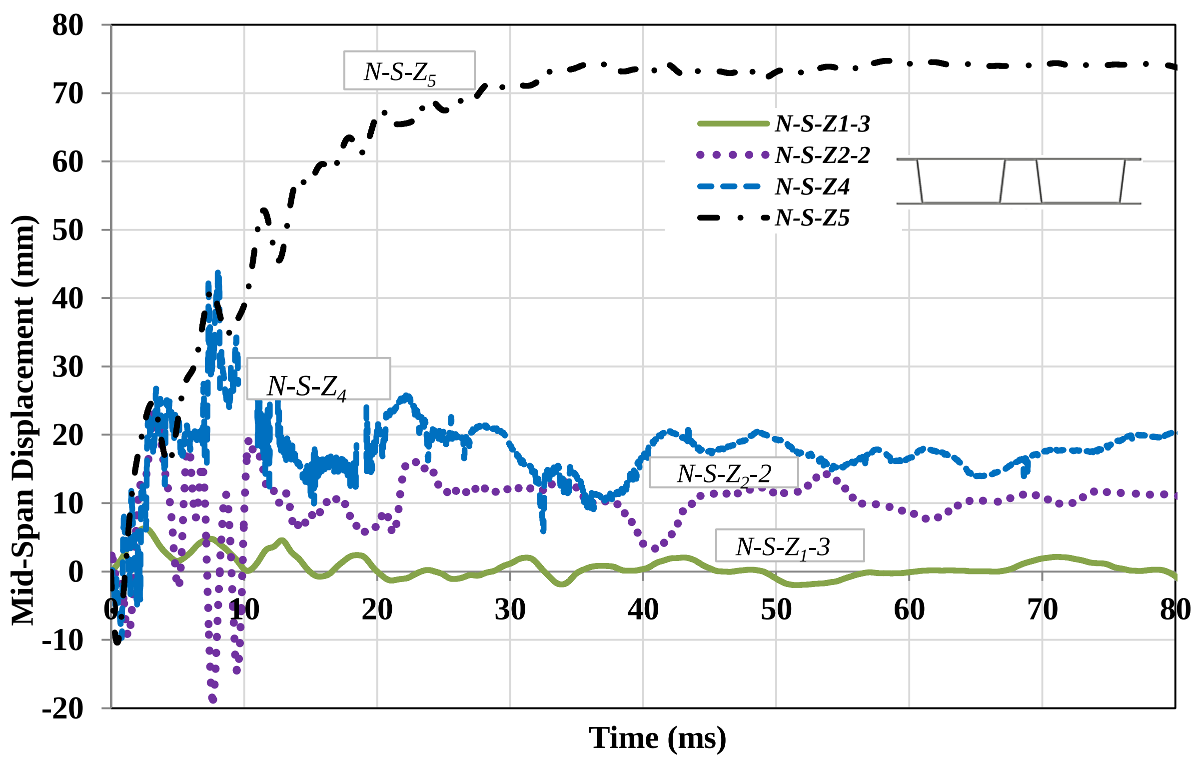

(b)

Fig. 5.6 Mid-span displacement time histories, (a) *Bi-directional* panels (*B-T*-core) and (b) *Uni-directional* panels (*N-S*-core).

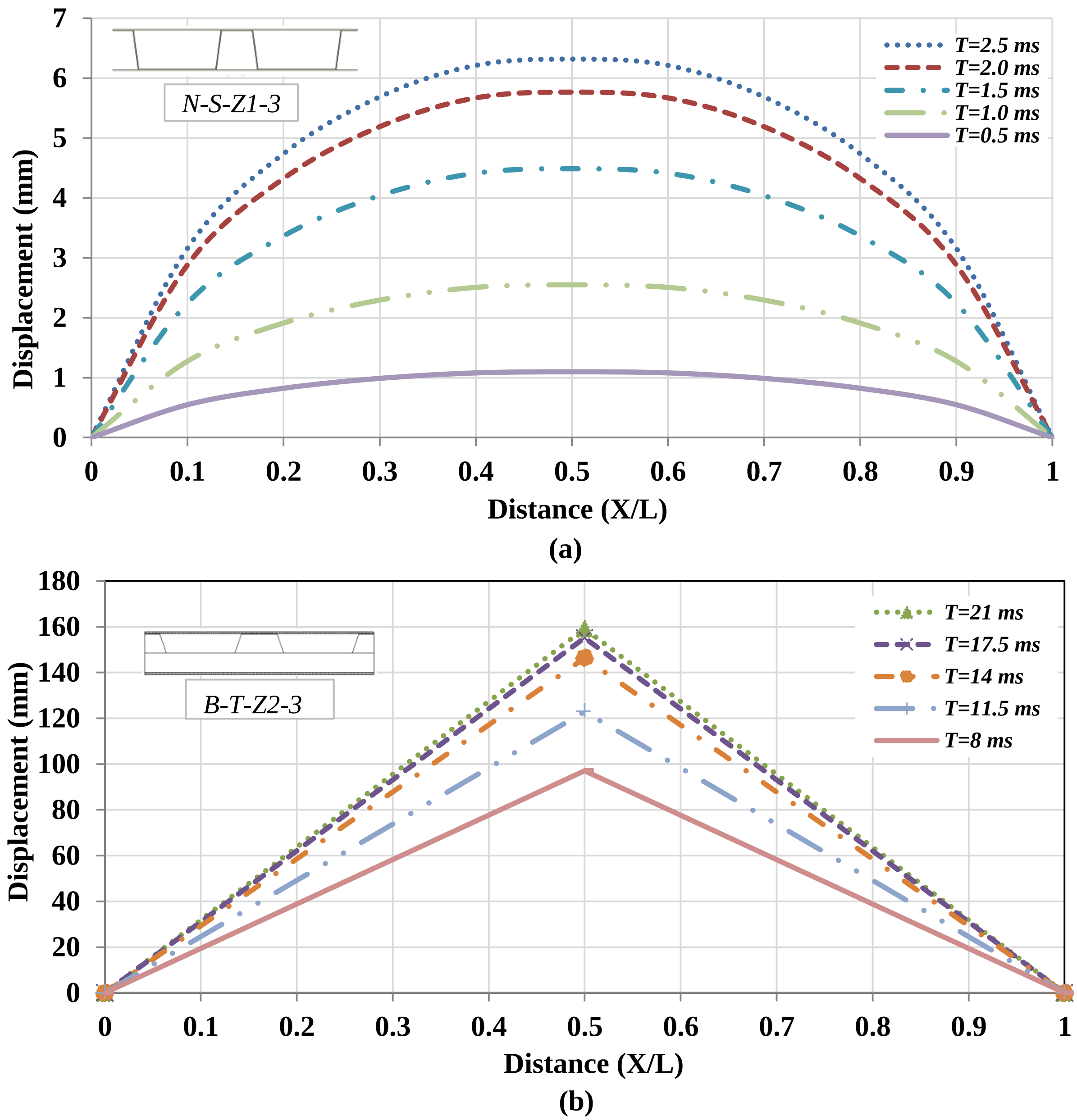

Fig. 5.7 Back face deflected shape at different instants of time, (a) *Uni-directional* panel at shot-3 (*N-S-Z1-3*) and (b) *Bi-directional* panel at shot-9 (*B-T*-Z_2-3).

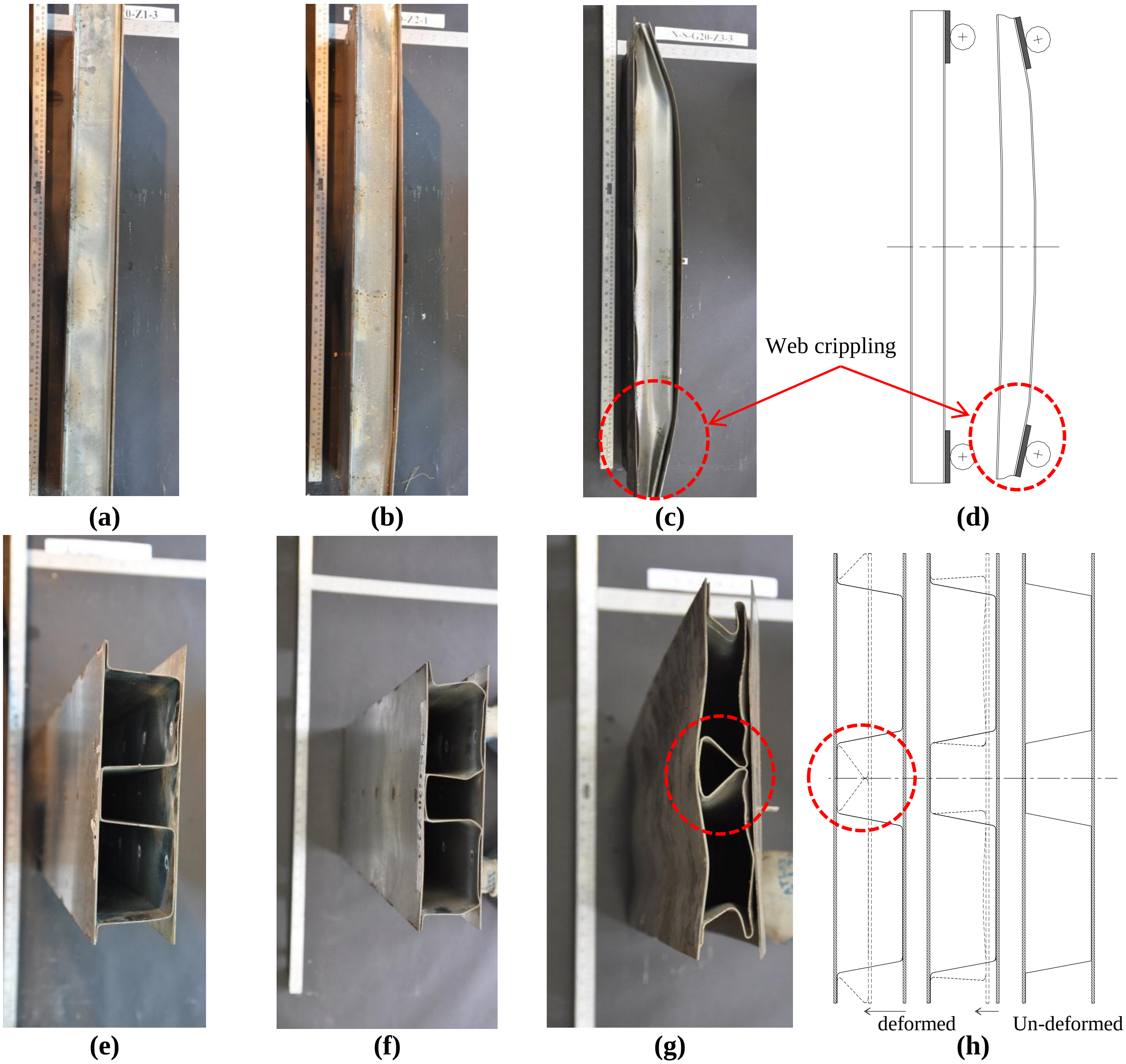

Fig. 5.8 Observed and expected failure modes of *N-S*-core sandwich panels, (a) & (e) for scale distance Z_1, (b) & (f) for scale distance Z_3, (c) & (g) for scale distance Z_4 and (d) & (h) expected failure mode shape.

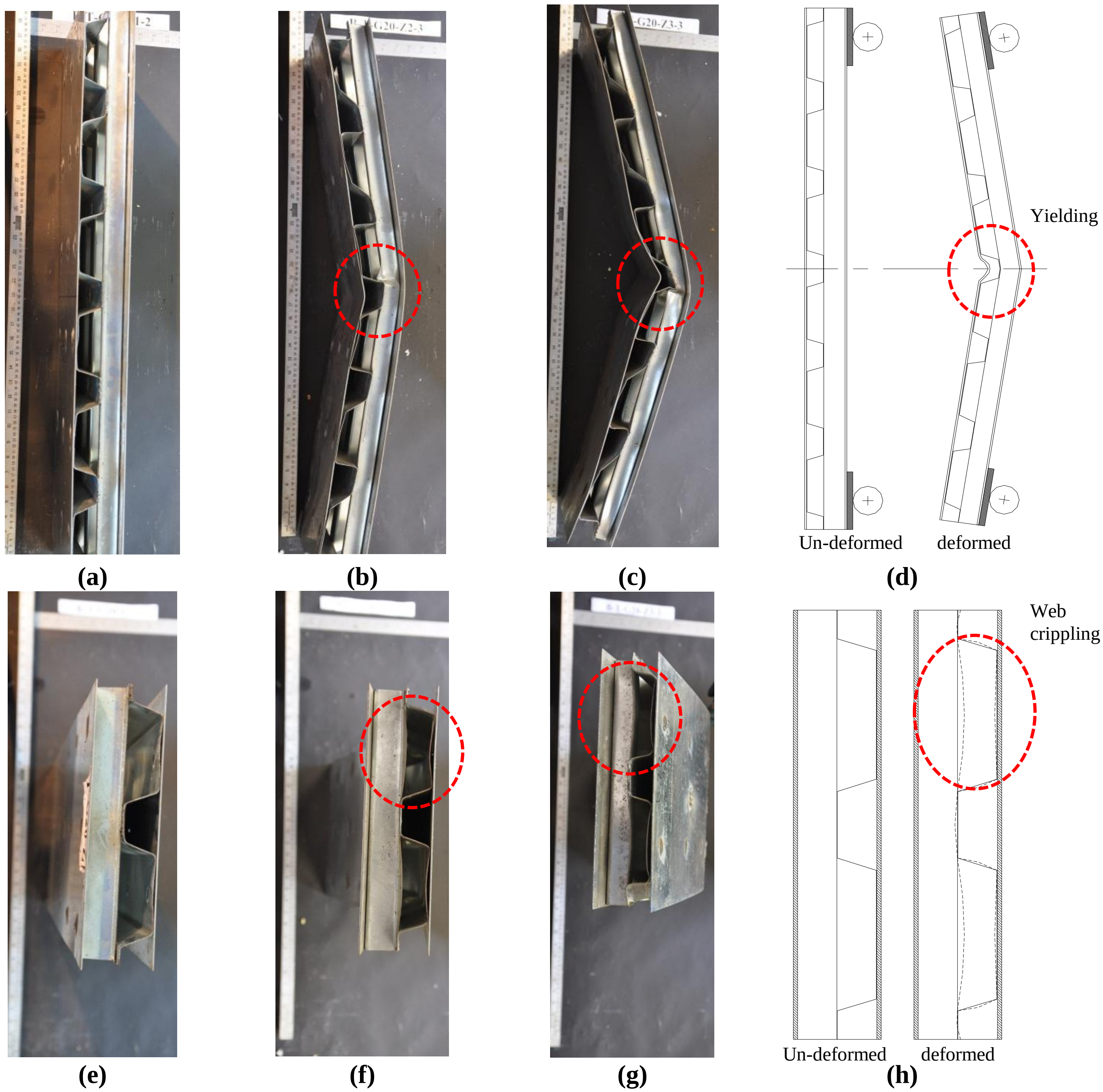

Fig. 5.9 Observed and expected failure modes of *B*-*T*-core sandwich panels, (a) & (e) for scale distance Z_1, (b) & (f) for scale distance Z_2, (c) & (g) for scale distance Z_3, and (d) & (h) expected failure mode shape.

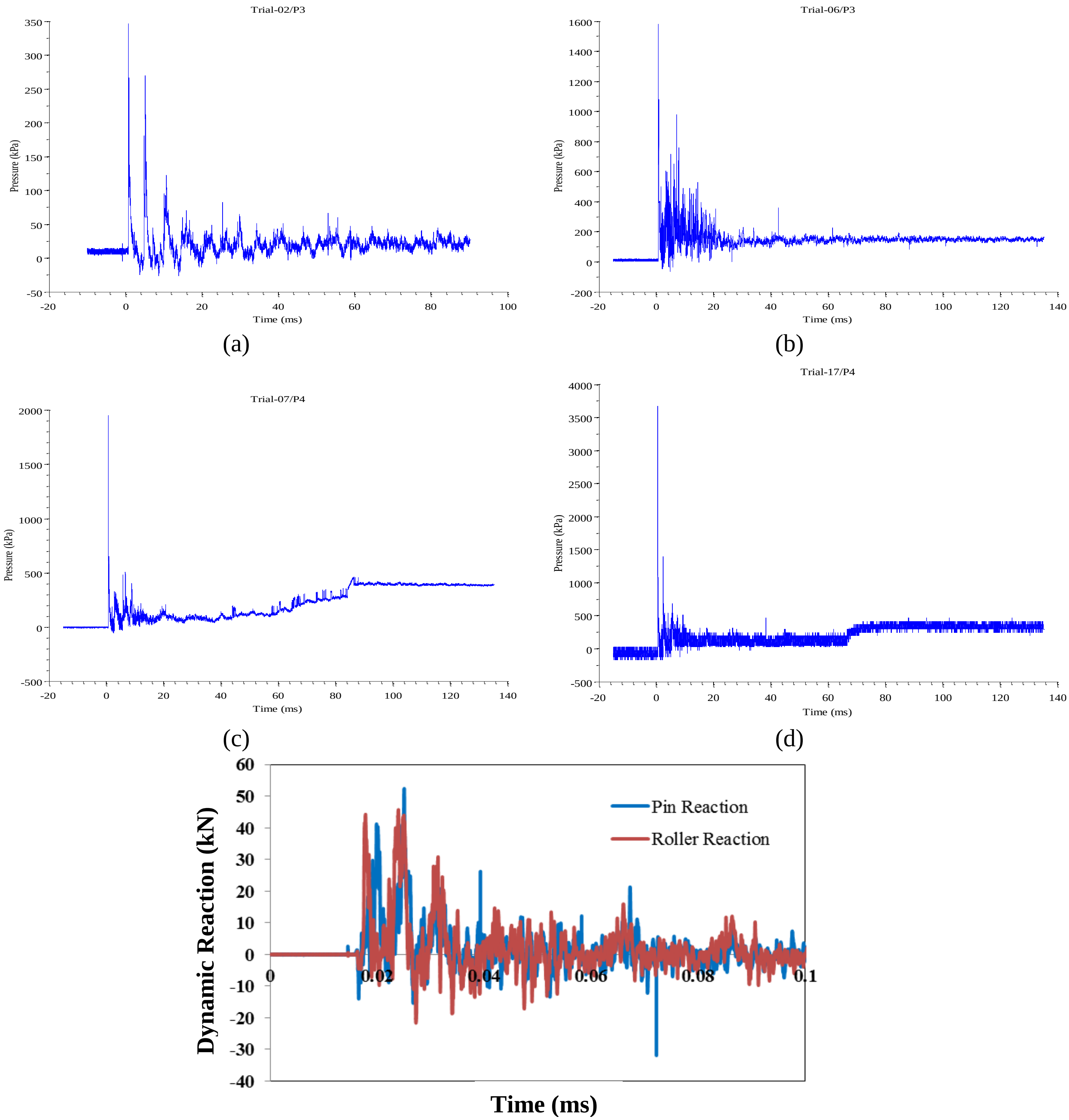

(e)

Fig. 5.10 Typical reflected pressure-time history and dynamic reaction for (a) Shot-2, scale distance Z_1, (b) Shot-6, scale distance Z_2, (c) Shot-7, scale distance Z_3, (d) Shot-17, scale distance Z_4 and (e) dynamic reaction.

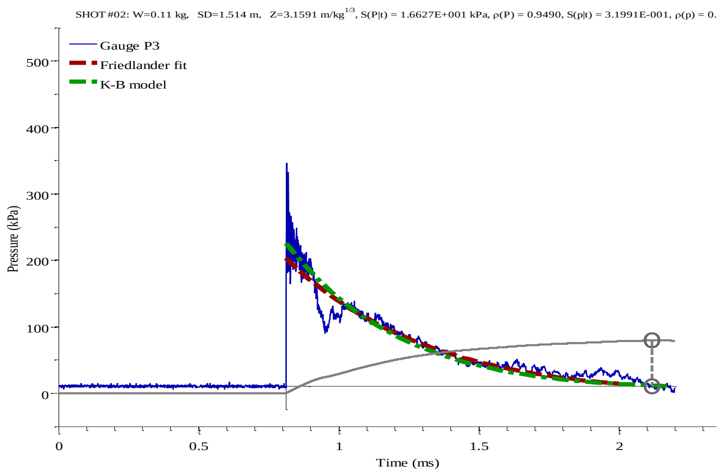

(a)

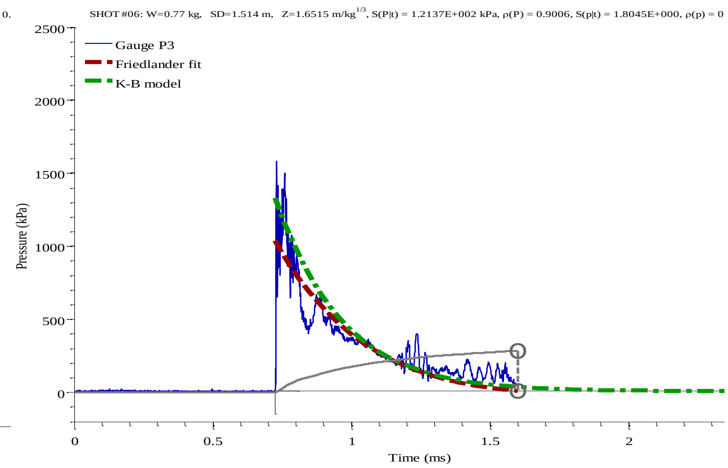

(b)

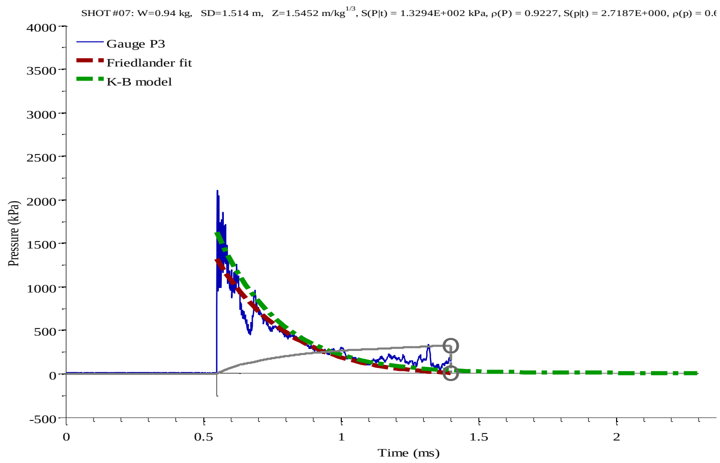

(c)

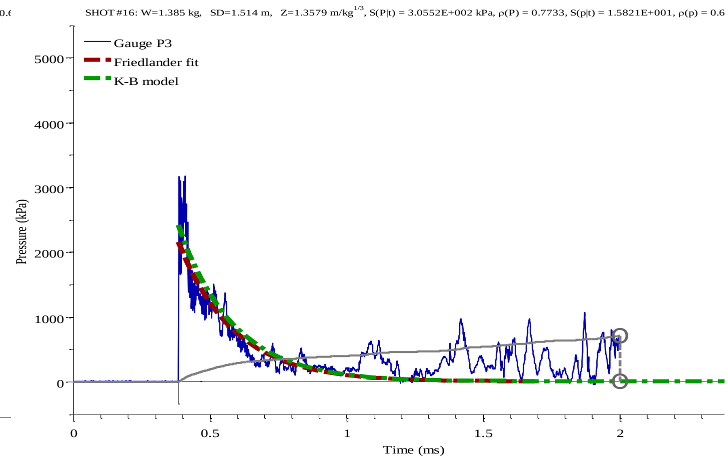

(d)

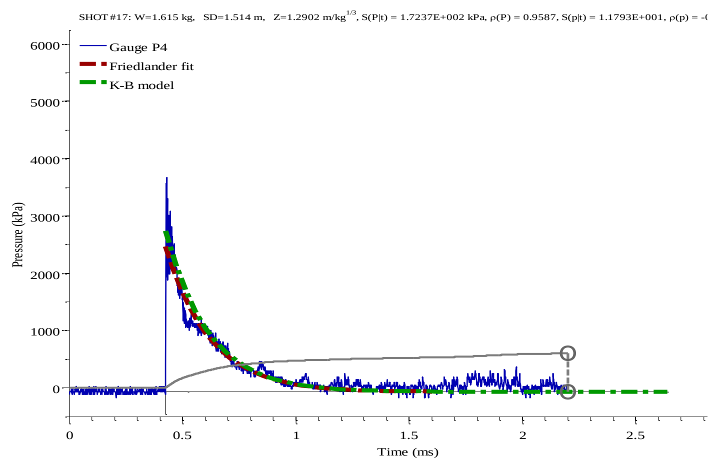

(e)

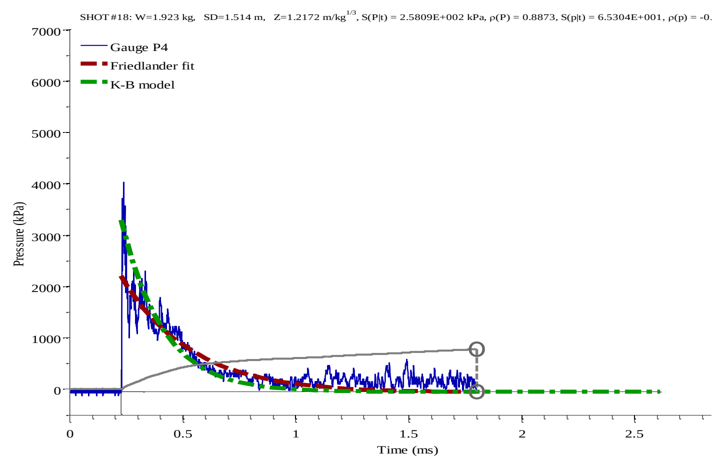

(f)

Fig. 5. 11 Typical reflected pressure, fitted Friedlander and ConWep expected pressure time histories of the first positive phase for (a) Shot-2, scale distance Z_1, (b) Shot-6, scale distance Z_2, (c) Shot-7, scale distance Z_3, (d) Shot-16, scale distance Z_4, (e) Shot-17, scale distance Z_5 and (f) Shot-18, scale distance Z_6.

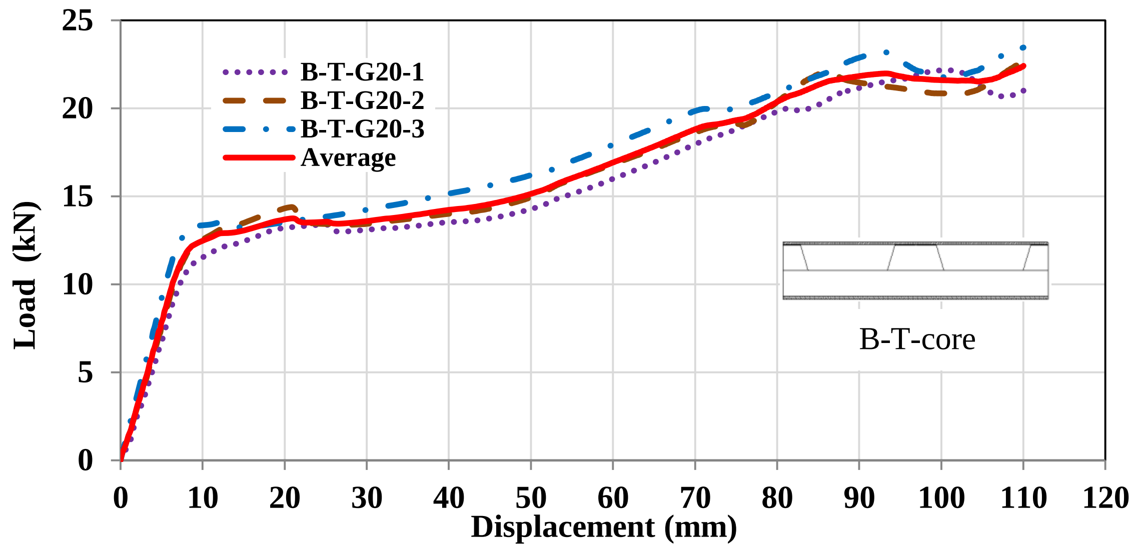

(a)

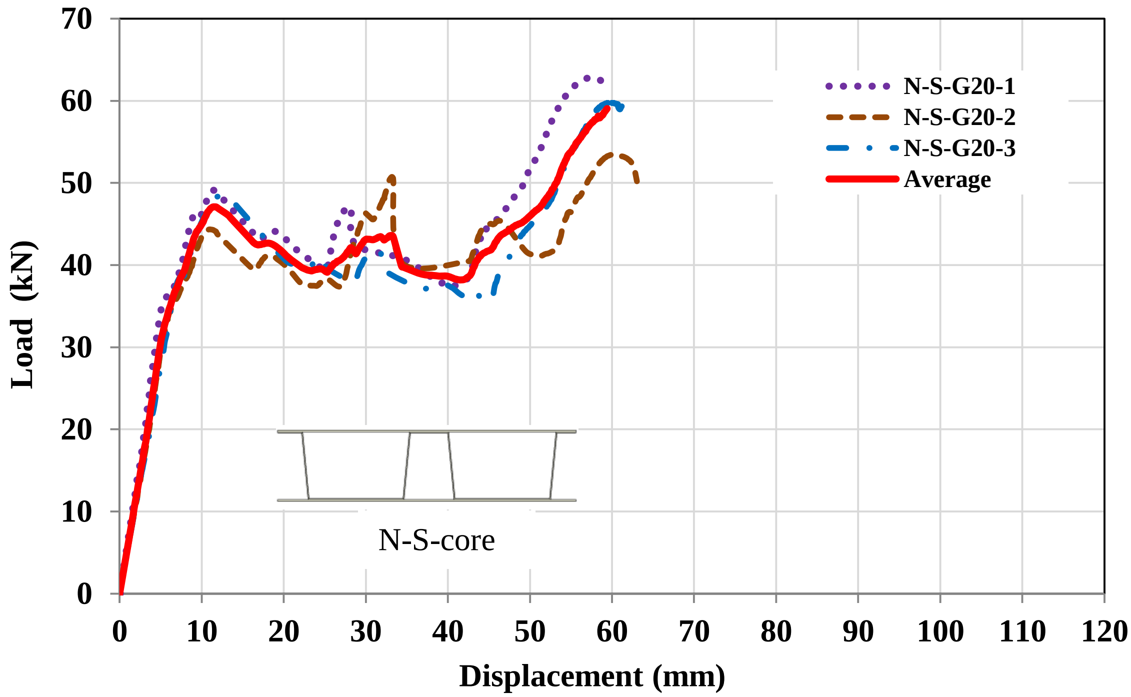

(b)

Fig. 5.12 Experimental and average resistance functions for: (a) *B-T-G20* sandwich panels and (b) *N-S-G20* sandwich panels.

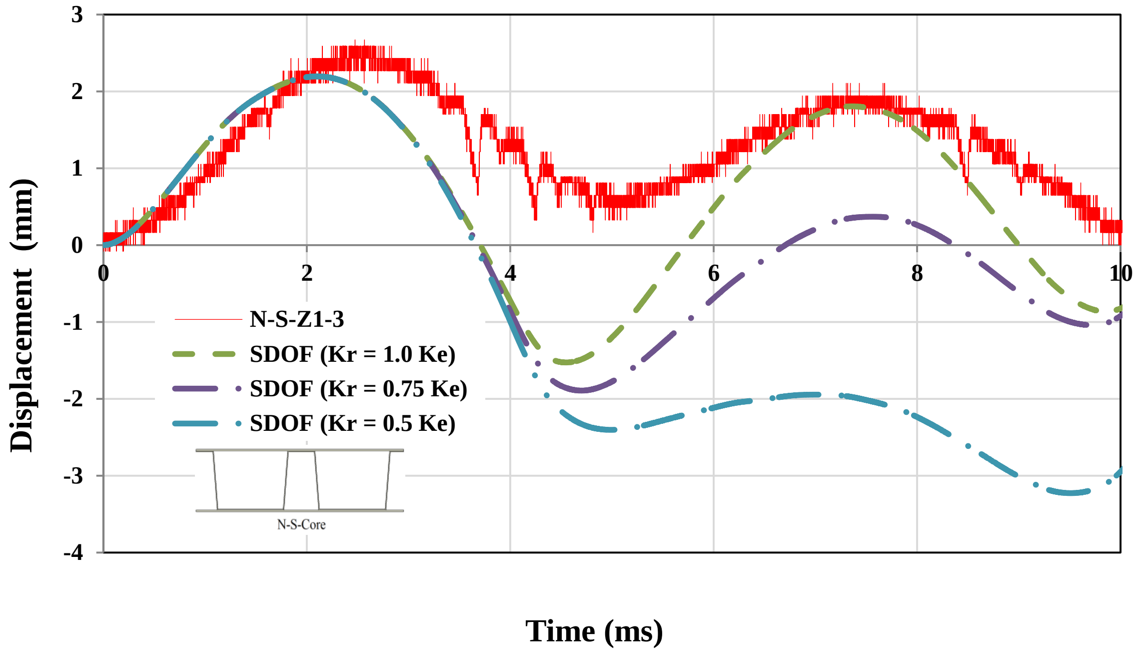

(a)

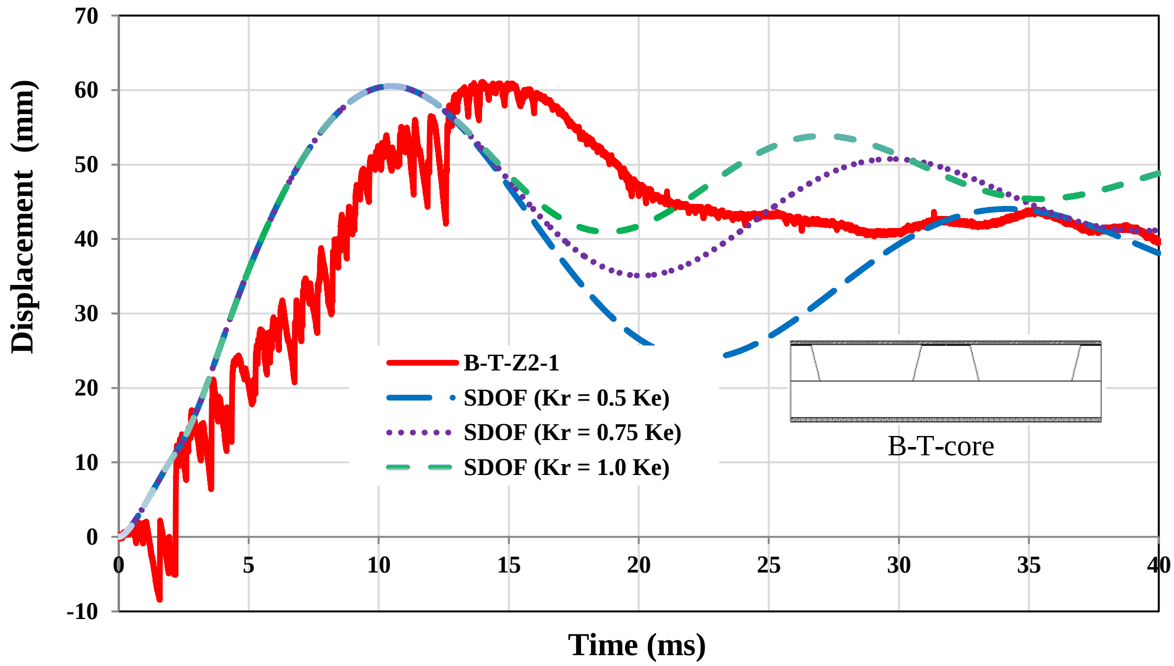

(b)

Fig. 5.13 Experimental and SDOF displacement-time histories (a) *N-S*-core, shot-3, scale distance Z_1 and (b) *B-T*-core, shot-7, scale distance Z_2.

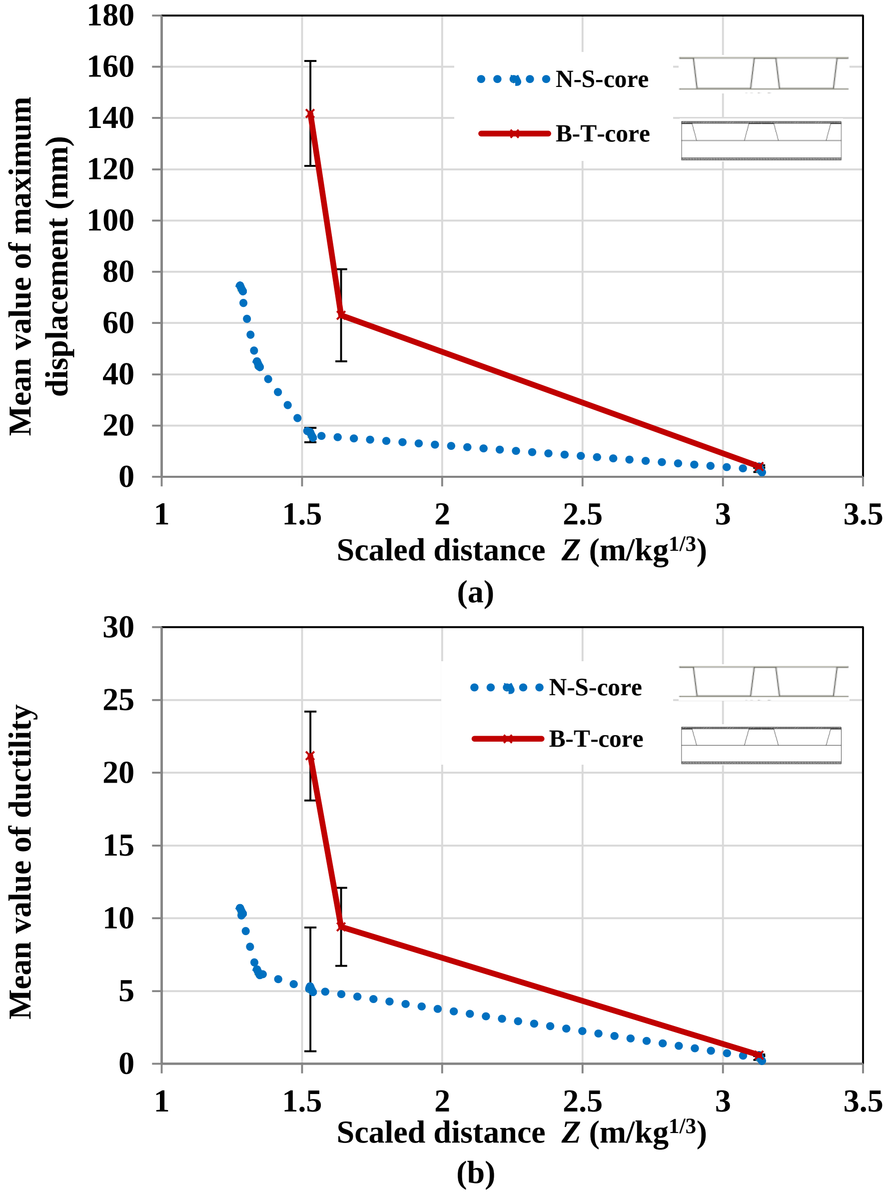

Fig. 5.14 Influence of core configuration on maximum displacement and ductility under different scaled distances, (a) mean value of maximum displacement-scaled distance and (b) mean value of ductility-scaled distance.

Chapter 6: Summary, Conclusions, and Recommendations for Future Research

6.1 Summary

This work represents the first phase (internal explosions) of a multi-phase research program that is focused on developing blast damage mitigation techniques for submerged systems. The dissertation focused on evaluating the performance of fifty-seven lightweight cost-effective sandwich panels under either static loads or confined blast loads. The sandwich panel configurations were developed to be employed as sacrificial cladding where confined explosion may occur. The confined and un-vented space in a submerged structure can make the consequences of a confined explosion more disastrous than open-air explosion, as a fewer amount of explosives can cause the same damage level of a much larger size of explosive device due to the occurrence of multiple reflections. Subsequently, this work attempted to assess the response of lightweight cold-formed steel sacrificial cladding to mitigate the risk of blast hazard in a cylindrical blast chamber simulating a submerged structure. The proposed sandwich panel systems offer superior energy absorption capabilities and possess high strength levels and high stiffness-to-weight ratios, which makes it ideal for blast hazard mitigation. In addition, the dissertation attempted to overcome some of the typical sandwich panel disadvantages associated with the high material cost and complex manufacturing techniques. Finally, it should also be noted that there is no general analytical approach available in literature to accurately predict the resistance function of sandwich panels, which is a key aspect in estimating the dynamic response of sacrificial cladding under blast loads. Consequently, there is a need to develop an experimental sandwich panel blast result database, to be used in predicting the dynamic response of the proposed panels.

In the current study, an analytical model was first introduced to predict the elastic static capacities of the proposed sandwich configurations and to define the expected failure mode(s). Followed by two stages of quasi-static tests were carried out, in order to accurately quantify the resistance function. Eighteen single layer core sandwich panels were included in the first stage, representing *longitudinal* and *transverse corrugated* core configurations, where various available off-the-shelf corrugated sheets profiles with different thicknesses were used in the manufacture of the panels' sandwich cores. The first stage results demonstrated an efficient strength and stiffness, but showed a lack in ductility and energy absorption capabilities. As such, different core configurations were developed and tested in the second, where twenty one panels including double layered core such as *Bi-directional* and *X-core* configurations, and a *Uni-directional* single layer core with an equivalent depth to the former core. The results of the second stage demonstrated significant improvement in the ductility and energy absorption capabilities compared to the panels tested in the first stage. Deformations and failure modes exhibited by all panels were documented and discussed. Yield loads, ultimate capacities, and corresponding displacement values characterized the static resistance function for each of tested panel. Furthermore, the influences of core configuration and core sheet thickness on the stiffness, ductility, and energy absorption were quantified.

Based on the quasi-static test results, two core configurations were selected to be further evaluated under live explosives. The selection criteria included the panels' ductility and energy absorption capabilities, in addition to their behavior beyond the elastic zone. The dynamic response of eighteen sandwich panels was evaluated under different scaled distances, in order to exhibit different damage states according to the American and Canadian blast standards (ASCE 2011, CSA 2012). In addition, blast wave characteristics such as the incident and reflected pressures were recorded, and a good agreement was found between the predicted and recorded pressure and impulse values of different shots for the first positive phase. Moreover, the observed post-blast damage and failure modes were determined and compared to the static failure modes.

In addition to the experimental work, a nonlinear *SDOF* model was developed to predict the dynamic response of the tested configurations, and the results were compared with the experimental data. In this respect, the experimental and numerical ductility levels and support rotation values were correlated to the different damage state specified by standards. Finally, the influence of core configuration on the dynamic behavior of the tested panels was discussed and assessed.

6.2 Conclusions

The static and dynamic performance of a lightweight cold-formed steel sacrificial cladding were investigated.. The tested panels showed different damage levels corresponding to different scaled distance scenarios. The conclusions from the experimental and analytical studies reported in the preceding chapters are as follows:

- A literature review shows that sandwich panels have the potential to serve as an ideal sacrificial blast cladding system due to its high capability of energy absorption, and its high stiffness/weight ratio.
- Literature also shows that although numerical and analytical methods might be capable of predicting the dynamic response of sandwich panels under blast loads, experimental

tests present the most realistic approach to quantify the panel response and to provide benchmark data to verify the analytical models.

- The proposed sandwich panels were efficiently manufactured within a relatively short time frame and using a cost effective fabrication technique. The effectiveness of the manufacturing technique was demonstrated as no weld failure was observed in any of the blast tested panels.
- An analytical model which could predict the yield load, yield displacement, elastic stiffness, corresponding energy absorption, web crippling load, and buckling load, was introduced. The analytical results were found in good agreements with the experimental measured values, where the error between the analytical and the experimental results was quantified and presented.
- The core configuration was found to affect the nominal yield of the tested panels. For the single layer (first stage) configurations, the highest nominal yield load was achieved by using the *V-S*-core configuration; while for the double layer core (tested within second stage) configurations the highest nominal yield value was exhibited by *B-X-G18*.
- The ultimate capacity was also influenced by core configuration, which has been illustrated by comparing values for various configurations dimensions for a given core sheet thickness. For all the tested configurations, the highest ultimate capacity exhibited by *N-S-G18* was found to have a value of 63.61, and also for *G20* configurations the highest ultimate capacity was achieved by the *N-S-G20* configuration.
- As a separate parameter, the core sheet thickness also had a significant effect on the nominal yield load. For single layer (first stage) sandwich panels, the most affected

configuration was the *B-S*-core, where an increase in the core sheet thickness from 0.9 mm (*G20*) to 1.2 mm (*G18*) was found to increase its nominal yield load by 35.6 %, while same increase in core sheet thickness in double layer (second stage) configurations resulted in an increase in nominal yield load by 68.7%, 45.7% and 13.4 % for the *B-T*-core, *B-X*-core and *N-S*-core, respectively.

- Similar to its influence on the nominal yield load, the core sheet thickness also had an influence on the ultimate panel capacity, where the mean values of ultimate capacity for the double layer configurations increased by 35.4 %, 59.3% and 23.0 % in the *B-X*-core, *B-T*-core, and *N-S*-core configurations respectively, corresponding to the increase of the core sheet thickness from *G20* to *G18*.
- The tested configurations of the single layer configurations (tested within the first stage) did not possess significant ductility, as the maximum ductility did not exceed 2.3. On the other hand, a significant enhancement in ductility exhibited by double layer configurations (tested within the second stage), where *B-T-G20* configuration exhibited the maximum ductility compared to all the tested configurations with a value of 14.2.
- Although increasing the core sheet thickness from 0.9 mm to 1.2 mm was found to increase both the nominal yield load and the ultimate panel capacity, it resulted in decreasing the ductility by 20.2%, 35.3%, and 13.1% for *B-X*-core, *B-T*-core, and *N-S*-core sandwich panels, respectively.
- As expected, the flexure elastic stiffness was also influenced by the core configuration. For example, the stiffness of the *B-S*-core was found to be 3.3 times greater than that for the *V-ST*-core. The flexure elastic stiffness was also affected by the core sheet thickness,

where the stiffness for the B-S-core configuration increased by 23% when the core sheet thickness was increased from 0.9 mm (G20) to 1.2 mm (G18)

- For the single layer (tested within the first stage) configuration, the maximum energy absorption exhibited by *V-S-G20* panels, while the B-T-G18 panels showed the maximum energy absorption among all test configurations.
- The energy absorption was found to increase by increasing the core sheet thickness, where an increase of 0.3 mm in the core sheet thickness was found to increase the energy absorption by 24.3%, 72.3%, and 7.2% for *B-X*-core, *B-T*-core, and *N-S*-core sandwich panels, respectively.
- When each stage configurations (i.e. single layer or double layer) are considered separately, the normalized energy curves were found to follow the same trend in terms of the energy variation with the ductility demand. Subsequently, a proposed equation was obtained to represent the normalized energy as a function in the normalized displacement for each stage configurations.
- Analyses of the blast test results showed that the post-blast dynamic failure modes were in good agreement with their static counterparts. This confirmed the assumption of the blast design standards that rely on the static resistance function to predict the dynamic response.
- The sandwich panels exhibited different damage states in accordance with the damage level classification in the ASCE 59-11 (ASCE 2011) and CSA S850-12 (CSA 2012) under different scaled distances.

- The measured blast wave characteristics for the first positive phase reasonably agreed with the predicted characteristics (pressure and impulse) using the ConWep (Hyde 1990) for open air spherical explosions where the errors in predicting the reflected impulse and the reflected pressure varied between +11 % to -22% and +17% to -33%, respectively.
- The predicted response using the developed explicit nonlinear *SDOF* model under blast loads was in a reasonable agreement with the experimental results, where the difference in the maximum displacement predictions ranged between 67% to 99% for the *Uni-directional*-core sandwich panels, and 67% to 98% for the *Bi-directional*-core panels.
- The blast response of the tested configurations was evaluated and findings suggest that it is viable to use the lightweight relatively cost-effective proposed panels as sacrificial cladding for blast risk mitigation.

6.3 Recommendations for future research

The research results reported in this dissertation included only the first of multi-phase research program that focused on blast damage mitigation in submerged structures, within which static and dynamic testing of lightweight sandwich panels had been performed. Detailed analyses for all stages of the experimental tests have been provided. However several aspects of interest require further research. This section suggests possible research areas to extend the current knowledge base with regard to response of sacrificial cladding systems under confined explosions:

- In this study, only flat sandwich panels were tested. Investigating the influence of the geometrical shape of panels on its dynamic response under blast loads can be very promising area, for example the influence of the panel curvature.

- Improving the resistance of the sandwich panels by filling lightweight polymer materials in the core of sandwich panels could also be an interesting area of investigation.
- One-way sandwich panels only were tested in the presented experimental program, investigating the dynamic performance of two-way sandwich panels under confined explosion need to be studied.
- The influence of boundary conditions on the dynamic behavior of sandwich panels can be an interesting area to be investigated, as only simply-supported one-way sandwich panels were evaluated in this study. Considering different boundary conditions with both one-way and two-way sandwich panels would be beneficial.
- The variability and uncertainties associated with the panel's response under confined explosions might call for a probabilistic analysis approach in order to give more confidence of the sacrificial cladding system performance under different level of blast hazard. Such approaches would also be very useful for the decision making process for blast risk mitigation.
- Finally, applying different techniques to optimize the shape of the panels for different applications and performance criteria is a key area that requires further investigation, especially when the material, dimensions, boundary conditions, cost, and other application-specific factors are accounted for.